LBL-17426
Preprint c. 2

Lawrence Berkeley Laboratory
UNIVERSITY OF CALIFORNIA

RECEIVED
LAWRENCE
BERKELEY LABORATORY

APR 17 1984

LIBRARY AND
DOCUMENTS SECTION

Submitted to Annual Review of Nuclear and Particle Science

THE ROLE OF ROTATIONAL DEGREES OF FREEDOM IN HEAVY ION COLLISIONS

L.G. Moretto and G.J. Wozniak

March 1984

TWO-WEEK LOAN COPY

This is a Library Circulating Copy which may be borrowed for two weeks. For a personal retention copy, call Tech. Info. Division, Ext. 6782.

LBL-17426 c.2

Prepared for the U.S. Department of Energy under Contract DE-AC03-76SF00098

DISCLAIMER

This document was prepared as an account of work sponsored by the United States Government. While this document is believed to contain correct information, neither the United States Government nor any agency thereof, nor the Regents of the University of California, nor any of their employees, makes any warranty, express or implied, or assumes any legal responsibility for the accuracy, completeness, or usefulness of any information, apparatus, product, or process disclosed, or represents that its use would not infringe privately owned rights. Reference herein to any specific commercial product, process, or service by its trade name, trademark, manufacturer, or otherwise, does not necessarily constitute or imply its endorsement, recommendation, or favoring by the United States Government or any agency thereof, or the Regents of the University of California. The views and opinions of authors expressed herein do not necessarily state or reflect those of the United States Government or any agency thereof or the Regents of the University of California.

LBL-17426

The Role of Rotational Degrees of Freedom in Heavy Ion Collisions

L. G. Moretto and G. J. Wozniak

Nuclear Science Division
Lawrence Berkeley Laboratory
University of California
Berkeley, California 94720

Nec ratio solis simplex et recta patescit
quo pacto aestivis e partibus aegocerotis
brumalis adeat flexus, atque inde revertens
cancri se ut vertat metas ad solstitialis,
lunaque mensibus id spatium videatur obire
annua sol in quo consumit tempora cursu
non inquam simplex his rebus reddita causast.

Lucretius, De rerum natura V 614-620

And it is not clear nor simple how the sun moves from the hot to the cold regions from solstice to solstice, nor how the moon in a month covers the journey that the sun covers in a year. There is not a simple explanation at hand for this.

This work was supported by the Director, Office of Energy Research, Division of Nuclear Physics of the Office of High Energy and Nuclear Physics of the U.S. Department of Energy under Contract DE-AC03-76SF00098.

CONTENTS

1 INTRODUCTION 1

2 ROLE OF ENTRANCE CHANNEL ANGULAR MOMENTUM IN EXIT CHANNEL DISTRIBUTIONS 10

2.1 Angular Distributions and the Classical Deflection Function 10

2.2 Width of the Angular Distributions: Quantal or Statistical Fluctuations? 17

2.3 Angular Distributions as a Function of Mass Asymmetry 20

2.4 Rigid Rotation and Angular Momentum Fractionation Along the Mass Asymmetry Coordinate 24

3 THE EXCITATION OF ANGULAR MOMENTUM BEARING MODES AND THE PARTITION OF ANGULAR MOMENTUM BETEWEEN ORBITAL AND INTRINSIC 29

3.1 The Rotational Degrees of Freedom of the Dinuclear Complex 29

3.2 Angular Momentum Misalignment 34

3.3 Angular Distributions of Sequential Fission and of Sequential Light Particle Emission 35

3.4 Gamma Ray Angular Distributions 40

3.5 Experimental Spin Alignment From Gamma-Ray Angular Distributions 44

3.6 Experimental Data From Sequential Decay 48

3.6.1 Sequential Alpha Emission 48

3.6.2 Sequential Fission 49

4 MORE AMBITIOUS MODELS 51

4.1 Time Dependent Hartree-Fock Model 51

4.2 Coherent Surface Excitation Model 51

4.3 Transport Models 52

5 CONCLUSION 56

LITERATURE CITED 58

FIGURE CAPTIONS 67

FIGURES 73

1 INTRODUCTION

Nuclear science, not unlike other human endeavors, has been both developed and defined by the tools at its disposal. As late as the early 1970's most accelerators provided a limited range of projectiles, typically protons, deuterons, tritons, ^{3}He and ^{4}He. The picture of nuclear reactions painted by means of these projectiles was remarkably one-sided, with hardly anyone noticing it. The extreme polarization that ensued can be appreciated in terms of the following modern classification. Two classes of processes were unveiled and studied: On the one hand, the elastic and the nearly elastic reactions involving elementary excitations of the target; on the other, the complete amalgamation of the projectile and the target giving rise to a fully equilibrated intermediate, or compound nucleus.

The former reactions were instrumental in defining the optical potential and the shell-model picture. Spectroscopy was the vogue, and anything not looking like a peak, and sharp at that, was inexorably discarded as annoying "background." Barely saved from such a "subtraction" of background were some broad structures like the single particle "strength" and the giant dipole resonance because of special interests and special projectiles, respectively.

The latter reactions, of a more democratic nature, determined the application of statistical mechanics to nuclear physics. The cavalier treatment of matrix elements, spectroscopic factors and the like, made possible the recognition and the treatment of particle evaporation spectra as more or less continuous entities, as well as of statistical branching ratios and excitation functions, but created a great chasm and an unsympathetic atmosphere between the two areas.

Of a special interest in the second class of reactions was the process of fission which, by involving the coherent motion of many particles at a time, earned the scornful derision of the spectroscopists but sensitized the compound nucleus observers to collective macroscopic effects. With hindsight, one can argue that the polarization between spectroscopy and equilibrium statistics was more in the mind of the practitioners than in the experimental spectra. The presence of large cross sections in the intermediate inelasticity range was well known (see for example: Kaufman & Wolfgang 1961, Galin et al. 1970), but what is now the virgin field of "illuminated" spectroscopists hunting for resonances was then the wasteland of their conservative forefathers.

The advent of heavy ion accelerators in the early seventies made available a range of projectiles and energies leading to reactions in which the complete fusion of the target and projectile was substantially depressed. The room left behind by the failure to form a compound nucleus became occupied by reactions with intermediate to complete inelasticities and with a variable amount of mass, charge, spin and isospin transfer (Artukh et al. 1973, Moretto et al. 1973, Kratz et al. 1974, Hanappe et al. 1974, Wolf et al. 1974). The failure of two nuclei to fuse into a compound nucleus can be understood in terms of the liquid drop model. The surface energy always favors fusion. Coulomb and centrifugal forces oppose it. From a static point of view it is possible to define the boundary of stability of (liquid drop) nuclei in terms of two parameters, $x = \frac{E_{coulomb}}{2E_{surface}}$, $y = \frac{E_{rotational}}{E_{surface}}$, where $E_{coulomb}$, $E_{surface}$ and $E_{rotational}$ are defined for the spherical configuration and rigid rotation. With increasing x and y, the disruptive forces increase and make the nucleus progressively more unstable towards fission. The limits of stability

(Swiatecki 1972, Cohen et al. 1974), corresponding to the fission barrier going to zero, are shown in Figure 1.

Unfortunately statics is not sufficient to establish whether two colliding nuclei are going to fuse. Dynamics plays a vital role in the fusion process. Early attempts (Bondorf et al. 1974, Tsang 1974, Gross & Kalinowski 1974) were made by treating the dynamics in a simplified fashion in terms of two spherical nuclei under the action of conservative forces (Coulomb, centrifugal and nuclear) and dissipative forces (radial and tangential friction). The angular momentum dependent potentials increase with decreasing internuclear distance. As the nuclei touch, the nuclear interaction (proximity force) may lead to the appearance of a minimum which eventually disappears (see Figure 2) with increasing orbital angular momentum. Fusion criteria were then adopted on the basis of the presence of a minimum in the relevant potential energy curve (Bass 1974) and also of a critical distance (Lefort 1975, Glas & Mosel 1975). If a system can dynamically reach the minimum, it will fuse. Tangential friction gives the additional possibility of jumping from the entrance-channel ℓ-wave potential energy curve to another at a lower ℓ-wave due to angular momentum transfer from orbital rotation to nuclear spin. Thus, even if the entrance channel ℓ-wave potential does not have a pocket, the system may still fuse if friction brings it down to a lower ℓ-wave potential with a pocket. These simple models have been extended by Deubler & Dietrich 1975, Birkelund et al. 1979, and Gross 1981.

A general theoretical model of fusion and reseparation, which allows the two nuclei to deform, to form a neck and amalgamate, has been presented by Swiatecki (1982). His approach explicitly considers the degrees of freedom that allow two nuclei to fuse. Thus such a model provides the most suitable

framework not only for the description of fusion but of reseparation as well. Unfortunately the illustration of this model goes beyond the scope and limits of this work.

Even if the two nuclei do not manage to fuse, they do, of course, interact. During the interaction phase, a variety of degrees of freedom is called into play (Galin 1976, Moretto & Schmitt 1976 & 1981, Schröder & Huizenga 1977, Lefort & Ngô 1979, Scott 1978, Volkov 1978, Nörenberg & Weidenmüller 1980). The coupling of the relative motion to the internal, or collective nuclear degrees of freedom leads to energy dissipation, the most manifest property of these reactions. In a similar manner, angular momentum is transferred from orbital motion to nuclear spin. The exchange of matter between the two fragments may lead to an evolution along the mass asymmetry degree of freedom as well as to a redressing of a possible imbalance in the neutron-to-proton ratio of the two fragments in contact.

These degrees of freedom, that are so intimately involved with the nucleus-nucleus interaction, have been previously encountered in the fission process. The attempt to study them in fission was not too successful due to the inability of the experimenter to control the initial conditions of some relevant variables. Rather, such conditions are statistically determined at the fission saddle point, and thus very little variety can be observed. In deep inelastic processes one has a broad choice of initial conditions for all the relevant degrees of freedom. The collision energy can be varied greatly and so can the entrance channel angular momentum. The overall mass and charge of the system is only limited by the availability of stable or nearly stable isotopes (e.g. $^{238}U + ^{248}Cm$ or heavier). The mass asymmetry can be easily explored in its whole range from extreme asymmetry (p, α + nucleus) to

symmetry (Ca + Ca, Nb + Nb, Pb + Pb etc.). The equilibration of the neutron-to-proton ratio can be explored by exploiting either the variety of isotopes available for a given atomic number Z (e.g. ^{40}Ca, ^{48}Ca,) or the progressive increase of the neutron excess with Z. It is no wonder that so many fission experts found the availability of such reactions a godsend and proceeded in becoming experts in deep inelastic processes.

The experimental observations provided a very tantalizing picture of the evolution of such degrees of freedom. While some modes seemed to relax all the way to the equilibrium limit, others seemed to hardly evolve away from their initial conditions. So it was soon apparent that energy was dissipated with inelasticities covering the whole range from elastic energies to Coulomb energies (Artukh et al. 1973, Moretto et al. 1973, Hanappe et al. 1974, Wolf et al. 1974). Yet, at every inelasticity the dissipated energy was divided between the fragments proportionally to their mass as required by statistical equilibrium (Eyal et al. 1978, Schmitt et al. 1978, Tamain et al. 1979, Hilscher et al. 1979, Gould et al. 1980). Similarly, the angular momentum was found to be partitioned between orbital motion and fragment spin from pure orbital motion all the way down to rigid rotation (Dyer et al. 1977, Glässel et al. 1977, Natowitz et al. 1978). Also, while the neutron-to-proton ratio was found to equilibrate rapidly (Gatty et al. 1975a & b, Jacmart et al. 1975, Galin 1976), the mass asymmetry mode seemed to develop extremely slowly (Moretto & Schmitt, 1976). Whatever the degree of relaxation happened to be for a given mode, the mean value was observed to be accompanied by a corresponding development of the width.

This state of affairs led naturally to the treatment of the time evolution of the involved variables in terms of transport equations. The earliest suggestions along this line were by Nörenberg (1974, 1975, 1976) who

described the energy dissipation in terms of a Fokker-Planck equation and by Moretto and Sventek (1975) who treated the evolution of the mass asymmetry degree of freedom by means of the Master equation. The two approaches are related to one another and are suitable for the description of the time evolution of distribution functions.

The Master Equation for a single variable describes the time evolution of a population $f(x,t)$ as follows:

$$\dot{f}(x,t) = \int dx' \left[\Lambda(x,x') f(x',t) - \Lambda(x',x) f(x,t) \right] \qquad 1.$$

where $\dot{f}$ is the time-derivative of f and $\Lambda(x,x')$, $\Lambda(x',x)$ are the direct and inverse transition probabilities. The first term in the square bracket is called a gain term while the second is the loss term. The simplicity of this equation arises from the assumption that the transition probabilities are local in space and time-independent. Under these conditions the Λ's must obey the relations required by microscopic reversibility:

$$\Lambda(x,x') = \lambda(x,x')\rho_x \qquad 2.$$

$$\Lambda(x',x) = \lambda(x',x)\rho_{x'} \qquad 3.$$

$$\lambda(x,x') = \lambda(x',x) \qquad 4.$$

where ρ_x, $\rho_{x'}$ are the level densities at x,x'. This guarantees that the system will approach equilibrium. In fact, for $\dot{f} = 0$:

$$f(x',t = \infty)/f(x,t = \infty) = \rho_{x'}/\rho_x \quad . \tag{5.}$$

The Fokker-Planck equation can be simply derived from the Master equation. If one sets $x' = x + h$ and expands all the quantities in powers of h about x one obtains:

$$\dot{f}(x,t) = -\frac{\partial}{\partial x}(\mu_1 f) + \frac{1}{2}\frac{\partial^2}{\partial x^2}(\mu_2 f) + \ldots \tag{6.}$$

where μ_1,μ_2 are the 1st and 2nd moments of the transition probabilities:

$$\mu_1 = \int h\Lambda(x,h)dh \quad ; \quad \mu_2 = \int h^2\Lambda(x,h)dh \quad . \tag{7.}$$

The physics is of course contained in the Λ's or alternatively in μ_1,μ_2.

The justifications and the applications of these equations have been widely discussed (Nörenberg & Weidenmuller 1980). It may suffice here to recall the two most general approaches. The first, introduced by Nörenberg (1975), calculates the transition probabilities in terms of shell model matrix elements, while the second, employed by Randrup (1978) and Feldmeier (1982), is based upon the one-body assumption following which the long nucleonic mean-free path allows one to deal with the nucleons as independent particles. In this framework mass, charge, energy and angular momentum are exchanged and/or dissipated through the nucleon exchange between the interacting nuclei.

An even simpler approach to the description of heavy ion reactions is the concept of conditional equilibrium (Moretto 1981). As discussed above, certain degrees of freedom equilibrate very fast while others are very slow. In this regime the former modes are essentially at equilibrium and smoothly

follow the evolution of the slow modes. These fast modes can be treated within the framework of equilibrium statistical mechanics. The advantage of this approach is the minimal amount of information needed to predict the distribution of the variables under discussion. This approach has been applied with success to the problem of energy partition between fragments (Morrissey & Moretto 1981), to the distribution of charge at fixed mass asymmetry (Gatty et al. 1975) and to the distribution of angular momentum among the angular momentum bearing modes (Moretto & Schmitt 1980). The latter problem will be discussed extensively later on.

So far we have attempted to paint in broad strokes the picture of the field of heavy ion reactions. It may already be apparent that angular momentum plays a very pervasive role in this class of reactions, starting from the definition of the range in which these processes become dominant with respect to fusion on one hand, and direct reactions on the other, and ending with detailed effects on most of the variables that have been explored so far.

In what follows we shall consider the role of angular momentum both in those modes whose excitation is associated with their ability to carry angular momentum, as well as in other modes, like the mass asymmetry mode, which do not carry angular momentum but whose effective potential energy is directly affected by angular momentum through the associated rotational energy.

We shall begin by discussing the effect of angular momentum on angular distributions and we shall show how it is still possible to retain the concept of a deflection function in this class of reactions. We shall then proceed to discuss how the entrance channel angular momentum is distributed or fractionated along the mass asymmetry degree of freedom. In this way the dependence of the angular distribution on mass asymmetry can be understood.

The introduction of the rotational degrees of freedom associated with the dinuclear complex will allow us to discuss their thermal or statistical excitation and to calculate the 1st and 2nd moments of the angular momentum associated with the fragments.

The resulting fragment angular momentum misalignment due to fluctuations is considered in its effects upon the angular distribution of the gamma rays, alpha particles and fission fragments sequentially emitted by the primary deep inelastic fragments. The experimental evidence on the first and second moments of the fragment angular momentum is discussed in detail.

In the last section, Time Dependent Hartree-Fock, the excitation of surface modes and transport models are discussed briefly. Finally the spin-spin correlation is discussed theoretically and the results of dynamical and equilibrium calculations are compared.

2 ROLE OF ENTRANCE CHANNEL ANGULAR MOMENTUM IN EXIT CHANNEL DISTRIBUTIONS

2.1 The Angular Distributions and the Classical Deflection Function

In general, the angular momentum plays an essential role in determining the angular distributions of reaction products. In the case of complete decoupling between entrance and exit channel (e.g. compound nucleus decay), the magnitude of the orbital angular momentum carried by the emitted particle together with the total angular momentum determines, generally speaking, the sharpness of the angular distribution. For instance, in compound nucleus decay, evaporated neutrons and protons which can carry little angular momentum are nearly isotropic, while fission fragments which carry the lion's share of angular momentum are strongly forward peaked, like $1/\sin\theta$. In the case of elastic scattering, such a decoupling does not exist, and a unique relation can be established between the entrance channel angular momentum ℓ (or the impact parameter b) and the exit channel angle θ. This relation can be obtained directly from energy and angular momentum conservation. From energy conservation we have:

$$\frac{1}{2} m\dot{r}^2 = E - V(r) - \frac{\ell^2}{2mr^2} \quad . \qquad 8.$$

From angular momentum conservation we have

$$\ell = mr^2\dot{\theta} \quad . \qquad 9.$$

By eliminating the time, we obtain

$$d\theta = -\frac{\ell}{mr^2}\left\{\frac{2}{m}\left(E - V(r) - \frac{\ell^2}{2mr^2}\right)\right\}^{-1/2} dr \quad . \qquad 10.$$

Setting $w = b/r$ and the impact parameter $b = \ell(2mE)^{-1/2}$, one obtains the deflection function Θ.

$$\Theta = \pi - 2\int_0^{b/r_{min}} \frac{dw}{\sqrt{1 - V(w)/E - w^2}} \quad . \qquad 11.$$

For the Coulomb potential, for instance

$$\Theta = 2\arctan\left(\frac{Z_1 Z_2 e^2}{2Eb}\right) \quad . \qquad 12.$$

The angular distribution is given by:

$$\frac{d\sigma}{d\Omega} = \frac{b}{\sin\theta}\left|\frac{db}{d\theta}\right| \quad . \qquad 13.$$

The presence of energy dissipation and the ability of nuclei to pick up angular momentum in the form of spin can also be dealt with within the framework of classical mechanics. The most general formulation of the problem requires the definition of a set of dynamical variables $q,\dot{q}$, of the corresponding Lagrangian $L(q,\dot{q}) = T - V$ and of the Raleigh dissipation function $R = \frac{1}{2}\ \Sigma\gamma_{\mu\nu}\dot{q}_\mu\dot{q}_\nu$ where $\gamma_{\mu\nu}$ is the dissipation tensor. The equation of motion is then:

$$\frac{d}{dt}\frac{\partial L}{\partial \dot{q}} - \frac{\partial L}{\partial q} + \frac{\partial R}{\partial \dot{q}} = 0 \quad . \qquad 14.$$

The simplest way to deal with such a problem is to consider the case of two rigid spheres interacting through the Coulomb field and the short range nuclear force. The friction tensor must be defined empirically or determined from some microscopic model (Nörenberg 1974). Such a simple formulation of the problem allows one already to define the maximum angular momentum for trapping with eventual compound nucleus formation, to determine the deflection function for the non trapped orbits and, to establish the exit channel fragment spin.

The transfer of angular momentum from the orbital motion to the fragments rotation can divided into three regimes (Tsang 1974, Lefort & Ngô 1978). Initially the two nuclei "slide" on top of each other and they are brought to rest relative to one another by tangential friction. At this stage the nuclei roll and are slowed down by "rolling" friction. When the nuclei stop rolling, they stick, the orbital rotation and the nuclear rotation share the same angular velocity, and the dinuclear system rotates rigidly. It is interesting, but not too useful, to appreciate that, in absence of rolling friction, one obtains the <u>rolling limit</u>, which, for spheres, implies the following relation

$$\ell_{rolling} = \frac{5}{7}\,\ell_{initial} \qquad 15.$$

independent of mass asymmetry. The angular momentum of each nucleus is defined by

$$\frac{I_1}{R_1} = \frac{I_2}{R_2} \qquad 16.$$

where R_i and I_i are the nuclear radius and spin, respectively. The rigid rotation limit on the other hand gives for the spin of one fragment:

$$I_{1,2} = \frac{\mathcal{J}_{1,2}}{\mathcal{J}_1 + \mathcal{J}_2 + \mu d^2} \ell_{initial} \quad , \qquad 17.$$

where $\mathcal{J}_1$ and $\mathcal{J}_2$ are the moments of inertia, μ is the reduced mass and d is the distance between centers of the fragments. For two touching spheres the spin of one fragment goes from $\frac{1}{7}\ell_{initial}$ to $\ell_{initial}$ as one goes from a symmetric system $(A_1 = A_2)$ to a progressively more asymmetric system. A completely fused system is of course made up of a single nucleus and its angular momentum must be equal to $\ell_{initial}$. Such a dependence on mass asymmetry can be readily written down for two touching spheres:

$$I_1 = \frac{\frac{2}{5} M_1 R_1^2}{\frac{2}{5}(M_1 R_1^2 + M_2 R_2^2) + \frac{M_1 M_2}{M_1 + M_2}(R_1 + R_2)^2} \ell_{initial} \quad . \qquad 18.$$

This dependence of the transferred spin on mass asymmetry has been frequently used to verify rigid rotation (Glässel et al. 1977, Natowitz et al. 1978, Babinet et al. 1980, Sobotka et al. 1981).

The calculated deflection functions show two possible regimes: near-side scattering and far-side scattering or orbiting. It is possible to verify such predictions experimentally. A useful way to examine the experimental data is to plot the doubly differential cross section $\frac{d^2\sigma}{dEd\theta}$ as contour lines in the plane E,θ. When this is done (Wilczynski 1973), as shown in Figure 3, one notices that, rather than observing a unique relation between E and θ, as predicted by the classical models, one obtains a broad spread of energies for a given angle and vice-versa. This means that the deflection function as well as the energy loss are not well defined and that fluctuations, quantal or statistical in nature, dominate the picture. Still at times it is possible to

observe ridges which suggest that both regimes, near-side scattering and orbiting can occur. For instance Figure 3a gives the distinct impression that the two ridges observed in the cross section do correspond to near side scattering and far side scattering for the high energy and low energy branch, respectively. Yet other reactions seem to indicate that near-side scattering alone is occurring. For this second class of reactions the angular distribution is side-peaked at all energy losses (Figure 3b). These two classes of reactions are qualitatively distinguished by the deflection function which dives to negative angles in the former case and which remains confined to positive angles in the latter.

It has been shown (Moretto & Schmitt 1976, Mathews et al. 1977) that the product of the interaction time and of the angular velocity, which determines the amount of forward swinging of the dinuclear system, is related to the ratio of the c.m. energy and the Coulomb barrier E/B. Typically, for $E/B > 1.5$, one observes forward peaking in the angular distribution associated with negative angle scattering and the corresponding two branches in the Wilczyński diagram, while for $E/B < 1.5$ one observes side peaking in the angular distribution or near-side scattering and only one branch in the Wilczyński diagram.

The definitive way to establish the above picture is to measure the polarization of the fragments spins. The polarization is defined as:

$$P = \left\langle \frac{m}{I} \right\rangle = \left\langle \sum P(m) \cdot m/I \right\rangle \qquad 19.$$

when I is the spin, m is its Z projection and $P(m)$ is the distribution of m values. If the spin transfer is induced by ordinary macroscopic friction, then P is positive for far side scattering and negative for near side scattering, as shown in Figure 4. The determination of the spin

polarization can be made by measuring the circular polarization of the emitted γ rays. Experiments performed so far are in general agreement with the above picture, provided one allows at times for some simultaneous near and far side scattering due to fluctuations (Trautman et al. 1977 & 1981, Lauterbach et al. 1978). Some data obtained for the reaction ^{58}Ni + 100 MeV ^{16}O are shown in Figure 5. For oxygen ejectiles one observes a large negative polarization in the quasi-elastic peak (near side scattering) evolving into a large positive polarization in the deep inelastic peak, as expected. Similar results have been obtained with a different technique (Ishihara et al. 1978).

Two different techniques have been developed in order to obtain an empirical deflection function. Wolschin (1979a) observed that the deflection angle Θ is related to the rotation angle $\Delta\theta$ by the relation

$$\Theta(\ell_{initial}) = \pi - \theta_i - \theta_f - \Delta\theta \qquad 20.$$

where θ_i and θ_f are the Coulomb angles in the entrance and exit channel and ℓ_i is the entrance-channel angular momentum. The above equation can be written as

$$\Theta(\ell_i) = \Theta_C(\ell_i) - \Theta_N(\ell_i) \qquad 21.$$

where Θ_C is the Rutherford deflection function and Θ_N is the nuclear part of the deflection fuction. The latter is parametrized as

$$\Theta_N(\ell_i) = \beta\, \Theta_C^{gr} \frac{\ell_i}{\ell_{gr}} \left(\frac{\delta}{\beta}\right)^{\ell_i/\ell_{gr}} \qquad 22.$$

where Θ_C^{gr} is the grazing angle; ℓ_{gr} is the grazing angular momentum

and β, δ are two free parameters. The quantity δ determines the deviation of the actual grazing angle from the Coulomb grazing angle, while β detemines the depth of the deflection function. The two parameters δ and β are fitted to the experimental gross angular distribution through the relation

$$\frac{d\sigma}{d\theta} = \frac{2\pi}{K^2} \sum \ell \left|\frac{d\theta}{d\ell}\right|^{-1} . \qquad 23.$$

Examples of deflections functions extracted in this manner are shown in Figure 6.

Another approach is based on the assumption that the dependence between entrance channel angular momentum and exit channel kinetic energy is monotonic (Schröder et al. 1978). Thus the reaction cross section can be divided up into energy bins and from the nearly triangular distribution of the cross section with ℓ one can assign an average angular momentum to each energy bin. At the same time the angular distribution in each energy bin gives the most probable angle to be associated with that angular momentum. The combination of the two quantities defines an empirical deflection function, of which an example is given in Figure 7.

It is clear that both approaches suffer from several basic criticisms. Both methods not only do not allow for fluctuations but also assume that the deflection function is independent of the mass of the actual fragments. The second method leaves an ambiguity in the way one should set the energy windows. In order to be correct one should be able to trace lines of constant entrance channel angular momentum for the map of the cross section vs. energy and atomic number. Unfortunately that would be equivalent to knowing the

answer at the outset, so different approaches have been suggested. On the one hand straight cuts have been used (Schröder & Huizenga 1977, Vandenbosch et al. 1976), on the other lines parallel (Moretto & Schmitt 1976, Rudolf et al. 1979) to the Coulomb-like line of the peaks of the deep inelastic bump. Neither are justified by a theoretical simulation (Sventek & Moretto 1978). Therefore the conclusions obtained in such a way are to be considered only approximate.

2.2 The Width of the Angular Distributions: Quantal or Statistical Fluctuations?

As we have seen in the section above, the use of a classical Lagrangian leads to the definition of an energy distribution function $E = E(\ell)$ and of a deflection function $\theta = \Theta(\ell)$ which relate the entrance channel angular momentum ℓ with the exit channel energy E and angle θ. The two observables E,θ can be correlated as can be seen in the so-called Wilczyński diagrams. Experimentally the cross section $\frac{\partial^2\sigma}{\partial\theta\partial E}$ shows at times ridges that remind us of the theoretical predictions, especially for small energy losses and for masses near that of the entrance channel. However, even under the best conditions it is apparent that fluctuations substantially smear the angular distribution and under the worst wash out any indication of a deterministic trajectory. Typically the experimental angular distributions vary from side-peaked to forward peaked, frequently in the same reaction, as the system moves toward ever more negative Q-values. Such a remarkable evolution is associated with a progressive increase in the interaction time on the one hand, and a corresponding increase in the width of the orbital angular momentum distribution on the other. The width of the distribution can arise from two

very different contributions, as was pointed out by Strutinsky (1973). We can expect a diffractive contribution arising from the width of the ℓ-packet associated with the process, and a "dynamical" contribution associated with the classical deflection function. The "diffractive" component can be estimated from the indetermination principle:

$$\sigma_{\theta,\mathrm{diff}} = \frac{1}{2\sigma_\ell} \quad . \qquad 24.$$

In other words, as one progressively narrows the ℓ-window, one observes a broadening of the angular range covered by the angular distribution. In particular, for a single ℓ-wave one expects to observe an angular distribution spread out over an angular range of 2π.

A purely classical width of dynamical origin is associated with the variation in scattering angle associated with the variation in ℓ:

$$\sigma_{\theta,\mathrm{dyn}} = \frac{d\theta}{d\ell}\,\sigma_\ell \quad . \qquad 25.$$

In this case an increase in the width of the ℓ distribution produces a corresponding increase in the width of the angular distribution. The two widths can be combined in quadrature:

$$\sigma_\theta^2 = \frac{1}{4\sigma_\ell^2} + \left(\frac{d\theta}{d\ell}\right)^2 \sigma_\ell^2 \quad . \qquad 26.$$

Which of the two terms dominates? It depends of course on the size of σ_ℓ. A calculation (Cassing & Friedrich 1980) performed with a purely classical Fokker-Planck approach is unable to reproduce the width of the angular distribution at small energy losses, as shown in Figure 8a. The deficiency of

this approach is related to the predicted smallness of σ_ℓ at small energy losses. In this model the variance σ^2 is proportional to the temperature T which in turn depends on the Q-value. Consequently σ_ℓ^2 tends to zero for Q tending to zero. However the very smallness of σ_ℓ^2 at small energy losses implies a large diffractive width. The inclusion of this quantal effect improves the theoretical picture quite dramatically, as shown in Figure 8b, and makes it almost indistinguishable from experiment.

Interestingly enough, this is not the end of the story. A different calculation (Feldmeier 1982) based upon a one-body diffusion model is quite realistic even at small Q-values despite the absence of quantal fluctuations, as shown in Figure 9. The introduction of quantal fluctuations hardly changes the picture, since the angular distributions are not appreciably broadened. The reason for this apparently contradictory behavior lies in the large dynamical σ_ℓ predicted by the one-body diffusion model even for small Q values. This large σ_ℓ generates a large "dynamical" contribution to σ_θ. However, the same large σ_ℓ implies a small "quantal" fluctuation. Therefore the introduction of quantal effects changes the picture almost imperceptibly.

For large energy losses, thermal fluctuations are almost certainly responsible for a great part of the effect. At the very least, they are simple to estimate. One of the possible fluctuations is associated with the angular momentum trade-off between orbital and intrinsic rotation (Moretto & Sobotka 1981). Given a total angular momentum I and a given orbital angular momentum ℓ, the rotational energy for a dinucleus composed of two equal touching spheres is:

$$E_R = \frac{\ell^2}{2\mathcal{J}^*} + \frac{I^2}{4\mathcal{J}} - \frac{I}{2\mathcal{J}} \qquad \text{where } \frac{1}{\mathcal{J}^*} = \frac{1}{\mu d^2} + \frac{1}{2\mathcal{J}} , \qquad 27.$$

$\mathcal{J}$ being the moment of inertia of one of the two spheres, μ the reduced mass of the system, and d is the distance between the centers of the two spheres. The statistical distribution in ℓ at fixed I at a given temperature T is

$$P(\ell)d\ell = (2\pi\mathcal{J}^*T)^{-1/2}\exp - \left[\frac{\ell^2}{2\mathcal{J}^*T} - \frac{I\ell}{2\mathcal{J}T} + I^2\frac{\mathcal{J}^*}{8\mathcal{J}^2T}\right] . \qquad 28.$$

This distribution at fixed I has the following variance

$$\sigma^2 = \frac{10}{7}\mathcal{J}T . \qquad 29.$$

Additional ℓ fluctuations at fixed I can arise if the two fragments are allowed to deform (Moretto & Sobotka 1981).

2.3 Angular Distributions as a Function of Mass Asymmetry

One of the more complex and less understood problems in heavy ion collisions is the distribution or fractionation of the entrance channel angular momentum along the mass asymmetry coordinate. This distribution is also reflected in the angular distributions of the fragments as a function of mass asymmetry, although in a very complex way. Experimentally the angular distributions are seen to be either forward peaked (Moretto et al. 1975) or side peaked (Hanappe et al. 1974). At times there is a smooth evolution from side peaking to forward peaking in the same reaction (Artukh et al. 1973) as one moves away from the entrance channel mass asymmetry or towards greater energy dissipation. An example of this evolution is given in Figure 10 for the reaction 620 MeV Kr + Au (Moretto et al. 1976). The angular distributions evolve from side peaked near $Z = 36$ to forward peaked as one moves away, either way, from $Z = 36$.

A single approach employing the Fokker-Planck equation nicely illustrates most of the important physics. For heavy systems and for asymmetries between the Businaro-Gallone mountains, the mass asymmetry potential is approximately parabolic for a broad range of angular momenta (Moretto & Schmitt 1976). Thus one can readily make use of the analytical solution of the Fokker-Planck equation in a parabolic potential (Moretto 1978) to calculate the charge distribution $\phi(Z,t)$.

Both the mass asymmetry potential energy and the diffusion rate depend upon the interpenetration of the fragments and their shapes. Furthermore, calculations of the interaction time τ require knowledge of the dynamics. In the absence of detailed information concerning the time evolution of the system, we shall limit ourselves to an extremely simplistic approach which nevertheless closely reflects the experimental data (Moretto 1978).

Let us first assume that the time-dependent curvature of the mass asymmetry potential can be replaced by a time-independent quantity which reflects the average shape of the system. Since we know that the mass asymmetry potential for interpenetrating spheres can qualitatively explain many of the experimental features, we shall make this assumption. The curvature is then easily obtained from a parabolic fit to the ridge line potential as calculated from the liquid drop model. The diffusion rate can be estimated in terms of the nucleonic fluxes.

The radial potential can be written as

$$V(D) = V_{prox} + \frac{Z(Z_T - Z)e^2}{d} + \frac{\hbar^2 \ell^2}{2\mathcal{J}(\ell)} \qquad 30.$$

$\mathcal{J}(\ell)$ being the appropriate moment of inertia.

It is not very clear how much the fragments must interpenetrate before the above equation breaks down. This makes it difficult to formulate the dynamical problem. We shall just use the above potential to calculate the average force $F_R(\ell)$ at the interaction distance d_{int}. From the knowledge of the reduced mass μ, the radial velocity v_R, and the radial force F_R for each ℓ value at the interaction radius, one can introduce the following two ansatz for the interaction time τ and the average interpenetration x of the fragments:

$$\tau(\ell) = \frac{2\mu v_R}{F_R} = \frac{2[2\mu(E - B)]^{1/2}}{F_R}\left(1 - \frac{\ell^2}{\ell_{max}^2}\right)^{1/2} \quad , \quad \bar{x}(\ell) = \frac{\alpha}{2}\frac{\mu v_R^2}{F_R} \quad . \qquad 31.$$

In a more serious attempt to fit the experimental data one could resort to a more detailed dynamical calculation. Obviously, it is a trivial matter to substitute the above ansatz with more reliable expressions. The diffusion along the asymmetry coordinate is then allowed to proceed with a form factor dependent upon $\bar{x}(\ell)$ for a time $\tau(\ell)$.

The tangential motion is treated assuming for the equation of motion the simple form:

$$F_T = \mu\gamma(\omega_0 - \omega_{rig}) \qquad 32.$$

where ω_0 and ω_{rig} are the two limiting orbital angular velocities corresponding to sliding and sticking. The constant γ is chosen to approximately reproduce the mean kinetic energies as a function of angle, assuming that all of the radial energy is lost.

The interaction times calculated for the reaction Au + Kr at three energies are shown in Figure 11a as a function of angular momentum. There is good experimental evidence for the angular momentum dependence predicted by our ansatz. It is interesting to notice the rather mild increase in the average lifetime with increasing bombarding energy. The average deflection function is also shown in Figure 11a. Notice the well-pronounced deep inelastic rainbow (minimum in the deflection function, which yields a maximum in the angular distribution), which moves from positive to negative angles as the bombarding energy increases. The 600 MeV curve predicts a rainbow angle of about 50° in excellent agreement with experiment. The movement of the rainbow angle towards smaller and eventually negative angles results from the combination of three factors: (i) increasing lifetime, (ii) increasing angular momentum, (iii) decreasing average moment of inertia due to the increasing average penetration.

At this point the cross section can be calculated as a function of exit channel asymmetry for each ℓ wave. Summing over ℓ waves yields the angle-integrated charge distribution. In figure (11b) the calculated angle-integrated Z distributions are compared with experiment for the reaction Au + Kr at 620 MeV. The agreement is reasonable over more than two orders of magnitude.

The angular distributions can be calculated from the angular deflections of the fragments during the interaction and from their deflection in the Coulomb field. Angular distributions for the Kr + Au reaction are shown in Figure 11c. The theory nicely tracks the experiment in predicting forward-peaked angular distributions at small Z values which develop into side-peaked angular distributions close to the projectile. For Z values above

the projectile, the angular distributions slowly lose their side peak and become forward-peaked. The satisfactory agreement with both the Z distribution and the angular distribution shows that the calculated dependence of the interaction times and of the diffusion constant upon angular momentum and radial velocity is reasonably good. Even better agreement should be expected with a more realistic treatment of the dynamics.

2.4 Rigid Rotation and Angular Momentum Fractionation Along the Mass Asymmetry Coordinate

It has been shown above that the limit of rigid rotation can be tested by observing the dependence of either the spin of one fragment or of the sum of the moduli of the spins of both fragments upon mass asymmetry. Historically this was the way in which rigid rotation was first demonstrated. Compound nucleus studies (Diamond & Stephens 1980) have shown that, under optimal circumstances, the spin of a nucleus can be inferred from the number of γ rays emitted in any given reaction (γ-ray multiplicity). The reason for this lies in the fact that the majority of the angular momentum is removed by stretched E2 γ-ray transitions, so that each E2 transition accounts for two units of angular momentum. In general one obtains a relation of the form

$$I \cong 2(M_\gamma - \alpha) \qquad 33.$$

where I is the average angular momentum, M_γ is the measured average γ-ray multiplicity and α is the number of "statistical" transitions that can be inferred from the γ-ray spectrum and that are weakly related to spin.

The measurement of the M_γ associated with heavy ion reactions allows one to infer the sum of the moduli of the spins of both fragments. Early measurements of M_γ as a function of energy loss (Figure 12a) depicted an initial strong increase across the quasielastic region followed by saturation in the deep inelastic region (Bock et al. 1977, Olmi et al. 1978, Regimbart et al. 1978). At large energy losses, Olmi et al. (1978) pointed out that the spin transfer exceeded the classical sticking limit (Figure 13), but were well described by a diffusion model which included statistical fluctuations of the dissipated angular momentum (Wolschin & Nörenberg 1978).

Measurement of M_γ as a function of the fragment mass or charge allows one to verify whether the limit of rigid rotation is in fact attained. Some measurements (Glässel et al. 1977 and Natowitz et al. 1978) presented in Figure 14 show that, indeed, M_γ increases rapidly with increasing mass asymmetry, or decreasing atomic number of the detected fragment, thus verifying the rigid rotation limit. However, measurements on heavier systems (Figure 12b) show that M_γ is essentially constant with the atomic number of one of the fragments (Bock et al. 1977, Aleonard et al. 1978, Olmi et al. 1978, Gerschel et al. 1979, Christensen et al. 1980).

The lack of rise of the M_γ with increasing asymmetry may, at first, suggest that the rigid rotation limit is not established and that some intermediate relaxation stage is prevailing. This is not easy to accept in view of the extensive relaxation observed in the kinetic energy spectra away from the entrance-channel mass asymmetry. It is significant that the reactions exhibiting the rise of the M_γ typical of rigid rotation are associated with a narrow angular momentum window, while the other reactions are associated with a very broad angular momentum range. Therefore it is

possible to explain the lack of rise of the M_γ and still retain the rigid rotation limit if, as it is the case, the process is associated with a broad ℓ window. In such cases a rather more stringent condition is required in order to obtain the rise in M_γ signalling rigid rotation, namely that each ℓ wave populates all mass asymmetries uniformly. This condition is not realized even in the equilibrium limit and it should not be expected to occur in the non equilibrium regime which is known to prevail for the mass asymmetry mode.

It is known from a variety of considerations that the interaction time (Agassi et al. 1978, 1979), τ, or the lifetime of the dinuclear system is a decreasing function of the entrance-channel angular momentum as shown, for instance in Figure 11a. The diffusion along the mass asymmetry coordinate can be characterized in terms of a gaussian whose centroid is drifting downhill on the potential energy surface and simultaneously spreading. If we consider the drift negligible, as can be observed in several circumstances, we can describe the mass distribution for a given ℓ wave as given by a gaussian with a variance

$$\sigma_A^2 = \sigma_A^2 (\tau(\ell)) \quad . \qquad 34.$$

For a large ℓ-wave we expect a narrow distribution while for a small ℓ-wave we expect a much broader distribution. Therefore a sample of the angular momentum near the entrance channel asymmetry should show a predominance of the high ℓ-waves, while far from the entrance channel, at greater asymmetries progressively lower ℓ-waves should be sampled.

As a consequence the mean total angular momentum is expected to decrease with increasing asymmetries. This decrease may well be sufficient to compensate for the rise in spin imposed by rigid rotation, as the asymmetry

increases. This is quantitatively borne-out by diffusion calculations (Figure 12b) that include the angular momentum dependence of the interaction time (Regimbart et al. 1978, Wolschin & Nörenberg 1978).

Angular momentum fractionation can occur not only due to the differential spreading of the various ℓ-waves, but can occur, in special cases, due to the change in driving forces with increasing angular momentum. The total energy of the system, including the rotational energy as a function of mass asymmetry is given by

$$E(x,A,\ell) = E(x,A)_{LD} + \frac{\ell^2}{2\mathcal{J}(x)} \quad . \qquad 35.$$

The driving force is

$$-\frac{dE}{dx} = -\frac{dE_{LD}}{dx} + \frac{\ell^2}{2\mathcal{J}(x)^2}\, d\,\frac{\mathcal{J}(x)}{dx} \quad . \qquad 36.$$

If we define $x = \frac{A_2 - A_1}{A_1 + A_2}$ and notice that $\mathcal{J}(x)$ decreases monotonically in going from 0 to 1, we see that that the centrifugal effect contributes a force that tends always to restore the system to symmetry.

The combination of the liquid drop and centrifugal terms is illustrated in Figure 15a where the potential energy is given as a function of mass asymmetry for a number of ℓ-waves (Moretto 1982). The system chosen in the figure is Ar + Tb and all the curves are normalized at the entrance channel asymmetry. It is evident that it would be quite difficult for the high ℓ-waves to populate the greater asymmetries to the left of the entrance channel asymmetry, while it would become progressively easier for the lower ℓ-waves. The experiment, shown in Fig. 15b, illustrates this effectively. The gamma ray multiplicity, which seems to rise going from right to left, as expected for rigid rotation (except for the sharp wedge at the entrance

channel asymmetry due to incomplete angular momentum relaxation) actually takes a steep plunge to the left of the entrance-channel mass asymmetry, indicating that only low ℓ-waves are feeding that region. The same figure portrays a calculation (solid dots) that incorporates the physics discussed above and that fits the experimental data satisfactorily (Moretto 1982).

3 THE EXCITATION OF ANGULAR MOMENTUM BEARING MODES AND THE PARTITION OF ANGULAR MOMENTUM BETWEEN ORBITAL AND INTRINSIC

3.1 The Rotational Degrees of Freedom of the Dinuclear Complex

Many of the degrees of freedom of the dinuclear system can carry angular momentum. If we simulate the dinuclear system with two equal touching spheres (Moretto & Schmitt 1980), these degrees of freedom can be easily identified (Figure 16). Let us fix a reference frame with the x-axis coincident with the line of centers and the y and z axes perpendicular to it. The two "bending" modes correspond to a rotation of one fragment parallel to the y or z axis associated with an opposite rotation of the other fragment. The "twisting" modes correspond to a rotation of one fragment about the x-axis associated with an opposite rotation of the other fragment. The two "wriggling" modes are rotations of both fragments parallel to the y or z axis compensated by a counter-rotation of the system as a whole about the same axis. Finally the "tilting" mode describes the inclination angle of the total angular momentum with respect to the x-axis.

The excitation of these modes may occur through a variety of mechanisms. For instance one of the two wriggling modes can be excited by a coupling with the relative motion mediated by tangential friction. Similarly multipole-multipole Coulomb and nuclear interactions, as well as particle exchange, can be responsible for this excitation. In general, since these collective modes are not exactly normal but are weakly coupled to the intrinsic modes, they can be "thermally" excited.

As an example, let us consider the relaxation of one wriggling mode that leads to the equilibration of the intrinsic rotation and the orbital rotation. If the total angular momentum is I and the spin fragment is s, the

energy for an arbitrary partition between orbital and intrinsic angular momentum is

$$E(s) = \frac{(I - 2s)^2}{2\mu r^2} + \frac{2s^2}{2\mathcal{J}} = \left(\frac{2}{\mu r^2} + \frac{1}{\mathcal{J}}\right) s^2 - \frac{2I}{\mu r^2} s + \frac{I^2}{2\mu r^2} \quad . \qquad 37.$$

The first term is the orbital and the second the intrinsic rotational energy, $\mathcal{J}$ being the moment of inertia of one of the two equal spheres.

The partition function is given by

$$Z \propto \int \exp\,[-E(s)/T]ds = \sqrt{\frac{\pi\mu r^2 \mathcal{J} T}{2\mathcal{J} + \mu r^2}} \exp\left[-\frac{I^2}{2T(2\mathcal{J} + \mu r^2)}\right] . \qquad 38.$$

The average spin for both fragments is given by

$$2\overline{s} = \frac{2\int s \exp\,[-E(s)/T]ds}{Z} = \frac{2\mathcal{J}}{\mu r^2 + 2\mathcal{J}} I = \frac{2}{7} I = 2I_R \quad , \qquad 39.$$

where $I_R = I/7$ is the spin per fragment expected from rigid rotation. The second moment $\overline{s^2}$ is given by

$$4\overline{s^2} = \frac{2\mu r^2 \mathcal{J} T}{\mu r^2 + 2\mathcal{J}} + \frac{4I^2\mathcal{J}^2}{(\mu r^2 + 2\mathcal{J})^2} \quad . \qquad 40.$$

From this we obtain the standard deviation

$$4\sigma_s^2 = \frac{2\mathcal{J}\,\mu r^2 T}{\mu r^2 + 2\mathcal{J}} = \frac{10}{7}\mathcal{J}T \quad . \qquad 41.$$

The result in Equation 39 is temperature independent, as one should have expected from the fact that Equation 37 is quadratic in s. It could in fact be obtained by solving the equation $dE/ds = 0$. This result corresponds to the mechanical limit of rigid rotation when the orbital and the intrinsic angular velocities are matched.

The result in Equation 41 could have been obtained also by appreciating that the thermal fluctuations about the average in Equation 39 are controlled by the second derivative of Equation 37 at the minimum, or $\sigma_s^2 = T/b$, where

$$b = \left[\frac{\partial^2 E}{\partial s^2}\right]_{\bar{s}} .$$

It is important to appreciate the meaning of Equation 41. The quantity $4\sigma^2$ represents the amount of angular-momentum trade-off allowed by the temperature, between orbital and intrinsic rotation.

In some instances, such as in γ-ray multiplicity measurements, one is interested in the average sum of the moduli of the fragment spins. This can be obtained from

$$2|\bar{s}| = \int 2|s| \exp[-E(s)/T]ds/Z , \qquad 42.$$

which yields

$$2|\bar{s}| = 2\left\{\left(\frac{\mu r^2 \mathcal{J} T}{\pi(\mu r^2 + 2\mathcal{J})}\right)^{1/2} \exp\left(-\frac{\mathcal{J} I^2}{\mu r^2 T(\mu r^2 + 2\mathcal{J})}\right) + \right.$$

$$\left. + I \frac{\mathcal{J}}{\mu r^2 + 2\mathcal{J}} \operatorname{erf}\left[I\left(\frac{\mathcal{J}}{\mu r^2 T(\mu r^2 + 2\mathcal{J})}\right)^{1/2}\right]\right\} , \qquad 43.$$

or, in dimensionless form,

$$\frac{2|\bar{s}|}{\sqrt{\mathcal{J}^* T}} = 2\left[\frac{1}{\sqrt{\pi}} \exp[-x^2] + x \operatorname{erf}(x)\right] , \qquad 44.$$

where $x = I_R(\mathcal{J}^* T)^{-1/2}$ and $\mathcal{J}^* = \mu r^2 \mathcal{J}/(\mu r^2 + 2\mathcal{J})$. The above expression is plotted in Figure 17. In the limit of large I, one recovers Equation 39:

$$2|\bar{s}| = \frac{2\mathcal{J} I}{\mu r^2 + 2\mathcal{J}} = \frac{2}{7} I . \qquad 45.$$

For small I,

$$\frac{2|\bar{s}|}{\sqrt{\mathcal{J}^* T}} \cong \frac{2}{\sqrt{\pi}} (1 + x^2) \qquad 46.$$

to order x^2, so for I = 0 one obtains

$$2|\bar{s}| = 2\sqrt{\frac{\mathcal{J} T}{\pi}} \left(\frac{\mu r^2}{\mu r^2 + 2\mathcal{J}}\right)^{1/2} = 2\sqrt{\frac{5\mathcal{J} T}{7\pi}} . \qquad 47.$$

The second moment, still given by Equation 40, can be rewritten as $4\overline{s^2} = 2\mathcal{J}^* T + 4I_R^2$. Notice that the fragment angular momentum at zero total angular momentum arises from the excitation of a collective mode (wriggling) in which the two fragments spin in the same direction, while the system as a whole rotates in the opposite direction in order to maintain I = 0.

The overall statistical treatment of the angular momentum bearing modes allows us to describe the angular momentum of one of two fragments in terms of a tridimensional Gaussian distribution in the angular momentum components I_x, I_y, I_z:

$$P(\underset{\sim}{I}) \propto \exp - \left(\frac{I_x^2}{2\sigma_x^2} + \frac{I_y^2}{2\sigma_y^2} + \frac{(I_z - \bar{I}_z)^2}{2\sigma_z^2} \right) \qquad 48.$$

where I_z is the rigid rotation component:

$$I_{z_i} = \frac{\mathcal{J}_i}{\mu d^2 + 2\mathcal{J}_i} I = \frac{1}{7} I \quad \text{for two equal touching spheres;} \qquad 49.$$

$$\sigma_x^2 = \sigma_{Tw}^2 + \sigma_{Ti}^2 = \frac{1}{2}\mathcal{J}T + \frac{7}{10}\mathcal{J}T = \frac{6}{5}\mathcal{J}T$$

$$\sigma_y^2 = \sigma_B^2 + \sigma_w^2 = \frac{1}{2}\mathcal{J}T + \frac{5}{14}\mathcal{J}T = \frac{6}{7}\mathcal{J}T$$

$$\sigma_z^2 = \sigma_B^2 + \sigma_w^2 = \frac{1}{2}\mathcal{J}T + \frac{5}{14}\mathcal{J}T = \frac{6}{7}\mathcal{J}T \quad . \qquad 50.$$

In the case of an asymmetric system one obtains qualitatively similar results (Schmitt & Pacheco 1982). The dependence of the three variances as a function of mass asymmetry is given in Figure 18. The presence of angular momentum fluctuations increases the average fragment spin over the value expected from simple transfer. An example of the role of fluctuations (Wolschin & Nörenberg 1978) is shown in Figure 19.

3.2 Angular Momentum Misalignment

The presence of fluctuating in-plane components in the fragment angular momentum leads to a misalignment of the fragment's spin which fluctuates with a given amplitude about the normal to the reaction plane. The angular momentum alignment can be expressed quantitatively in terms of the polarization P and the alignment P_{zz} which are given by

$$P = \langle \frac{m}{I} \rangle = \langle \sum_m P(m)\, m/I \rangle_I = \langle \cos\theta \rangle \qquad 51.$$

and

$$P_{zz} = \langle \frac{3}{I(2I-1)} \left[\sum_m P(m) m^2 - I(I+1) \right] \rangle_I \cong \frac{3}{2} \langle \frac{m^2}{I^2} \rangle - \frac{1}{2} \qquad 52.$$

where P(m) is the probability distribution of a given projection. In terms of the σ's we can obtain

$$P_{zz} \cong \frac{1}{1 + (\sigma_x^2 + \sigma_y^2 + \sigma_z^2)/\bar{I}_z^2} \quad . \qquad 53.$$

Such misalignment is expected to affect the angular distributions of the particles and γ rays emitted by the fragments. It is rather straightforward to incorporate the angular momentum fluctuations into general expressions for the angular distributions. We deal first with the angular distribution of sequential α-particles and fission fragments and later with the gamma ray angular distributions.

3.3 Angular Distributions of Sequential Fission and of Sequential Light Particle Emission

We have shown elsewhere (Moretto 1975) that the angular distribution of fission fragments and of light particles emitted by a compound nucleus can be treated within a single framework. The direction of emission of a decay product (fission fragment, α-particle, etc.) is defined by the projection K of the fragment angular momentum on the disintegration axis. Simple statistical mechanical considerations show that the distribution in K values is Gaussian.

Specifically for any given K the particle width can be written as (Moretto 1981):

$$\Gamma_K^I \, dK = \Gamma^o \exp\left[-\frac{\hbar^2 I^2}{2T}\left(\frac{1}{\mathcal{J}_\perp} - \frac{1}{\mathcal{J}_c}\right)\right] \exp\left(-\frac{K^2}{2K_o^2}\right)\frac{dK}{I} \qquad 54.$$

where Γ^o is an angular momentum independent quantity; T is the temperature; $K_o^2 = \hbar^{-2}(1/\mathcal{J}_{\parallel} - 1/\mathcal{J}_\perp)^{-1}T$; $\mathcal{J}_{\parallel}$, $\mathcal{J}_\perp$ are the principal moments of inertia of the decaying system, with particle and residual nucleus just in contact, about an axis parallel and perpendicular to the disintegration axis, respectively; $\mathcal{J}_c$ is the moment of inertia of the compound nucleus.

Similarly, the neutron decay width, integrated over all the neutron emission directions is

$$\Gamma_N \cong \Gamma_N^o \exp\left[-\frac{\hbar^2 I^2}{2T}\left(\frac{1}{\mathcal{J}_N} - \frac{1}{\mathcal{J}_c}\right)\right] \quad . \qquad 55.$$

In this expression $\mathcal{J}_N = \mathcal{J}_R + \mu R^2$, corresponding to $\mathcal{J}_\perp$ in Equation 54, is the sum of the moment of inertia of the residual nucleus after neutron decay and the orbital moment of inertia of the neutron at the surface of the nucleus.

Let us now express the particle decay width in terms of the emission angle α measured with respect to the angular momentum direction. Since $K = I\cos\alpha$ and $dK = I\, d(\cos\alpha) = I\, d\Omega$, we obtain:

$$\Gamma^I(\alpha)d\Omega = \Gamma^0 \exp\left[-\frac{\hbar^2 I^2}{2T}\left(\frac{1}{\mathcal{J}_\perp} - \frac{1}{\mathcal{J}_c}\right)\right]\exp\left(-\frac{I^2\cos^2\alpha}{2K_0^2}\right)d\Omega \quad . \qquad 56.$$

If the angular momentum has an arbitrary orientation with respect to our chosen frame of reference, defined by its components I_x, I_y, I_z, the angular distribution can be easily rewritten by noticing that

$$K = I\cos\alpha = \underset{\sim}{I} \cdot \underset{\sim}{n} = I_x \sin\theta\cos\phi + I_y \sin\theta\sin\phi + I_z\cos\theta \quad , \qquad 57.$$

where $\underset{\sim}{n}$ is a unit vector pointing along the direction of particle emission with polar angles θ, ϕ. If the orientation of the angular momentum is controlled by the distribution in Equation 48, we can integrate over the distribution of orientations and obtain, dropping angular momentum independent factors (Broglia et al. 1979, Moretto et al. 1981):

$$\Gamma^I(\theta,\phi)d\Omega \propto \exp\left[-\frac{\hbar^2 I^2}{2T}\left(\frac{1}{\mathcal{J}_\perp} - \frac{1}{\mathcal{J}_c}\right)\right]\frac{1}{S(\theta,\phi)}\exp\left(-\frac{I^2\cos^2\theta}{2S^2(\theta,\phi)}\right)d\Omega \qquad 58.$$

where:

$$S^2(\theta,\phi) = K_0^2 + (\sigma_x^2\cos^2\phi + \sigma_y^2\sin^2\phi)\sin^2\theta + \sigma_z^2\cos^2\theta \quad . \qquad 59.$$

In Equation 58 we have set $I_z = I$, in other words we have averaged over the

orientation but we have allowed the decay width to depend only upon the average angular momentum set equal to its z component. This expression should then be considered only as a high angular momentum limit ($\sigma/I \ll 1$).

The final angular distribution is obtained by integration over the fragment angular momentum distribution which is assumed to reflect the entrance-channel angular momentum distribution through the rigid rotation condition:

$$\frac{d\sigma}{d\Omega} \propto \int_{I_{min}}^{I_{max}} 2I dI \frac{\Gamma^I}{\Gamma_N} \qquad 60.$$

where we have assumed $\Gamma_T \cong \Gamma_N$. More precisely:

$$W(\theta,\phi) \propto \int_{I_{min}}^{I_{max}} \frac{2I}{S} \exp\left[-I^2\left(\frac{\cos^2\theta}{2S^2} - \beta\right)\right] dI \qquad 61.$$

or

$$W(\theta,\phi) = \frac{1}{S}\left[\frac{I_{min}^2}{A_{min}} \exp(-A_{min}) - \frac{I_{max}^2}{A_{max}} \exp(-A_{max})\right] . \qquad 62.$$

If $I_{min} = 0$, then

$$W(\theta,\phi) = \frac{1}{SA}\left[1 - \exp(-A)\right] , \qquad 63.$$

where

$$A = A_{max} = I^2_{max}\left(\frac{\cos^2\theta}{2S^2} - \beta\right) \; ; \quad A_{min} = I^2_{min}\left(\frac{\cos^2\theta}{2S^2} - \beta\right) \; ;$$

$$\beta = \frac{\hbar^2}{2T}\left(\frac{1}{\mathcal{J}_n} - \frac{1}{\mathcal{J}_\perp}\right) . \qquad 64.$$

The quantity $\mathcal{J}_n$ is the moment of inertia of the nucleus after neutron emission, $\mathcal{J}_\perp$ is the perpendicular moment of inertia of the critical shape for the decay (e.g., saddle point). It is important to notice that the angular momentum dependence of the particle/neutron competition or fission/neutron competition is explicitly taken into account through β.

The final ingredient necessary for an explicit calculation of the angular distributions is the quantity K_o^2. This quantity can be expressed in terms of the principal moments of inertia of the critical configuration for the decay:

$$K_o^2 = \frac{1}{\hbar^2}\left(\frac{1}{\mathcal{J}_\parallel} - \frac{1}{\mathcal{J}_\perp}\right)^{-1} T = \mathcal{J}_{eff} T \; . \qquad 65.$$

For fission $\mathcal{J}_{eff}$ can be taken from liquid drop calculations (Cohen et al. 1974). For light particle emission, the calculation of $\mathcal{J}_{eff}$ can be worked out trivially. Let m, M, A be the masses of the light, residual and total nucleus. One obtains:

$$\mathcal{J}_\parallel = \frac{2}{5} MR^2 + \frac{2}{5} mr^2$$

$$\mathcal{J}_\perp = \frac{2}{5} MR^2 + \frac{mM}{A}(R + r)^2$$

$$\frac{\mathcal{J}_{eff}}{\mathcal{J}_{sph}} = \left(\frac{M}{A}\right)^{5/3}\left[1 + \frac{2}{5}\frac{A}{m}\left(\frac{R}{R + r}\right)^2\right] , \qquad 66.$$

where r and R are the radii of the light particle and residual nucleus, respectively.

This result is adequate if m << M and if the charge of the light particle is small. If the charge of the light particle is not negligible, one has to consider the shape polarization induced on the heavy fragment at the "ridge point," as discussed in Moretto (1975). Since the shape polarization affects the asymptotic kinetic energy of the emitted particle as well, one can in principle utilize the particle kinetic energy spectra to verify that the shape of the system at the ridge point and its principal moments of inertia have been properly chosen. Again a more complete discussion on this point is available in Moretto (1975).

Now we are in the position to calculate both in-plane and out-of-plane anisotropies (Moretto et al. 1981). The in-plane anisotropy is given by:

$$\left.\frac{W(\phi = 90^\circ)}{W(\phi = 0^\circ)}\right|_{\theta=90^\circ} = \left(\frac{K_0^2 + \sigma_x^2}{K_0^2 + \sigma_y^2}\right)^{1/2} . \qquad 67.$$

Since in most cases K_0^2 is fairly large, or at least comparable with σ_x^2 or σ_y^2, it is difficult to obtain a sizable in-plane anisotropy. Even by letting $\sigma_x = 0$ one needs $\sigma_y^2 = 3\,K_0^2$ just to obtain an anisotropy of 2! The out-of-plane anisotropy is somewhat more complicated. For a fixed angular momentum I one has:

$$\left.\frac{W(\theta = 90^\circ)}{W(\theta = 0^\circ)}\right|_{\phi=0^\circ} = \left(\frac{K_0^2 + \sigma_z^2}{K_0^2 + \sigma_x^2}\right)^{1/2} \exp\left(\frac{I^2}{2(K_0^2 + \sigma_z^2)}\right) . \qquad 68.$$

For the usual angular momentum distribution one obtains:

$$\left.\frac{W(\theta = 90^\circ)}{W(\theta = 0^\circ)}\right|_{\phi=0^\circ} = \frac{1}{\beta}\left(\frac{K_0^2 + \sigma_z^2}{K_0^2 + \sigma_x^2}\right)^{1/2}\left(\beta - \frac{1}{2(K_0^2 + \sigma_z^2)}\right)$$

$$\times \quad \frac{1 - \exp \beta I_{max}^2}{1 - \exp I_{max}^2\left(\beta - \frac{1}{2(K_0^2 + \sigma_z^2)}\right)} \quad . \qquad 69.$$

At $\phi = 90^\circ$ the anisotropy is obtained from the above equation by interchanging σ_x with σ_y.

3.4 Gamma Ray Angular Distributions

Fragments with large amounts of angular momentum are expected to dispose of it mainly by stretched E2 decay (Diamond & Stephens 1980). The relative amounts of dipole and quadrupole radiation depends mainly upon the ability of the nucleus to remain a good rotor over the whole angular momentum range. If the angular momentum of the fragment is aligned, the typical angular pattern of the quadrupole radiation should be observed. Any misalignment should decrease the sharpness of the angular distribution. If the distribution of the angular momentum components I_x, I_y I_z is statistical, it is straightforward to derive analytical expression for the angular distributions (Moretto et al. 1981).

For a perfectly aligned system:

$$W(\alpha) = \frac{3}{4}(1 + \cos^2\alpha); \quad \text{for E1} \qquad W(\alpha) = \frac{5}{4}(1 - \cos^4\alpha). \quad \text{for E2} \qquad 70.$$

If the angular momentum is not aligned with the z axis, one must express α in terms of θ, ϕ which define the direction of the angular momentum vector. In particular:

$$\cos\alpha = \frac{\underset{\sim}{I} \cdot \underset{\sim}{n}}{I} = \frac{I_x \sin\theta \cos\phi + I_y \sin\theta \sin\phi + I_z \cos\theta}{\left[I_x^2 + I_y^2 + I_z^2\right]^{1/2}} \quad . \qquad 71.$$

For any given I, the angular distribution is obtained by integration over the statistical distribution $P(\underset{\sim}{I})$ of the angular momentum components:

$$W(\theta,\phi) = \int W(\alpha) P(\underset{\sim}{I}) d\underset{\sim}{I} \quad . \qquad 72.$$

It is not possible to obtain exact analytical expression for the general case. However, an expansion to order $\sigma_x^2/\overline{I}_z^2$, $\sigma_y^2/\overline{I}_z^2$, etc. allows one to obtain expressions in closed form.

For the dipole decay:

$$W(\theta,\phi) = \frac{3}{4}(1 + \cos^2\theta) + \frac{3}{4}\left[(\sin^2\theta\cos^2\phi - \cos^2\theta)\frac{\sigma_x^2}{\overline{I}_z^2} + (\sin^2\theta\sin^2\phi - \cos^2\theta)\frac{\sigma_y^2}{\overline{I}_z^2}\right] \quad . \qquad 73.$$

Notice that there is no dependence upon σ_z^2. In the case in which $\sigma_x = \sigma_y = \sigma$, we obtain the simplified expression:

$$W(\theta,\phi) = \frac{3}{4}(1 + \cos^2\theta) + \frac{3}{4}(\sin^2\theta - 2\cos^2\theta)\frac{\sigma^2}{\overline{I}_z^2} \quad . \qquad 74.$$

A weak in-plane anisotropy is possible:

$$\left.\frac{W(\phi = 0^\circ)}{W(\phi = 90^\circ)}\right|_{\theta=90^\circ} = \frac{1 + \sigma_x^2/\bar{I}_z^2}{1 + \sigma_y^2/\bar{I}_z^2} \cong 1 + \frac{\sigma_x^2 - \sigma_y^2}{\bar{I}_z^2} \quad . \qquad 75.$$

The out-of-plane anisotropy is:

$$\frac{W(0^\circ)}{W(90^\circ)} = 2\,\frac{(1 - \sigma^2/\bar{I}_z^2)}{(I + \sigma^2/\bar{I}_z^2)} \cong 2(1 - 2\sigma^2/\bar{I}_z^2) \quad . \qquad 76.$$

For the quadrupole decay we have:

$$W(\theta,\phi) = \frac{5}{4}\,(1 - \cos^4\theta) - \frac{5}{2}\left[(3\,\sin^2\theta\cos^2\theta\cos^2\phi - \cos^4\theta)\,\frac{\sigma_x^2}{\bar{I}_z^2} + (3\,\sin^2\theta\cos^2\theta\sin^2\phi - \cos^4\theta)\,\frac{\sigma_y^2}{\bar{I}_z^2}\right] \quad . \qquad 77.$$

Again, no dependence upon σ_z^2 is predicted. If one assumes $\sigma_x = \sigma_y = \sigma$ as before, one obtains:

$$W(\theta) = \frac{5}{4}(1 - \cos^4\theta) - \frac{5}{2}\,(3\,\sin^2\theta\cos^2\theta - 2\,\cos^4\theta)\sigma^2/\bar{I}_z^2 \qquad 78.$$

and

$$\frac{W(0^\circ)}{W(90^\circ)} \cong 4\,\frac{\sigma^2}{\bar{I}_z^2} \quad . \qquad 79.$$

For the in-plane anisotropy we have:

$$\left.\frac{W(\phi = 0^\circ)}{W(\phi = 90^\circ)}\right|_{\theta=90^\circ} \sim 1 \qquad 80.$$

to order $\sigma^2/\bar{I}_z^2$. This can be easily understood. The rms misalignment is $\sim\sigma/I$, thus, at $\theta = 90°$:

$$W(90) = 1 - \cos^4\left(90° - \frac{\sigma}{I}\right) \cong 1 - \frac{\sigma^4}{I^4} \quad . \qquad 81.$$

Thus, no second order term exists. This result shows that it is very difficult to study anisotropies in the angular momentum misalignment by means of γ-ray angular distribution. The range of validity of the above expressions is rather limited due to the low order expansion. In particular, the equations should not be trusted for $\sigma^2/\bar{I}_z^2 > 0.05$.

However, if we are willing to assume $\sigma_x^2 = \sigma_y^2 = \sigma_z^2 = \sigma$ then an exact result can be obtained. For the E1 distribution one obtains:

$$W(\theta)_{E1} = \frac{3}{4}\ [1 + \cos^2\theta + \beta^2(1 - D(\beta))(1 - 3\cos^2\theta)] \quad . \qquad 82.$$

For the E2 distribution one obtains:

$$\begin{aligned} W(\theta)_{E2} = \frac{5}{4}\Bigg[1 - \cos^4\theta - 2\beta^2\Bigg\{ & 3\sin^2\theta\cos^2\theta - 2\cos^4\theta \\ & - \frac{3}{4}\ D(\beta)(\sin^2\theta - 4\cos^2\theta)\sin^2\theta\Bigg\} \\ & -3\beta^4\left\{4\cos^4\theta + \frac{3}{2}\ \sin^4\theta - 12\sin^2\theta\cos^2\theta\right\}(1 - D(\beta))\Bigg] \ . \end{aligned}$$

83.

In these equations $\beta = \sigma/\bar{I}_z$ and $D(\beta) = \sqrt{2}\,\beta\ F(\sqrt{1/2}\ \beta)$ where

$$F(x) = e^{-x^2}\int_0^x e^{t^2}dt \qquad 84.$$

is the Dawson's integral. One can verify immediately that both expressions behave as expected in the limits of $\beta = 0$ and $\beta = \infty$. The anisotropy $W(0)/W(90^\circ)$ tends to 1 when β tends to infinity both for E1 and E2 transitions, while it tends to 0 for E2 and to 2 for E1 when $\beta = 0$.

These results are graphically summarized in Figure 20 where the anisotropy is plotted as a function of the fraction of E1 radiation for various values of $\sigma^2/\bar{I}_z^2$. The two extreme possibilities of stretched and non-stretched E1 decay are considered. If one has a fairly good experimental idea of the amount of E1 radiation to be expected from a given fragment and of its degree of stretching, the measurement of the anisotropy yields directly the value of $\sigma^2/\bar{I}_z^2$, which is of course the most direct information about the misalignment.

3.5 Experimental Spin Alignment From Gamma-Ray Angular Distributions

Discrete γ-rays in coincidence with deep-inelastic fragments were observed to have large anisotropies, indicating a high degree of spin alignment with the normal to the reaction plane (Van Bibber et al. 1977, Puchta et al. 1979, Puigh et al. 1980, Mouchaty et al. 1984). Because the deep-inelastic reaction strength is typically spread over a large number of final products, only low lying γ-ray transitions have been observed at small Q-values with modest statistics. These limitations and problems related to doppler broadening and side feeding have given impetus to continuum γ-ray studies.

Early attempts to observe continuum γ-ray anisotropies due to fragment spin alignment led to surprisingly small values of the alignment parameter P_{zz} (Berlanger et al. 1976, Bock et al. 1977, Natowitz et al. 1978, Lauterbach et al. 1978, Dayras et al. 1979 & 1980, Puchta et al. 1979, Aguer et al. 1979, Namboodiri et al. 1979, Puigh et al. 1980). The failure to observe substantial anisotropies was due to several causes. First, to the presence of sizeable amount of "statistical" isotropic E1 transitions; second to the possible presence of stretched M1 transitions under the E2 bump whose angular distribtion is exactly out-of-phase with the stretched E2 transitions; third to the integration over the deep inelastic part of the Q-value spectrum where the fluctuations are dominant and tend to decrease the alignment substantially. Once the above causes were understood, it was easy to choose suitable conditions under which strong anisotropies could be observed. In particular, it is important to maximize the number of stretched E2 transitions by selecting reaction products that are mostly good rotors, namely located in the region of the heavy rare earth nuclei.

An extensive study of the continuum γ-ray anisotropy in heavy ion reactions has been carried out for the reaction Ho + Ho at 8.5 MeV/A first (Wozniak et al. 1980, McDonald et al. 1982) and extended (Pacheco et al. 1983) to Ho + Yb, Sm, Ag always at the same energy. The Q-value spectrum was divided into a series of energy bins for which the γ-ray multiplicity, energy spectra and anisotropy were measured.

The sum of the spins obtained from the γ-ray multiplicity as a function of Q-value is shown in Figure 21. As in other reactions (Bock et al. 1977, Olmi et al. 1978, Regimbart et al. 1978, Puigh et al. 1980, Christensen et al. 1980), an increase in energy loss leads to an initially rapid transfer of

angular momentum to the fragments, followed by a relatively slow decrease as one moves towards the greatest inelasticies. These data (Figure 21), already corrected for the angular momentum removed by neutrons, show that the fragments can pick up as much as 35-40$\hbar$ of angular momentum each. Furthermore there is some evidence that, at least for large negative Q-values, rigid rotation is obtained. The scaling of the Q-value in terms of the common fragment temperature and of the spin in terms of the maximum spin expected for rigid rotation collapses all the data on a single curve (Figure 22). This scaling suggests that rigid rotation is indeed reached.

The anisotropy of the γ-rays (in the region of the γ-ray spectrum dominated by quadrupole radiation) as a function of Q-value is shown in Figure 23. In all cases, but more visibly for Ho + Yb, the anisotropy rises initially with increasing energy dissipation to values as high as two, and then declines slowly with further energy dissipation.

Qualitatively, the rise and fall of the γ-ray anisotropy with increasing energy dissipation is easily understood if studied simultaneously with the spin transfer. For small energy dissipations there is a small amount of angular momentum transferred to the fragments which in turn can be easily depolarized by in-plane components arising from detailed spectroscopic effects. As the energy dissipation increases, angular momentum is rapidly transferred to the fragments. This transferred angular momentum is aligned and is little perturbed by the in-plane thermal fluctuating components which increase very slowly with excitation energy ($\sigma^2 \propto T \propto Q^{1/2}$). The resulting strong alignment is manifested in the substantial rise of the γ-ray anisotropy.

A further increase in the energy dissipation does not increase the transferred angular momentum but it increases the excitation energy and thus the thermal fluctuations of the in-plane components. As a consequence the total angular momentum becomes progressively more misaligned and the γ-ray anisotropy decreases.

Of course there are additional sources of angular momentum misalignment, like particle evaporation from the primary fragments, but it appears that the main cause of angular momentum misalignment is the "thermal" excitation of the angular momentum bearing modes. This is shown by Figure 24 where all the sources of angular momentum misalignment have been included with the exception of the thermal fluctuations. The calculated anisotropies clearly over estimate the corresponding experimental values. On the other hand, the inclusion of thermal fluctuations provides us with a much improved picture, almost coincident with the experimental data, as seen in Figure 25. It should be pointed out that the calculation uses the experimental M_γ as an input for the fragment angular momentum and uses the theory only to calculate the σ's. In this way we can extend the use of the theory even in Q-value regions where the full equilibrium limit has not beeen attained, since it is well known that fluctuations tend to their equilibrium limit a great deal faster than the average values.

From the above analysis one can calculate the alignment for each individual fragment, although this decomposition is far less certain than the calculation of the anisotropy. In Figure 25 the alignment P_{zz} is shown for each of the two fragments. In general alignments as great as 0.7 are observed with the greatest alignment being associated with the heavier partner.

3.6 Experimental Data From Sequential Decay

3.6.1 Sequential Alpha Emission

Inspection of Equations 65, 67, 68 shows that if the σ's are comparable or smaller than K_0^2, it is difficult to differentiate between uncertainties in K_0^2 which are intrinsic to the sequential emission process and the angular momentum fluctuations arising from the deep inelastic process. In the case of alpha emission K_0^2 is indeed quite large in comparison with the σ's. As a consequence, the only quantity that one can hope to extract from angular distribution data is the spin of the emitting fragment (Babinet et al. 1980, Kühn et al. 1980, Sobotka et al. 1981a & b). In studies of the reaction Ar + Ni, Babinet et al. (1980) showed that the alphas from the Ni-like fragment could be isolated, that their angular distributions were peaked in-plane and that the resulting spins agreed with the rigid rotation assumption (Figure 26). No account was taken of the angular momentum fluctuations. In a subsequent experiment, Kr + Ag, the out-of-plane angular distribution of the alpha particles was measured for a broad range of Ag-like fragments (Sobotka et al. 1981a & b). The angular distributions are shown in Figure 27a. It is apparent that the anisotropy of the alpha particles increases with increasing asymmetry, indicating an increase of the Ag-like fragment spin with increasing atomic number. The fit to the angular distributions is shown in the same figure and the resulting spins are also shown in Figure 27c. The spin fluctuations were calculated on the basis of the thermal model described above. The measured spins are in excellent agreement with rigid rotation if one assumes that both fragments are prolate spheroids touching by their tips with a ratio of major to minor axes of $c/a = 2$. In this way it is also possible to reproduce the exit channel kinetic energy distribution as shown in Figure 27b.

From the scission configuration we can reconstruct the sum of the two spins. This quantity can also be inferred from M_γ, which was measured simultaneously in the experiment. A comparison between the sum of the spins measured in both ways is shown in Figure 27c. The agreement implies that not only the trends but also the absolute values of the spins measured with either technique can be relied upon. Similar agreement has also been observed in studies of heavier systems (Sobotka et al. 1983).

3.6.2 Sequential Fission

In the case of fission the quantity K_0^2 is comparable or smaller than the three σ's so that sequential fission can provide information not only about the spin of one of the fragments, as in the case of the alpha emission, but about the degree of alignment as well (Dyer et al. 1977, Wozniak et al. 1978). The first experiment (Dyer et al. 1977), performed for the reaction 610 MeV ^{86}Kr + Bi, showed that the sticking limit had been achieved. The out-of-plane anisotropy is quite strong as expected due to the exponential in Equations 61 & 68. Many other systems (Dyer et al. 1979, Puigh et al. 1979, Harrach et al. 1979, Le Brun et al. 1982, Morrissey et al. 1982a & b) have been studied. Alignments comparable to those extracted from the γ-ray work have been obtained (see Figure 28).

The angular distributions of γ rays and α particles are rather insensitive to differences in the in-plane projections of the random spin component. In contrast, the angular distributions of sequential fission fragments are more sensitive to such differences in that they can produce a substantial in-plane anisotropy. A complete measurement of the in-plane and out-of-plane distributions is necessary for this purpose. The anisotropies observed in-plane (Dyer et al. 1977 & 79, Puigh et al. 1979, Le Brun et al.

1982, Morrissey et al. 1982a & b) are much weaker than out-of-plane ones as suggested by Equation 67. However the measurement of in-plane anisotropies is quite worthwhile since it provides a sensitive test for the statistical model. In particular, as the mass asymmetry increases, the tilting mode becomes progressively softer, thus increasing σ_x^2 with respect to σ_y^2. The dependence of the three variances with mass asymmetry is shown in Figure 18. Thus the statistical model makes the following prediction for the in-plane angular distribution, namely the anisotropy is expected to be small for symmetric exit channels and to become more pronounced for asymmetric ones. Some data are shown in Figure 29. For very negative Q-values in the very asymmetric $^{20}Ne + ^{238}U$ reaction, the prediction seems to hold; for more symmetric systems smaller in-plane anisotropies have been observed (Dyer et al. 1979, Puigh et al. 1979, Zisman et al. 1982, Le Brun et al. 1982). More measurements are needed at intermediate mass asymmetries to determine whether the statistical model is successful even in this rather fine point.

4 MORE AMBITIOUS MODELS

4.1 Time-Dependent Hartree-Fock Model

The success of the self-consistent Hartree Fock approach in describing low-lying nuclear stationary states prompted the attempt to adapt this kind of calculation to the time evolution of complex nuclear systems. The resulting theory called Time Dependent Hartree Fock (Davies et al. 1978, Davies & Koonin 1981, Negele 1982) relies on the fact (or hope) that the complicated two body reactions can be substituted by a time-dependent mean field on which the nucleons move as free particles. This approach, while it can be considered as fundamental as any in nuclear physics, unfortunately produces rather limited predictions. One of its most serious limitations is its inability to produce dispersions in the relevant variables of a magnitude comparable to experiment, thus falling short of a qualitatively satisfying description, as shown in Figure 9. On the other hand, it appears that the mean energy dissipation and the mean angular momentum transfer are reproduced more or less adequately (Figure 30). The generalization of this model to include two-body interactions with the expected extensive thermalizations is not technically obvious. Still the trained eye of the experimentalist can discern in the data the extended degree of thermalization that the present calculations have not had the ability to portray as yet.

4.2 Coherent Surface Excitation Model

A program was undertaken by the Copenhagen group to verify the extent to which collective modes, excited through the mutual interaction of the two nuclei, could be responsible for energy and angular momentum transfer (Broglia

et al. 1978, 1979, 1982). In this approach, the surface modes are computed in the RPA approximation insofar as this strength distribution is concerned . These modes are further described in terms of equivalent damped oscillators. The results are mixed. Contrary to experiment, both fragments become loaded with approximately equal amount of energy: $\frac{Q_1}{Q_2} \cong \left(\frac{A_2}{A_1}\right)^{1/3}$ and the overall energy dissipation is inadequate by a factor of ~2. The introduction of particle exchange together with the surface modes provides an adequate amount of energy dissipation and of angular momentum transfer as well. The latter result does not prove much. In a regime in which the radial energy is rapidly dissipated, the damping of the tangential energy goes hand in hand with angular momentum transfer. The merit of this model is that of stressing the role of collective modes and the important microscopic connection to standard nuclear theory.

4.3 Transport Models

We have already mentioned some phenomenological transport theories. The two theories that come close to satisfying most requirements, like the incorporation of a sufficient number of degrees of freedom, including that of relative motion, and like the microscopic qualification of the diffusion coefficients, are that pioneered by Nörenberg (1975 & 1978), Ayik et al. (1978), Wolschin (1979a,b,c) and Li & Wolschin (1983) on the one hand, and those based upon one body theory promoted by Randrup (1978, 1979, 1983) and Feldmeier (1982) on the other. Their success has also been mixed. Most problems regarding the mass drift and the partition of the dissipated energy have not reached a satisfactory solution as yet. Also many of the successful predictions of the second moments and, at times, the first moment of dynamical

variables as well have been preempted in their significance by the fact that the same quantities are predicted in the equilibrium limit. Thus no support can come to these theories from the reproduction of the equilibrium limit.

Insofar as the angular momentum partition is concerned, we have seen that the equilibrium statistical model does a good job in describing the experiment. However some interesting theoretical results (Randrup 1981) have been obtained that show distinct differences between the equilibrium and the diffusion model in predicting the spin-spin correlation between the two fragments.

In order to attain statistical equilibrium of the spin distribution during a reaction, the appropriate relaxation times should be sufficiently short when compared with the reaction time. In the one body picture, the primary excitations occur through the transfer of individual nucleons between the two reaction partners. A system of Fokker-Planck equations for the resulting evolution of the mean values and covariances of the spin distribution in the two nuclei can be derived.

The long-time limit solution to the equations is given by rigid rotation for the mean spin vectors, and by the statistical model for the variances and covariances. For a symmetric collision, one can obtain analytic expressions for the characteristic relaxation times for approach towards equilibrium (Døssing & Randrup 1984). One should note that a different convention has been chosen in this work. The line of centers of the dinuclear system and the orbital angular momentum have been chosen to be the z- and y-axes, respectively. The relaxation times for the positive spin modes (in which the fragments are rotating in the same sense, wriggling and tilting) are denoted by t_{++} and t_{+z}, respectively. The relaxation times for the negative

spin modes (in which the fragments are rotating in the opposite sense, bending and twisting) are denoted by t_{--}. Figure 31 shows the relaxation times calculated for the collision of 1400 MeV ^{165}Ho with ^{165}Ho. This theory predicts (see Figure 31) that the wriggling modes (t_{++}) are strongly excited and reach equilibrium in most cases, the negative modes (t_{--}) get partially excited, and the tilting mode (t_{+z}) receives only little excitation. These conclusions are also valid for results obtained by solving numerically the system of equations and performing the necessary transformations to the external coordinate system and to distributions not gated by impact parameters, but by total kinetic energy loss.

Figure 32 shows variances and covariances of the spins $\vec{S}^A$ and $\vec{S}^B$ of the projectile-like and target-like reaction products (for example $\sigma^{AB}_{XZ} \equiv \langle S^A_S \; S^B_Z \rangle - \langle S^A_X \rangle \langle S^B_Z \rangle$). The left hand part of the figure shows the result obtained with the Transfer Induced Transport theory, and the right hand part shows the predictions of the statistical model for the same collision. The principal variances σ^{AA}_{ii} within one nucleus all increase steadily with TKEL (except for a slight decrease of σ^{AA}_{YY} at the largest TKEL; this may be an artifact of the upper bound imposed on TKEL by the calculation). The covariance between the spins in the two nuclei along the normal direction, σ^{AB}_{YY}, is always positive, due to the dominance of the positive wriggling mode for small TKEL, and due to the contributions from quite a wide range of ℓ waves at large TKEL. The dependence of the relaxation times on ℓ-wave, as shown in Figure 31, is reflected in the dependence of the in-plane covariances σ^{AB}_{XX} and σ^{AB}_{ZZ} on TKEL. The larger in-plane component, σ^{AB}_{XX}, first increases to substantial positive values for small TKEL, due to the very short relaxation time for the wriggling mode, and for large TKEL, σ^{AB}_{XX} decreases

and finally becomes rather small due to the increasing excitation of the negative in-plane bending mode. For large ℓ-waves, the tilting relaxation time, t_{+z}, is smaller than the twisting relaxation time t_{--}, and the smaller in-plane component of the covariance, σ_{ZZ}^{AB}, attains small positive values for small TKEL. With decreasing ℓ the twisting relaxation time becomes smaller and the tilting time longer. Consequently, with increasing TKEL, σ_{ZZ}^{AB} changes sign and finally, for large TKEL, attains substantial negative values.

In contrast to this behavior, the dispersions calculated with the statistical model grow roughly as the fourth root of the total kinetic energy loss. For the normal variances and covariances, σ_{YY}^{AA} and σ_{YY}^{AB}, one should not attach so much significance to the difference between the two results, since part of the result in the dynamical case comes from integration over impact parameter at fixed TKEL. A similar integration in the statistical model would diminish the difference between the two results. The in-plane variances and covariances, on the other hand, can be directly compared, and here the dynamical results display a much stronger anisotropy, and a quite different characteristic behavior as function of TKEL, as compared to the statistical model result, which would be obtained in the dynamical calculations if the relaxation times all were very short.

Thus, the nucleon exchange transport model predicts strong correlations between the two fragment spins. The detailed structure of such spin-spin correlations can be probed in a fission-fission angular correlation experiment. Most notably, the existence of covariances between the two nuclear spins implies that the detection of fission from one nucleus breaks the reflection symmetry of the angular correlation of fission from the other nucleus.

5. CONCLUSION

We tried to show how important the role of angular momentum is in deep inelastic collisions. Angular momentum defines the range of existence of this very process and its boundaries as well, with complete fusion on one side and direct reactions on the other. The angular distribution of the ensuing products is controlled by angular momentum in more than one way. On one hand the interaction time is angular momentum dependent, and so is the angular velocity. On the other, the orbital angular momentum that is dissipated, as well as the dissipated kinetic energy both depend on the angular momentum. Furthermore, the different exit channel asymmetries are fed by different ℓ waves. All this contributes to making the angular distributions dependent on just about any variable in the Hamiltonian. The relaxation of angular momentum leads to the secular equilibrium of the system which can rotate like a rigid body. However, the presence of angular momentum bearing degrees of freedom allows for fluctuations that can misalign the aligned component of the fragment angular momentum. The excitation of these modes can be studied through the angular distribution of particles and gamma rays emitted by the fragments.

The present understanding of the role of angular momentum has crystallized in a variety of theories ranging from conditional equilibrium statistical theories, to assorted transport theories and including Time Dependent Hartree Fock. At this stage it may be premature to say if any given theory satisfies all the details brought to light by experiment. It is also clear that, at this point one ought to broaden the discussion to the overall field of heavy ion collisions. Such an extension is beyond the

scope of this publication. We just ask forgiveness if our zeal in telling the whole story has been stronger at times than our commitment to a part of it albeit an important one.

This work was supported by the Director, Office of Energy Research, Division of Nuclear Physics of the Office of High Energy and Nuclear Physics of the U.S. Department of Energy under Contract DE-AC03-76SF00098.

LITERATURE CITED

Agassi, D., Ko, C. M., Weidenmüller, H. A. 1978. Phys. Rev. C18:223

Agassi, D., Ko, C. M., Weidenmüller, H. A. 1979. Ann. Phys. 117:407

Aguer, P., Schmitt, R. P., Wozniak, G. J., Habs, D., Diamond, R. M., Ellegaard, C., Hillis, D. L., Hsu, C. C., Mathews, G. J., Moretto, L. G., Rattazzi, G. U., Roulet, C. P., Stephens, F.S. 1979. Phys. Rev. Lett. 43:1778

Aleonard, M. M., Wozniak, G. J., Glässel, P., Deleplanque, M. A., Diamond, R. M., Moretto, L. G., Schmitt, R. P., Stephens, F. S. 1978. Phys. Rev. Lett.40:622

Artukh, A. G., Gridnev, G. F., Mikheev, V. L., Volkov, V. V., Wilczyński, J. 1973. Nucl. Phys. A215:91

Ayik, S., Wolschin, G., Nörenberg, W. 1978. Z. Phys. A286:271

Babinet, R., Cauvin, B., Girard, J., Alexander, J. M., Chiang, T. H., Galin, J., Gatty, B., Guerreau, D., Tarrago, X. 1980. Z. Phys. A295:153

Bass, R. 1974. Nucl. Phys. A231:45

Berlanger, M., Deleplanque, M. A., Gerschel, C., Hanappe, F., Le Blanc, M., Mayault, J. F., Ngô, C., Paya, D., Perrin, N., Péter, J., Tamain, B., Valentin, L. 1976. J. de Phys. Lett. 37:L323

Birkelund, J. R., Tubbs, L. E., Huizenga, J. R., De, J. N., Sperber, D. 1979. Phys. Lett. C56:107

Bock, R., Fischer, B., Gobbi, A., Hildenbrand, K., Kohl, W., Lynen, U., Rode, I., Stelzer, H., Auger, G., Galin, J., Lagrange, J. M., Back, B. B., Albrecht, R. 1977. Nucleonika 22:529

Bondorf, J. P., Sobel, M. I., Sperber, D. 1974. Phys. Lett. 15C:83

Broglia, R. A., Civitarese, O., Dasso, C. H., Winther, A. 1978. Phys. Lett. 73B:405

Broglia, R. A., Dasso, C. H., Pollarolo, G., Winther, A. 1978. Phys. Rev. Lett. 41:25

Broglia, R. A., Dasso, C. H., Winther, A. 1982. Proc. Int. School of Physics, "Enrico Fermi," Varenna, Italy, July 1979 (North Holland, Amsterdam, 1982) 327

Broglia, R. A., Pollarolo, G., Dasso, C. H., Døssing, T. 1979. Phys. Rev. Lett. 43:1649

Cassing, W., Friedrich, H. 1980. Z. Phys. A298:129

Christensen, P. R., Folkmann, F., Hansen, O., Nathan, O., Trautner, N., Videbaek, F., Van Der Werf, S. Y. 1980. Nucl. Phys. A349:217

Cohen, S., Plasil, F., Swiatecki, W. J. 1982. Ann. of Phys. 82:557

Davies, K. T. R., Maruhn-Rezwani, V., Koonin, S. E., Negele, J. W. 1978. Phys. Rev. Lett. 41:632

Davies, K. T. R., Koonin, S. E. 1981. Phys. Rev. C23:2042

Dayras, R. A., Stokstad, R. G., Fulmer, C. B., Hensley, D. C., Halbert, M. L., Robinson, R. L., Snell, A. H., Sarantites, D. G., Westerberg, L., Barker, J. H. 1979. Phys.Rev. Lett. 42:697

Dayras, R. A., Stokstad, R. G., Hensley, D. C., Halbert, M. L., Sarantites, D. G., Westerberg, L., Barker, J. H. 1980. Phys. Rev. C22:1485

Deubler, H. H., Dietrich, K.1975. Phys. Lett. 56B:241

Diamond, R. M., Stephens, F. S. 1980. Ann. Rev. Nucl. Part. Sci. 30:85

Dossing, T., Randrup, J. 1984. Lawrence Berkeley Laboratory Report No. LBL-16825

Dossing, T., Randrup, J. 1984. Lawrence Berkeley Laboratory Report No. LBL-16826

Dünnweber, W. 1982. International School of Physics "Enrico Fermi," Varenna, Italy

Dyer, P., Puigh, R. J., Vandenbosch, R., Thomas, T. D., Zisman, M. S. 1977. Phys. Rev. Lett. 39:392

Dyer, P., Puigh, R. J., Vandenbosch, R., Thomas, T. D., Zisman, M. S., Nunnelley, L. 1979. Nucl. Phys. A322:205

Eyal, Y., Gavron, A., Tserruya, I., Fraenkel, Z., Eisen, Y., Wald, S., Bass, R., Gould, G. R., Kreyling, G., Renfordt, R., Stelzer, K., Zitzmann, R., Gobbi, A., Lynen, U., Stelzer, H., Rode, I., Bock, R. 1978. Phys. Rev. Lett. 41:625

Feldmeier, H. 1982. International School of Physics "Enrico Fermi," Varenna, Italy

Galin, J. 1976. J. Physique 37:C5 83

Galin, J., Guerreau, D., Lefort, M., Péter, J., Tarrago, X., Basile, R. 1970. Nucl. Phys. A159:461

Gatty, B., Guerreau, D., Lefort, M., Pouthas, J., Tarrago, X., Galin, J., Cauvin, B., Girard, J., Nifenecker, H. 1975a. Z. Phys. A273:65

Gatty, B., Guerreau, D., Lefort, M., Tarrago, X., Galin, J., Cauvin, B., Girard, J., Nifenecker, H. 1975b. Nucl. Phys. A253:511

Gerschel, C., Deleplanque, M. A., Ishihara, M., Ngô, C., Perrin, N., Péter, J., Tamain, B., Valentin, L. 1979. Nucl. Phys. A317:473

Glas, D., Mosel, U. 1975. Nucl. Phys. A237:439

Glässel, P., Simon, R. S., Diamond, R. M., Jared, R. C., Lee, I. Y., Moretto, L. G., Newton, J. O., Schmitt, R., Stephens, F. S. 1977. Phys.Rev. Lett. 38:331

Gould, C. R., Bass, R., Czarnecki, J. v., Hartmann, V., Stelzer, K., Zitzmann, R., Eyal, Y. 1980. Z. Phys. A294:323

Gross, D. H. E., Kalinowski, H. 1974. Phys. Lett. 48B:302

Gross, D. H. E. 1981. Nukleonika 26:985

Hanappe, F., Lefort, M., Nĝo, C., Péter, J., Tamain, B. 1974. Phys. Rev. Lett. 32:738

Harrach, D. v., Glässel, P., Civelekoglu, Y., Männer, R., Specht, H. J. 1979. Phys. Rev. Lett. 42:1728

Hilscher, D., Birkelund, J. R., Hoover, A. D., Schröder, W. U., Wilcke, W. W., Huizenga, J. R., Mignerey, A. C., Wolf, K. L., Breuer, H. F., Viola, V. E., Jr. 1979. Phys. Rev. C20:576

Ishihara, M., Tanaka, K., Kammuri, T., Matsuoka, K., Sano, M. 1978. Phys. Lett. 73B:281

Jacmart, J. C., Colombani, P., Doubre, H., Frascaria, N., Poffé, N., Riou, M., Roynette, J. C., Stéphan, C. 1975. Nucl. Phys. A242:175

Kaufmann, R., Wolfgang, R. 1961. Phys. Rev. 121:192

Kratz, J. V., Norris, A. E., Seaborg, G. T. 1974. Phys. Rev. Lett. 33:502

Kühn, W., Albrecht, R., Damjantschitsch, H., Ho, H., Ronningen, R. M., Slemmer, J., Wurm, J. P., Rode, I., Scheibling, F. 1980. Z. Phys. A298:95

Lauterbach, C., Dünnweber, W., Graw, G., Hering, W., Puchta, H., Trautmann, W. 1978. Phys. Rev. Lett. 41:1774

Le Brun, C., Le Colley, J. F., Lefebvres, F., L'Haridon, M., Osmont, A., Patry, J. P., Steckmeyer, J. C., Chechik, R. 1982. Phys. Rev. C25:3212

Lefort, M. 1975. Lecture Notes in Physics, 33:275

Lefort, M., Ngô, C. 1979. Riv. Nuovo Cim. 2:1

Li, J. Q., Wolschin, G. 1983. Phys. Rev. C27:590

Mathews, G. J., Wozniak, G. J., Schmitt, R. P., Moretto, L. G. 1977. Z. Phys. A283:247

McDonald, R. J., Pacheco, A. J., Wozniak, G. J., Bolotin, H. H., Moretto, L. G., Schück, C., Shih, S., Diamond, R. M., Stephens, F. S. 1982. Nucl. Phys. A373:54

Moretto, L. G. 1975. Nucl. Phys. A247:211

Moretto, L. G. 1978. J. Phys. Soc. Japan 44:Suppl. 7 361

Moretto, L. G. 1981. Lawrence Berkeley Laboratory Report No. LBL-12596

Moretto, L. G. 1982. Proceedings of the International Conference on Selected Aspects of Heavy Ion Reactions, Saclay France, LBL-14283

Moretto, L. G., Babinet, R. P., Galin, J., Thompson, S. G. 1975. Phys. Lett. 58B:31

Moretto, L.G., Blau, S. K., Pacheco, A. J. 1981. Nucl. Phys. A364:125

Moretto, L. G., Cauvin, B., Glässel, P., Jared, R., Russo, P., Sventek, J., Wozniak, G. 1976. Phys. Rev. Lett. 36:1069

Moretto, L. G., Heuneman, D., Jared, R. C., Gatti, R. C., Thompson, S. G. 1973. Physics and Chemistry of Fission, Vienna, Vol. 2, 351 pp.

Moretto, L. G., Schmitt, R. P. 1976. J. Physique 37:C5 109

Moretto, L. G., Schmitt, R. P. 1980. Phys. Rev. C21:204

Moretto, L. G., Schmitt, R. P. 1981. Rep. Prog. Phys. 44:533

Moretto, L. G., Sobotka, L. G. 1981. Z. Phys. A303:299

Moretto, L. G., Sventek, J. S. 1975. Phys. Lett. 58B:26

Morrissey, D. J., Moretto, L. G. 1981. Phys. Rev. C23:1835

Morrissey, D. J., Wozniak, G. J., Sobotka, L. G., Pacheco, A. J., Hsu, C. C., McDonald, R. J., Moretto, L. G. 1982a. Z. Phys. A305:131

Morrissey, D. J., Wozniak, G. J., Sobotka, L. G., Pacheco, A. J., McDonald, R. J., Hsu, C. C., Moretto, L. G. 1982b. Nucl. Phys. A389:120

Mouchaty, G., Haenni, D. R., Nath, S., Garg, U., Schmitt, R. P. 1984 (in press)

Namboodiri, M. N., Natowitz, J. B., Kasiraj, P., Eggers, R., Adler, L., Gonthier, P., Cerruti, C., Simon, S. 1979. Phys. Rev. C20:982

Natowitz, J. B., Namboodiri, M. N., Kasiraj, P., Eggers, R., Adler, L., Gonthier, P., Cerruti, C., Alleman, T. 1978. Phys. Rev. Lett. 40:751

Negele, J. W. 1982. Rev. Mod. Phys. 54:913

Nörenberg, W. 1974. Phys. Lett. 53B:289

Nörenberg, W. 1975. Z. Phys. A274:241

Nörenberg, W. 1976. J. Physique 37:C5 141

Nörenberg, W. Lectures presented at the Predeal International School in Physics, Predeal, Romania, 1978

Nörenberg, W., Weidenmüller, H. A. 1980. Lecture Notes in Physics 51, Springer-Verlag, Berlin 1980

Olmi, A., Sann, H., Pelte, D., Eyal, Y.,Gobbi, A., Kohl, W., Lynen, U., Rudolf, G., Stelzer, H., Bock, R. 1978. Phys. Rev. Lett. 41:688

Pacheco, A. J., Wozniak, G. J., McDonald, R. J., Diamond, R. M., Hsu, C. C. Moretto, L. G., Morrissey, D. J., Sobotka, L. G., Stephens, F. S. 1983 Nucl. Phys. A397:313

Puchta, H., Dünnweber, W., Hering, W., Lauterbach, C., Trautmann, W., 1979. Phys. Rev. Lett. 43:623

Puigh, R. J., Doubre, H., Lazzarini, A., Seamster, A., Vandenbosch, R., Zisman, M. S., Thomas, T. D. 1980. Nucl. Phys. A336:279

Puigh, R. J., Dyer, P., Vandenbosch, R., Thomas, T. D., Nunnelley, L., Zisman, M. S. 1979. Phys. Lett. 86B:24

Randrup, J. 1978. Nucl. Phys. A307:319

Randrup, J. 1979. Nucl. Phys. A327:490

Randrup, J. 1981. Phys. Lett. 110B:25

Randrup, J. 1982. Nucl. Phys. A383:468

Regimbart, R., Behkami, A. N., Wozniak, G. J., Schmitt, R. P., Sventek, J. S., Moretto, L. G. 1978. Phys. Rev. Lett. 41:1355

Rudolf, G., Gobbi, A., Stelzer, H., Lynen, U., Olmi, A., Sann, H., Stokstad, R. G., Pelte, D. 1979. Nucl. Phys. A330:243

Schmitt, R. P., Bizard, G., Wozniak, G. J., Moretto, L. G. 1978. Phys. Rev. Lett. 41:1152

Schmitt, R. P., Pacheco, A. J. 1982. Nucl. Phys. A379:313

Schröder, W. U., Birkelund, J. R., Huizenga, J. R., Wolf, K. L., Viola, V. E., Jr. 1978. Phys. Lett. C45:301

Schröder, W. U., Huizenga, J. R. 1977. Ann. Rev. Nucl. Sci. 27:465

Scott, D. K. 1978. Notas de Fisica 1, No. 5

Sobotka, L. G., Hsu, C. C., Wozniak, G. J., Morrissey, D. J., Moretto, L. G. 1981a. Nucl. Phys. A371:510

Sobotka, L. G., Hsu, C. C., Wozniak, G. J., Rattazzi, G. U., McDonald, R. J., Pacheco, A. J., Moretto, L. G. 1981b. Phys. Rev. Lett. 46:887

Sobotka, L. G., McDonald, R. J., Wozniak, G. J., Morrissey, D. J., Pacheco, A. J., Moretto, L. G. 1983. Phys. Rev. C28:219

Strutinsky, V. M. 1973. Phys. Lett. 44B:245

Sventek, J. S., Moretto, L. G. 1978. Phys. Rev. Lett. 40:697

Swiatecki, W. J. 1972. J. de Physique 33:C5-45

Swiatecki, W. J. 1982. Nucl. Phys. A376:275

Tamain, B., Chechik, R., Fuchs, H., Hanappe, F., Morjean, M., Ngô, C., Péter, J., Dakowski, M., Lucas, B., Mazur, C., Ribrag, M., Signarbieux, C. 1979. Nucl. Phys. A330:253

Trautmann, W., Dahme, W., Dünnweber, W., Hering, W., Lauterbach, C., Puchta, H., Kühn, W., Wurm, J. P. 1981. Phys. Rev. Lett. 46:1188

Trautmann, W., de Boer, J., Dünnweber, W., Graw, G., Kopp, R., Lauterbach, C., Puchta, H., Lynen, U. 1977. Phys. Rev. Lett. 39:1062

Tsang, C. F. 1974. Phys. Scr. 10A:90

Van Bibber, K., Ledoux, R., Steadman, S. G., Videbaek, F., Young, G., Flaum, C. 1977. Phys. Rev. Lett. 38;334

Vandenbosch, R., Webb, M. P., Thomas, T. D., Zisman, M. S. 1976. Nucl. Phys. A269:210

Volkov, V. V. 1978. Phys. Lett. C44:93

Wilcke, W. W., Birkelund, J. R., Hoover, A.D., Huizenga, J. R., Schröder, W. U., Viola, V. E., Jr., Wolf, K. L., Mignerey, A. C. 1980. Phys. Rev. C22:128

Wilczyński, J. 1973. Phys. Lett. 47B:484

Wolf, K. L., Unik, J. P., Huizenga, J. R., Birkelund, J. R., Freiesleben, H., Viola, V. E. 1974. Phys. Rev. Lett. 33:1105

Wolschin, G. 1979a. International School of Physics "Enrico Fermi," Varenna, Italy

Wolschin, G. 1979b. Phys. Lett. 88B:35

Wolschin, G. 1979c. Nucl. Phys. A316:146

Wolschin, G., Nörenberg, W. 1978. Phys. Rev. Lett. 41:691

Wozniak, G. J., McDonald, R. J., Pacheco, A. J., Hsu, C. C., Morrissey, D. J., Sobotka, L. G., Moretto, L. G., Shih, S., Schück, C., Diamond, R. M., Kluge, H., Stephens, F. S. 1980. Phys. Rev. Lett. 45:1081

Wozniak, G. J., Schmitt, R. P., Glässel, P., Jared, R. C., Bizard, G., Moretto, L. G. 1978. Phys. Rev. Lett. 40:1436

Zisman, M. S., Puigh, R. J., Vandenbosch, R., Thomas, T. D., Nunnelley, L. 1982. Lawrence Berkeley Laboratory Report No. LBL-13366:93

FIGURE CAPTIONS

Fig. 1 A classification of rotating systems according to the rotational parameter y and the fissility parameter x. With increasing angular momentum, rotating systems first deform into a flat shape (below Y_I), then into a triaxial shape (beween Y_I and Y_{II}), and finally the fission barrier vanishes along curve Y_{II} (Cohen et al. 1974).

Fig. 2 (a) Potential energies as a function of r/r_0 for various values of $\eta = \ell/\ell_{max}$. (b) Schematic showing the trajectories in the presence of weak (full curve), moderate (dotted curve) and strong (broken curve) radial friction (Schröder & Huizenga 1977).

Fig. 3 Contours of constant cross section for (a) potassium ions produced in the reaction 388 MeV $^{40}Ar + ^{232}Th$ (Wilczyński 1973) and (b) all products produced in the reaction 1130 MeV $^{136}Xe + ^{209}Bi$ (Schröder et al. 1978).

Fig. 4 Relation between the spin polarization and the sign of the deflection angle in a frictional collision (Dünnweber 1982).

Fig. 5 (a) Particle spectra in coincidence with γ rays, (b) circular polarization of the energy-integrated γ radiation and (c) average in-plane/out-of-plane intensity ratio of stretched quadrupole transitions (Lauterbach et al. 1978).

Fig. 6 Mean deflection function for Xe + Bi and Kr + Er at two different incident energies (Wolschin 1979).

Fig. 7 The experimentally deduced deflection function as a function of the angular momentum is compared to classical trajectory calculations, using potential and friction form factors as indicated. No deformations are taken into account (Wilcke et al. 1980).

Fig. 8 Wilczyński plot calculated without (a) and with (b) quantal fluctuations (Cassing & Friedrich 1980).

Fig. 9 Wilczyński plot calculated from a one-body diffusion model without quantal fluctuations (Feldmeier 1982).

Fig. 10 Center-of-mass angular distributions for products (Z = 20 - 47) from the reaction 620 MeV $^{86}Kr + ^{197}Au$ (Moretto et al. 1976).

Fig. 11 (a) Calculated deflection functions (A, 600 MeV; B, 800 MeV; C, 1000 MeV) and interaction times (D, 1000 MeV; E, 800 MeV; F, 600 MeV) for the reaction $^{86}Kr + ^{197}Au$ at three bombarding energies. For the 620 MeV $^{86}Kr + ^{197}Au$ reaction, (b) calculated (full curves) and experimental (points), angle-integrated charge distributions and (c) C.M. angular distributions for selected atomic numbers. The broken curves are to guide the eye (Moretto 1978).

Fig. 12 (a) M_γ vs. total kinetic energy (TKE) for the reactions 618 MeV $^{86}Kr + ^{107,109}Ag$, ^{165}Ho, ^{197}Au. (b) M_γ vs. atomic number for the reactions Kr + Ag and Kr + Ho. The full and open symbols are data for a TKE gate on the deep inelastic and quasielastic reactions, respectively. The full curves are diffusion model calculations (Regimbart et al. 1978).

Fig. 13 Internal spin of the fragments as a function of the entrance channel angular momentum. The straight line indicates the sticking limit of two spheres for the Kr - Er exit channel (Olmi et al. 1978).

Fig. 14 γ-ray multiplicity vs. atomic number for the reactions 175 MeV ^{20}Ne + Ag (open circles) and 237 MeV ^{40}Ar + ^{89}Yb (filled circles) (Glässel et al. 1977, Natowitz et al. 1978).

Fig. 15 (a) Potential energy vs. mass asymmetry (Z) for various ℓ-waves for the system 340 MeV ^{40}Ar + ^{159}Tb. (b) γ-ray multiplicity data (diamonds) as a function of mass asymmetry for the same system. The solid dots represent a diffusion model calculation using the potential energy surfaces in (a).

Fig. 16 (left) Schematic illustrating the twisting mode and the doubly-degenerate bending modes for a two equal spheres model. In each case the spin vectors of the fragments (symbolized by arrows) are of equal length but point in opposite directions. (right) Schematic illustrating the tilting mode and the doubly-degenerate wriggling modes for the equal spheres model. The short arrows represent the spin vectors of the fragments. The long arrows originating at the point of tangency of the two spheres represent the orbital angular momentum vectors (Moretto & Schmitt 1980).

Fig. 17 Total spin of the fragments arising from wriggling as a function of the spin arising from rigid rotation alone plotted in dimensionless form. The upper solid curve shows the result for both wriggling modes while the lower solid curve corresponds to the excitation of a single wriggling mode. The limiting behavior for both small and large values of x are indicated in both cases (Moretto & Schmitt 1980).

Fig. 18 The variances of the normal modes of a dinuclear complex are shown as a function of mass asymmetry of the complex. The variances are shown in dimensionless units after division by $\mathcal{J}_{sym}T$, the moment of inertia of a mass-symmetric spherical fragment times the temperature Morrissey et al. 1982)

Fig. 19 The total angular momentum $I_{tot}(Z_1)$ as a function of fragment atomic number and corresponding M_γ data (Olmi et al. 1978) for ^{86}Kr (5.99 MeV/nucleon) + ^{166}Er. The solid curve includes statistical fluctuations and the dashed curve does not.

Fig. 20 Calculated γ-ray anisotropies for mixtures of stretched E1 and E2 transitions as a function of the fraction of E1 radiation for various values of $\sigma^2/\bar{I}_z^2$ (Moretto 1981).

Fig. 21 Sum of the spin magnitudes $(I_1 + I_2)$ as a function of Q-value for three reaction systems (Pacheco et al. 1983).

Fig. 22 The sum of the spins in reduced units as a function of temperature. The angular momentum axis has been scaled according to the rigid rotation limit (Pacheco et al. 1983).

Fig. 23 γ-ray anisotropy as a function of Q-value, for heavy ions detected near the grazing angle. Error bars for the three systems are similar and are only shown for ^{165}Ho + ^{176}Yb (Pacheco et al. 1983).

Fig. 24 Comparison between the experimental anistropies (open symbols) and a calculation (solid symbols) that does not include the effect of the thermal fluctuations (Pacheco et al. 1983).

Fig. 25 (left) Comparison between experimental (circles) anisotropies of γ-rays (E_γ = 0.80 - 0.95 MeV) and a calculation based on the equilibrium statistical model (squares) as a function of Q-value. Lines are drawn through the calculated points to guide the eye. (right) Alignment parameter P_{ZZ} as a function of Q-value, for each of the two deep-inelastic fragments in the three reactions (Pacheco et al. 1983).

Fig. 26 Experimental intrinsic spins of the individual fragments compared with the results of calculations for the sticking limit for rigid bodies (Babinet et al. 1980).

Fig. 27 (a) Alpha particle angular distributions (points) as a function of out-of-plane angle for several Z-bins. Each bin is 3Z units wide and is labeled by the median Z-value. These distributions are expressed in units of differential multiplicity and the solid curves are fits to the data.

(b) Center-of-mass energies as a function of the charge of the light fragment. The curves are calculations for two equally deformed spheroids separated by 1 fm and are labelled by the ratio of axes.

(c) Plotted are: the spin of the heavy ion fragment extracted from the α-particle distributions (solid circles), the sum of the spins calculated from the α-particle data (squares), and M_γ data (open circles). The size of the solid symbols indicates the statistical error only (Sobotka et al. 1981).

Fig. 28 Dependence of the angular momentum J transferred to the heavy fragment and the alignment P_{ZZ} of the transferred angular momentum on Q-value (Puigh et al. 1979).

Fig. 29 In-plane angular distributions of sequential fission fragments from the ^{20}Ne + ^{238}U system for several different Q-values (Morrissey et al. 1983).

Fig. 30 Quantitative summary of TDHF results for the 494MeV ^{84}Kr + ^{208}Pb reaction (Davies et al. 1978).

Fig. 31 Calculated local relaxation times for the reaction 1400 MeV ^{165}Ho + ^{165}Ho for various values of the total angular momentum ℓ. The relaxation times for the two positive perpendicular modes (wriggling) are denoted t_{++}, while the one of the positive longitudinal mode (tilting) is denoted T_{+z}. The relaxation time for the three negative modes (bending and twisting) is denoted t_{--} (Døssing & Randrup 1984).

Fig. 32 The spin dispersions along the principal directions as functions of the incurred energy loss TKEL, as calculated with the Transfer Induced Transport theory (left) and the statistical model (right) for the reaction 1400 MeV ^{165}Ho + ^{165}Ho by integrating over all ℓ-values (Døssing & Randrup 1984).

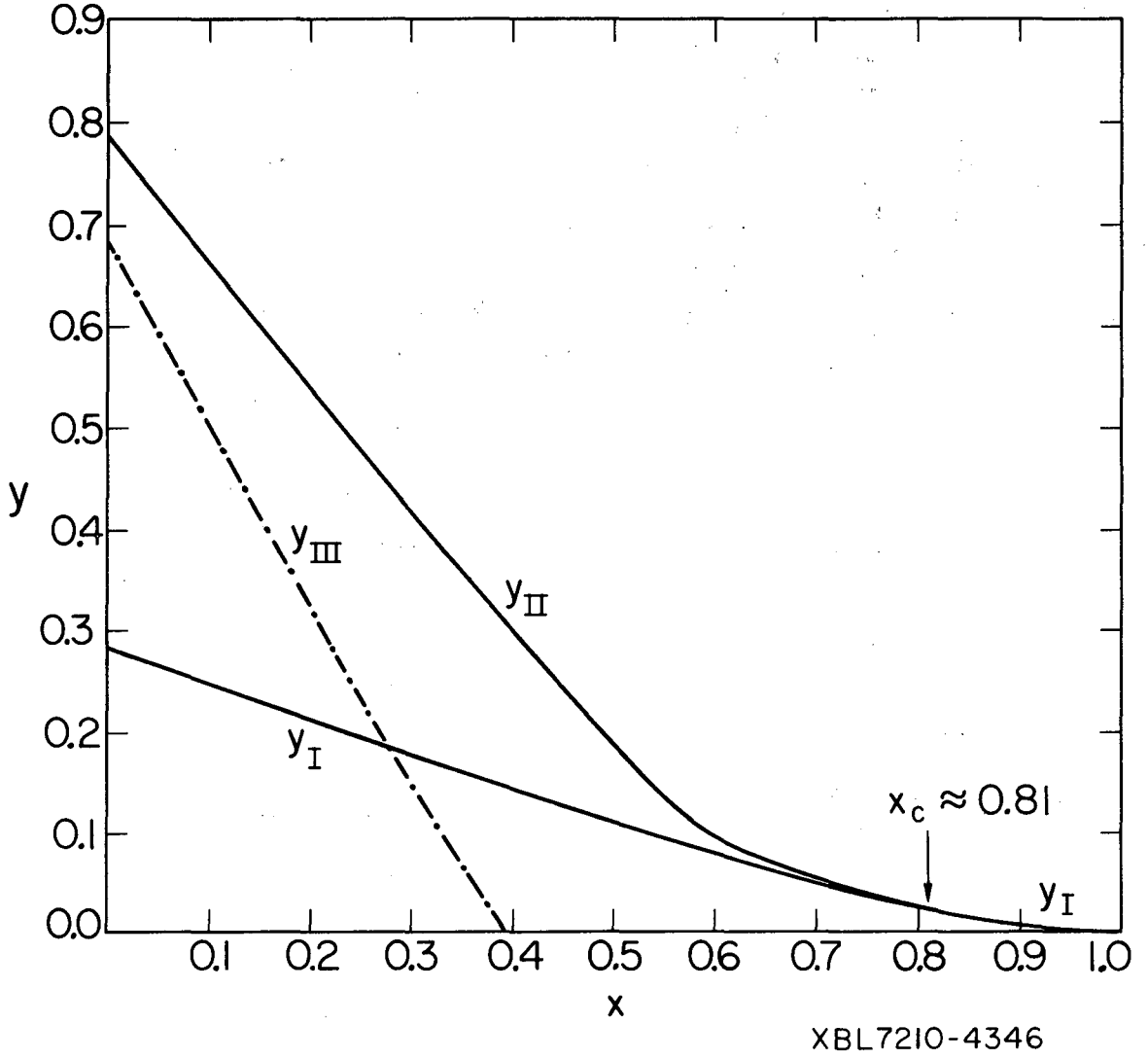
0.9
0.8
0.7
0.6
0.5
0.4
0.3
0.2
0.1
0.0
y
0.1
0.2
0.3
0.4
0.5
0.6
0.7
0.8
0.9
1.0
x
y_{III}
y_{II}
y_I
$x_c \approx 0.81$
y_I
XBL7210-4346

Fig. 1

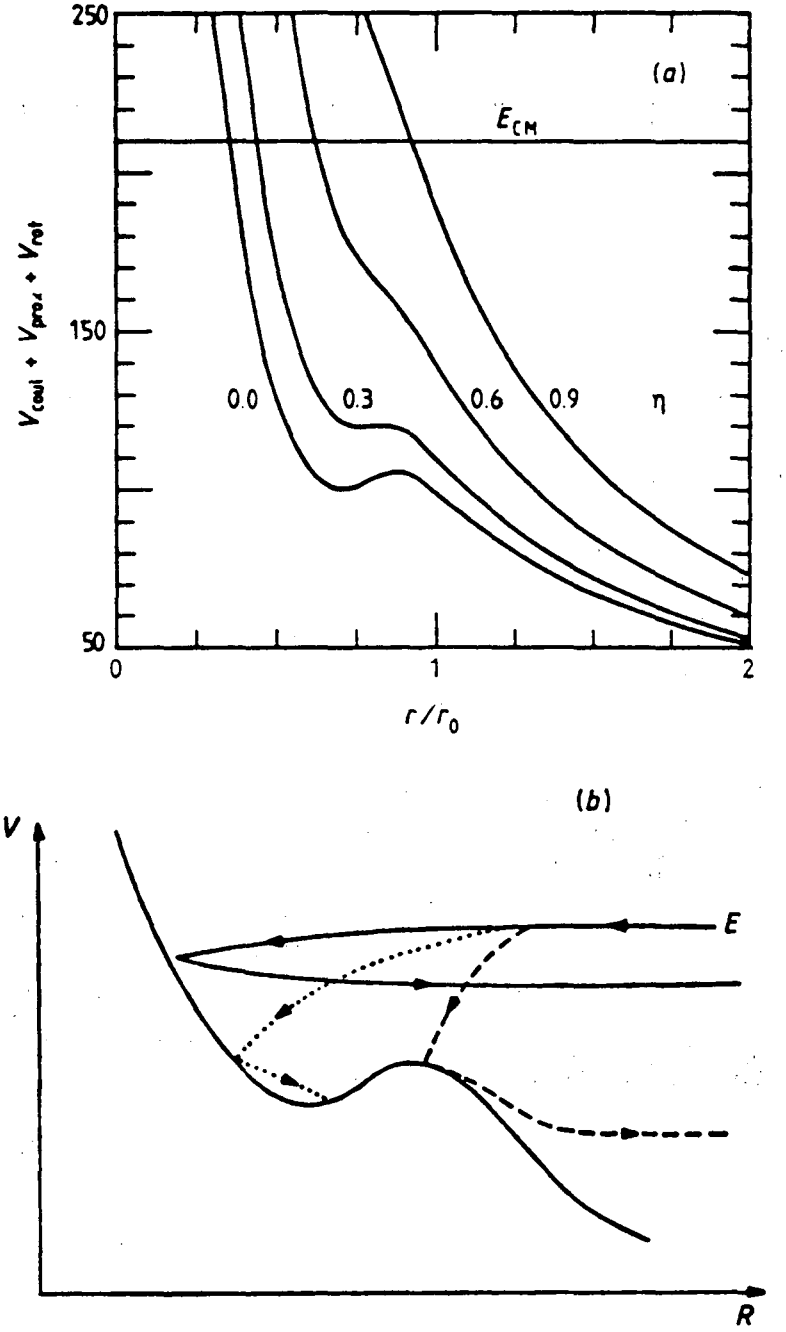

XBL 841-485

Fig. 2

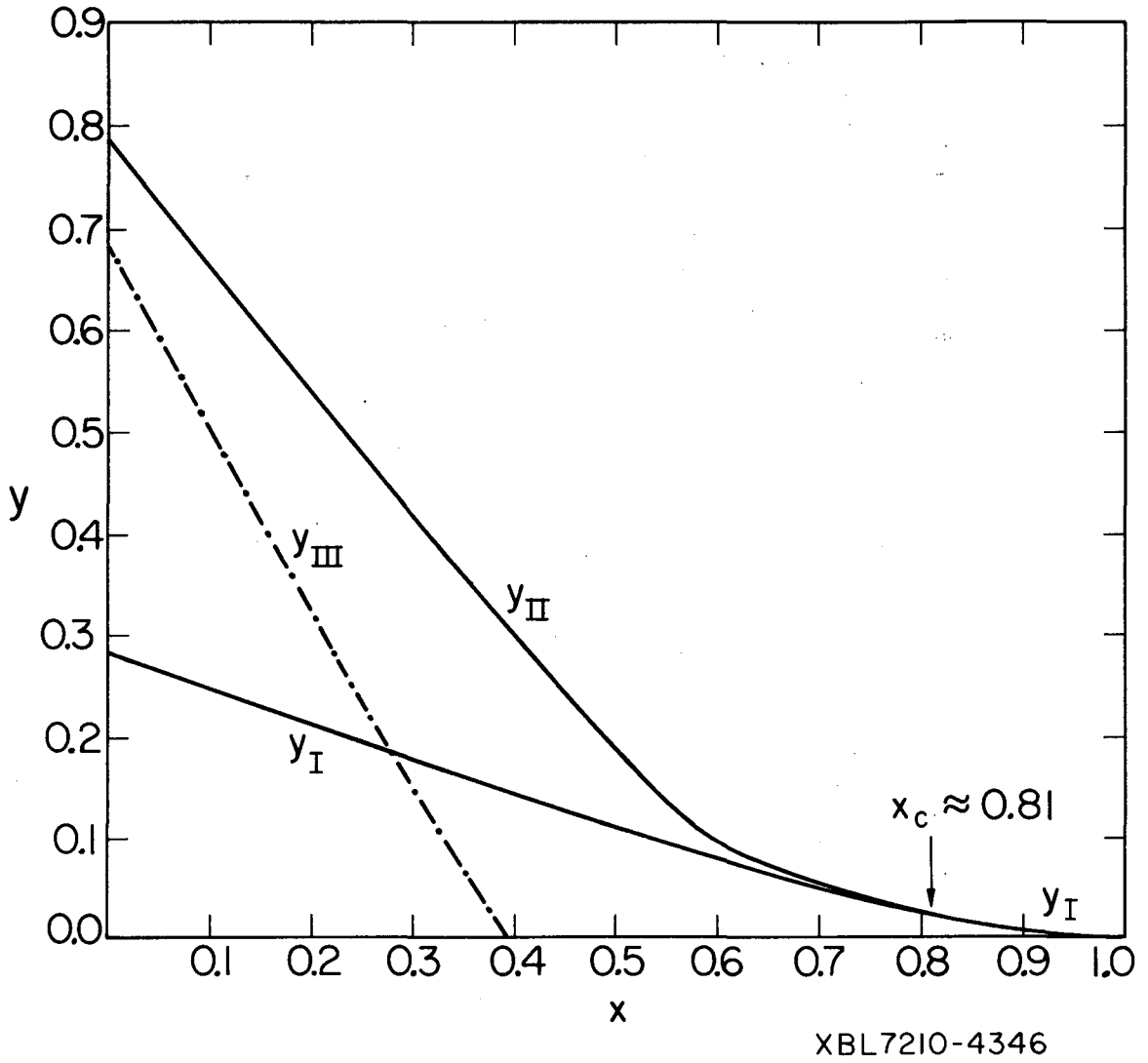
0.9
0.8
0.7
0.6
0.5
0.4
0.3
0.2
0.1
0.0
y
0.1
0.2
0.3
0.4
0.5
0.6
0.7
0.8
0.9
1.0
x
y_{III}
y_{II}
y_I
$x_c \approx 0.81$
y_I
XBL7210-4346

Fig. 1

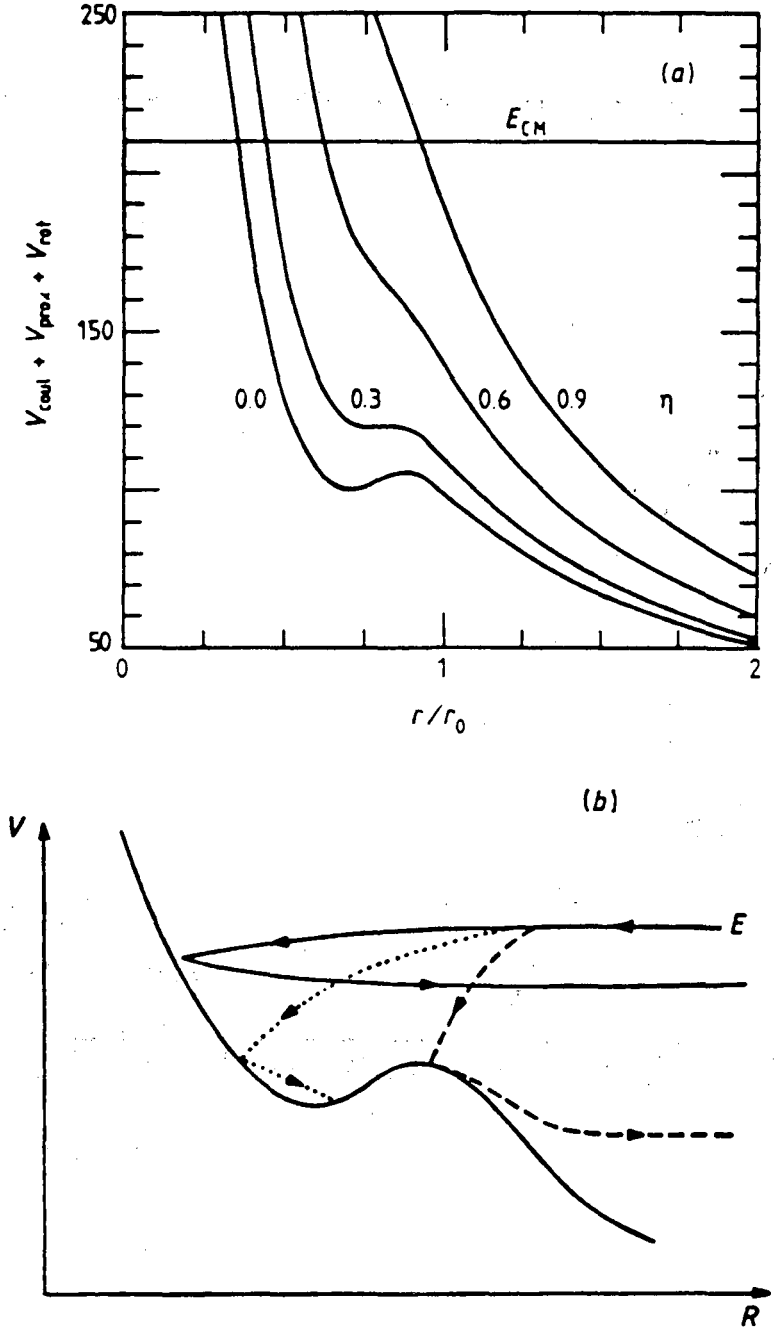

XBL 841-485

Fig. 2

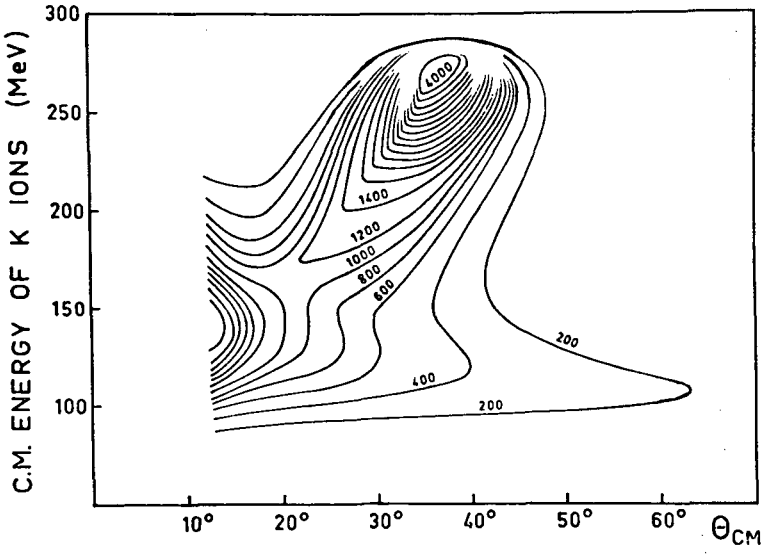

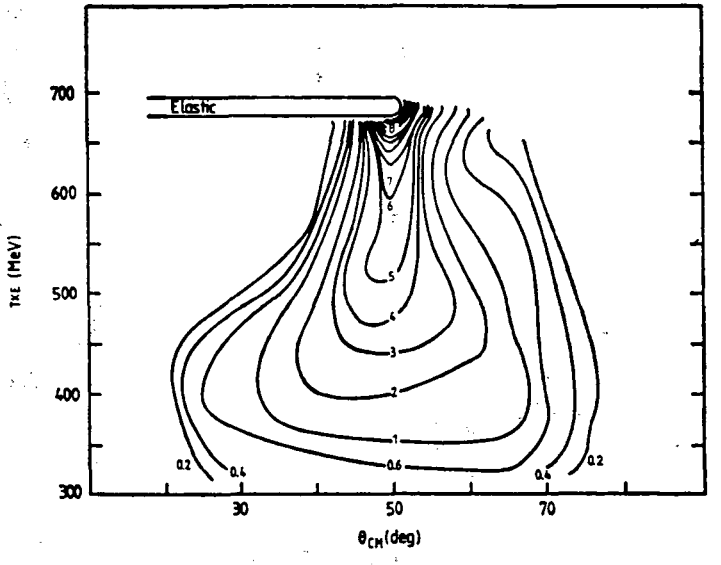

XBL 841-484A

Fig. 3

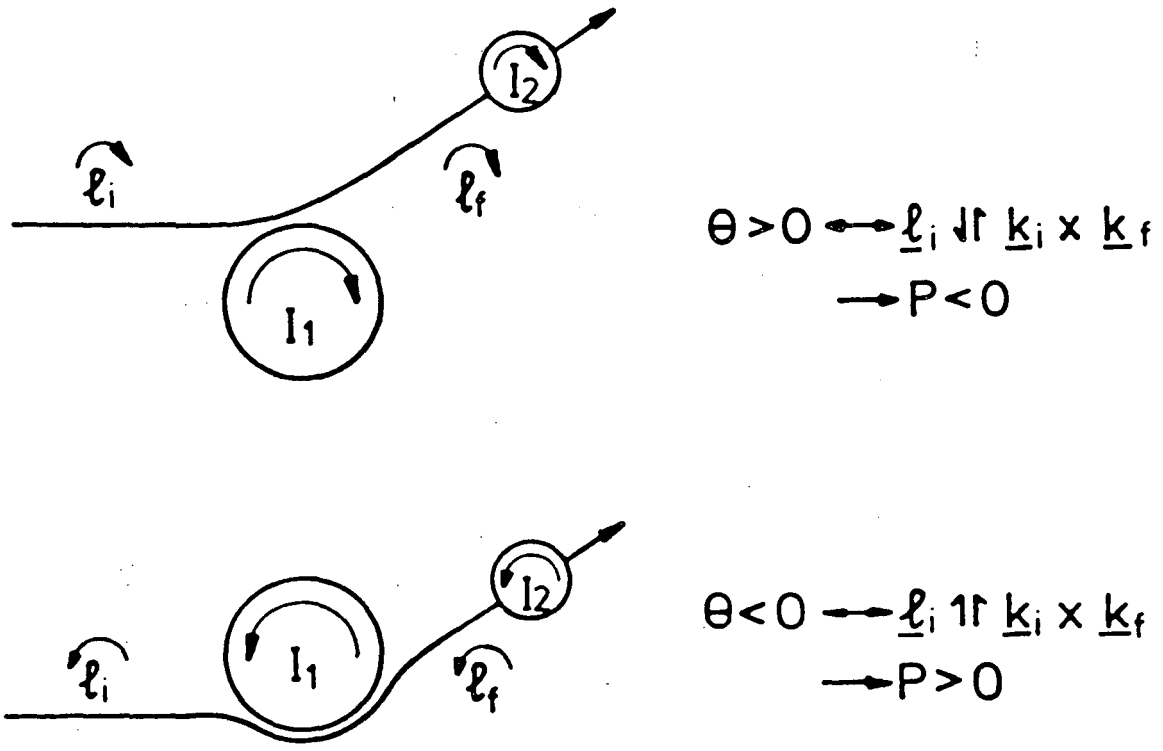

XBL 841-480

Fig. 4

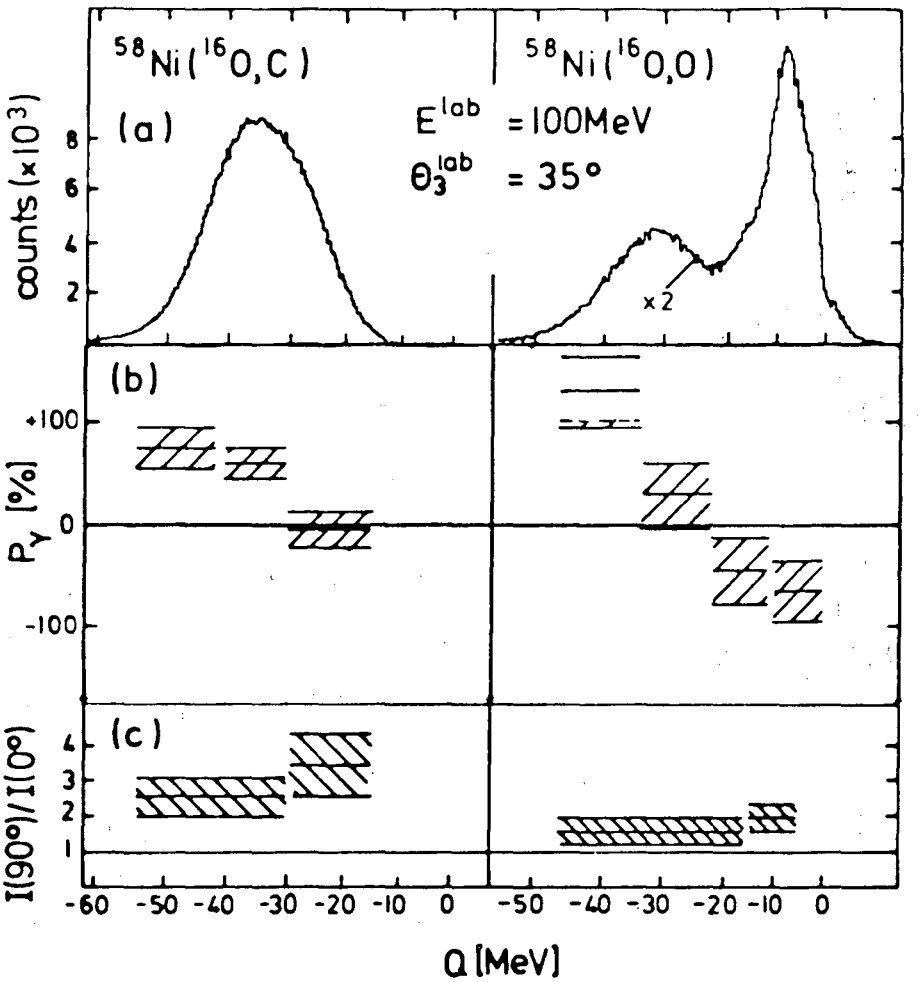

XBL 841-481

Fig. 5

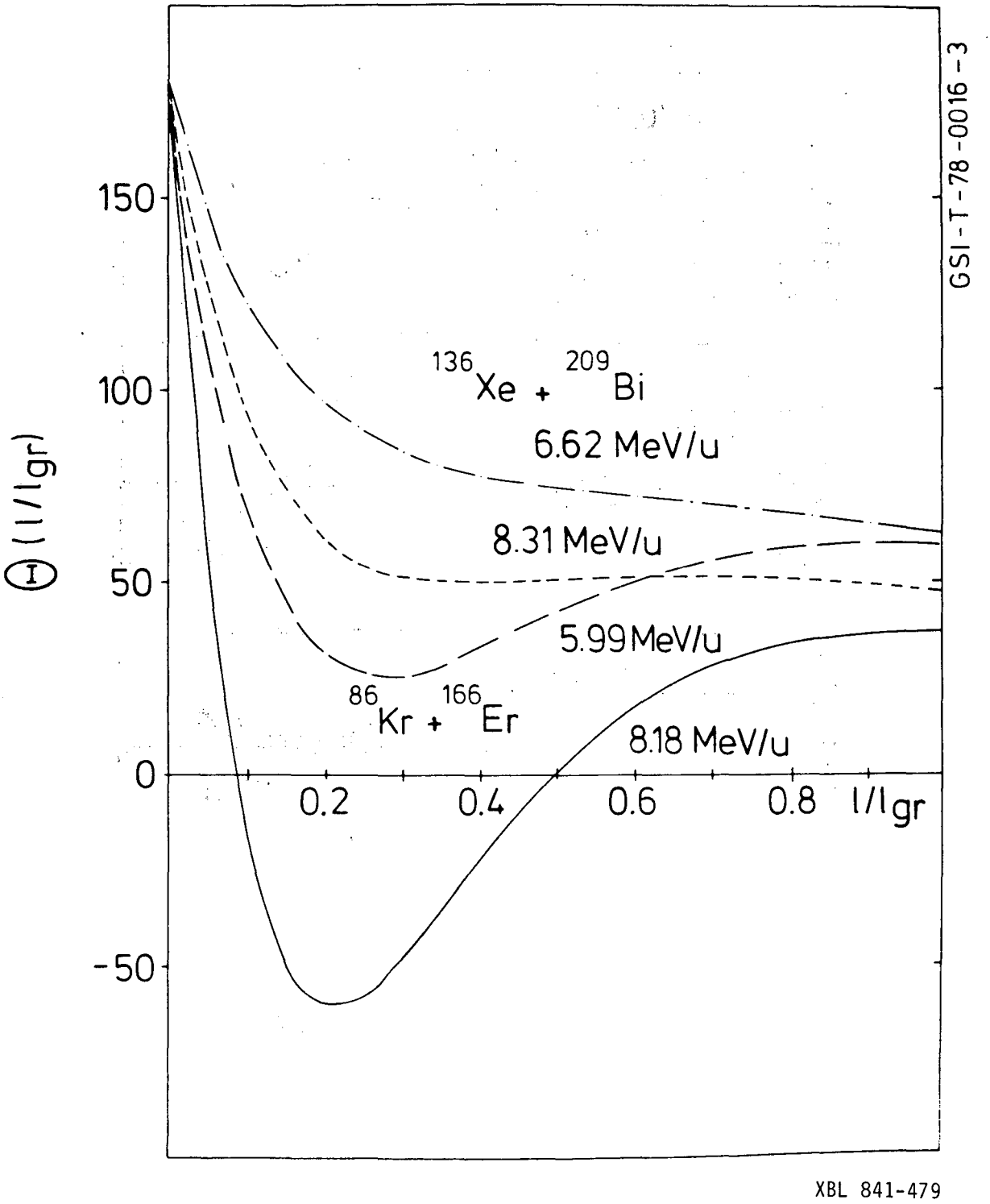
150
100
50
0
-50
Θ (I/Igr)
0.2
0.4
0.6
0.8
I/Igr
136Xe + 209Bi
6.62 MeV/u
8.31 MeV/u
5.99 MeV/u
86Kr + 166Er
8.18 MeV/u
GSI-T-78-0016-3
XBL 841-479

Fig. 6

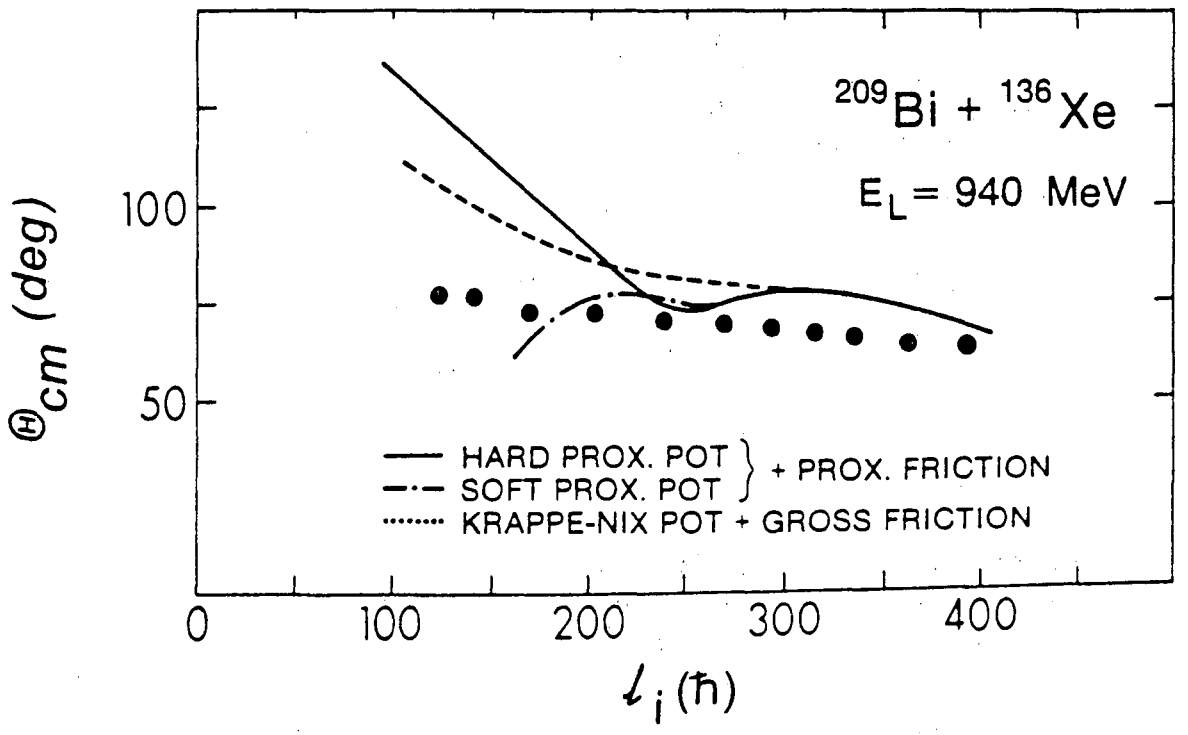

XBL 841-482

Fig. 7

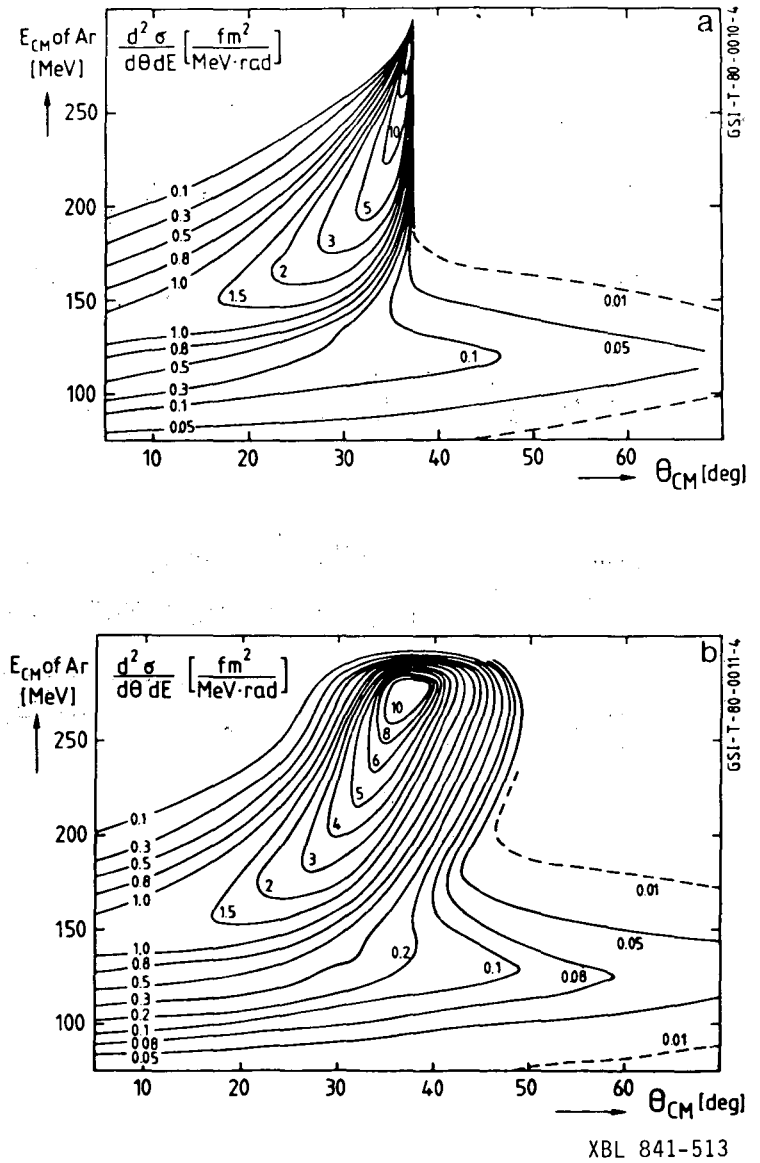
a
GSI-T-80-0010-4
E_{CM} of Ar [MeV]
$\frac{d^2\sigma}{d\theta dE}\left[\frac{fm^2}{MeV\cdot rad}\right]$
250
200
150
100
10
20
30
40
50
60
θ_{CM} [deg]
b
GSI-T-80-0011-4
E_{CM} of Ar [MeV]
$\frac{d^2\sigma}{d\theta dE}\left[\frac{fm^2}{MeV\cdot rad}\right]$
XBL 841-513

Fig. 8

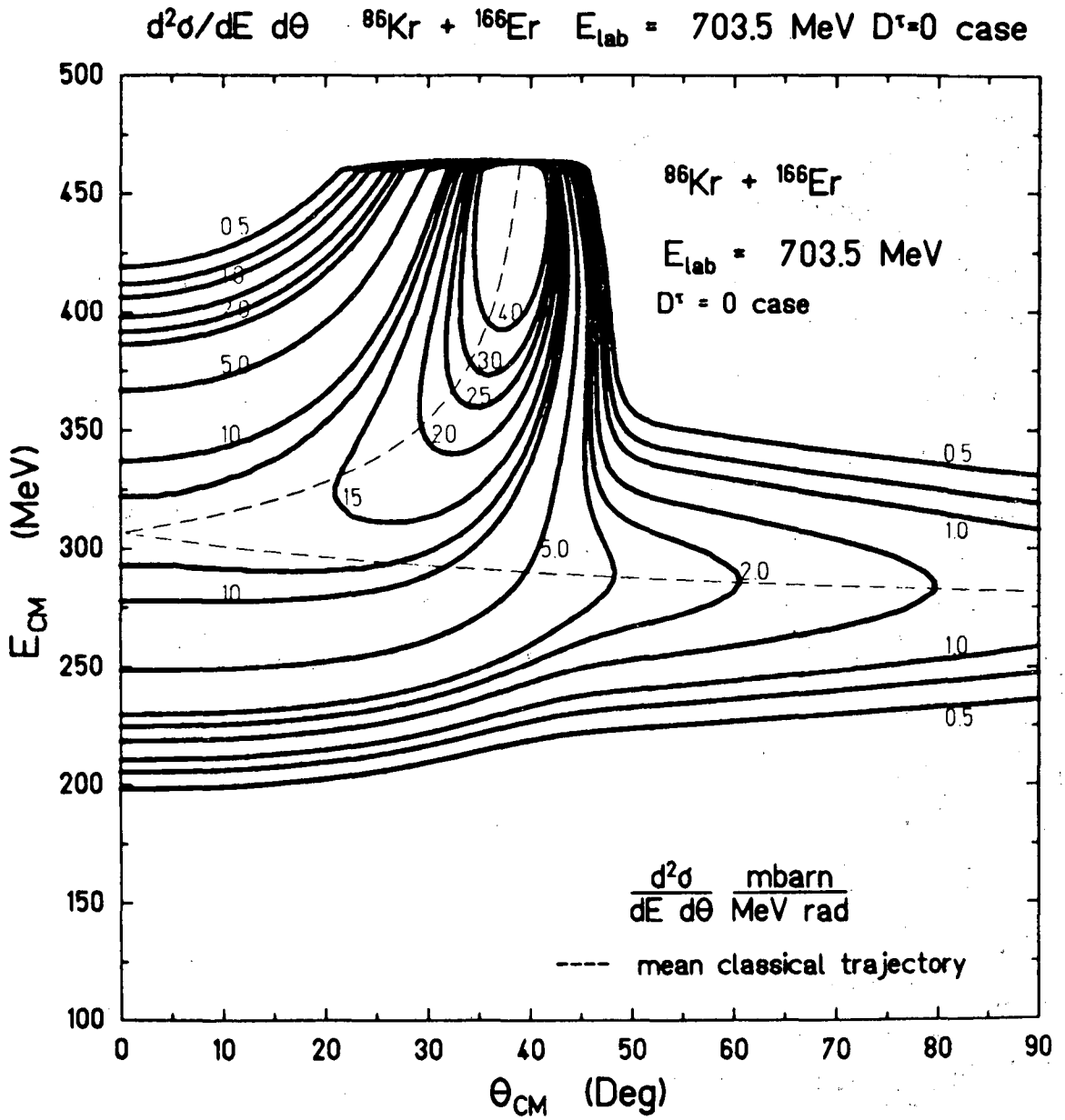

XBL 841-514

Fig. 9

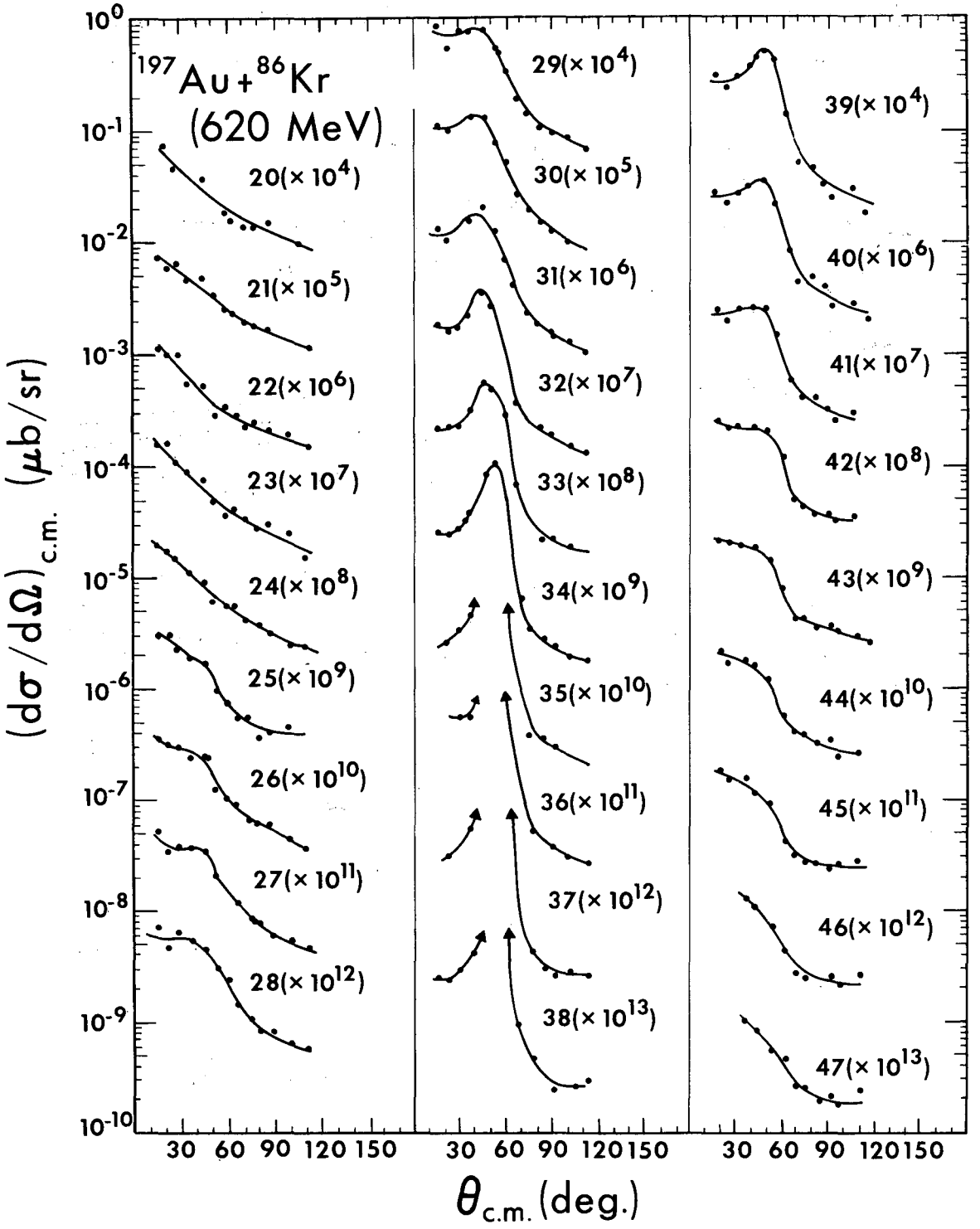
^{197}Au+^{86}Kr
(620 MeV)
20(× 10^4)
21(× 10^5)
22(× 10^6)
23(× 10^7)
24(× 10^8)
25(× 10^9)
26(× 10^{10})
27(× 10^{11})
28(× 10^{12})
29(× 10^4)
30(× 10^5)
31(× 10^6)
32(× 10^7)
33(× 10^8)
34(× 10^9)
35(× 10^{10})
36(× 10^{11})
37(× 10^{12})
38(× 10^{13})
39(× 10^4)
40(× 10^6)
41(× 10^7)
42(× 10^8)
43(× 10^9)
44(× 10^{10})
45(× 10^{11})
46(× 10^{12})
47(× 10^{13})
$(d\sigma/d\Omega)_{c.m.}$ (μb/sr)
$\theta_{c.m.}$ (deg.)
XBL 7512-9891

Fig. 10

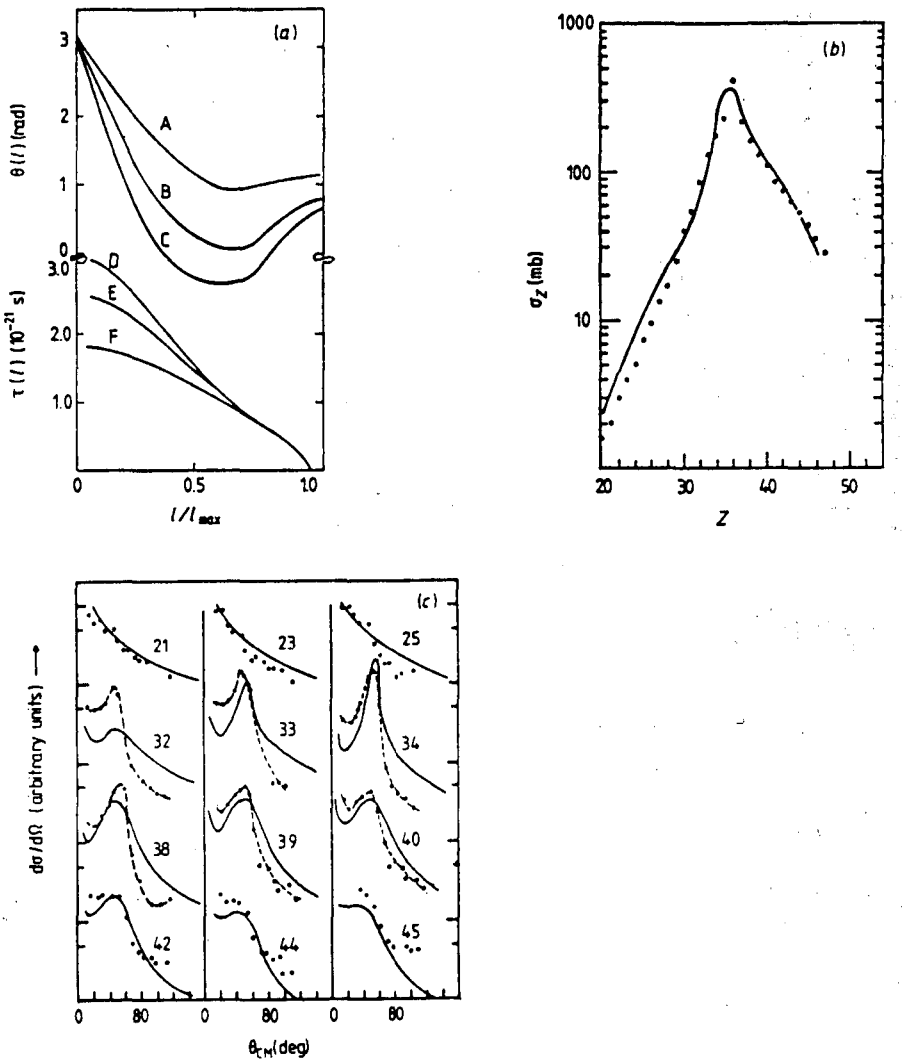

XBL 841-478

Fig. 11

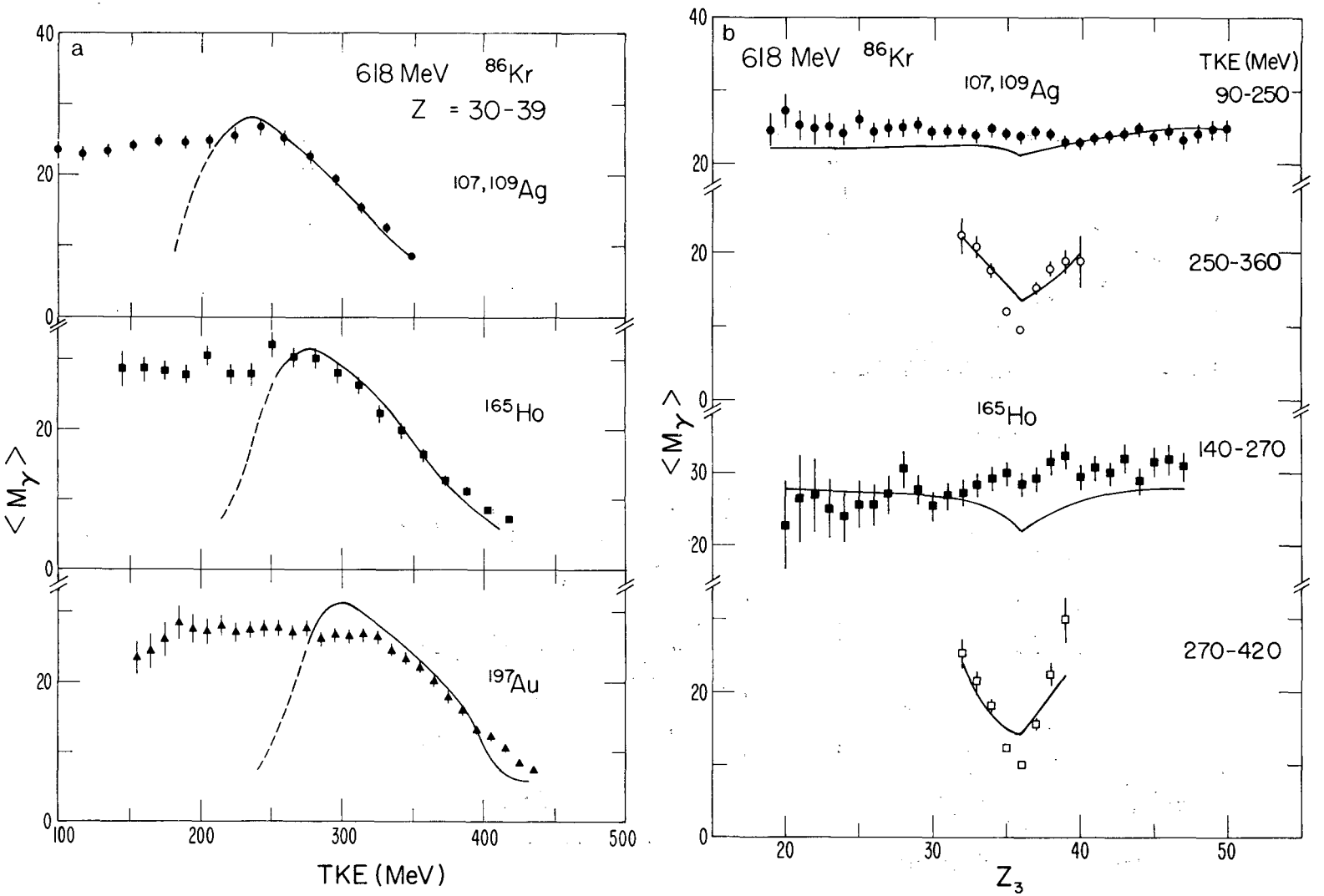

XBL 786-2556A

Fig. 12

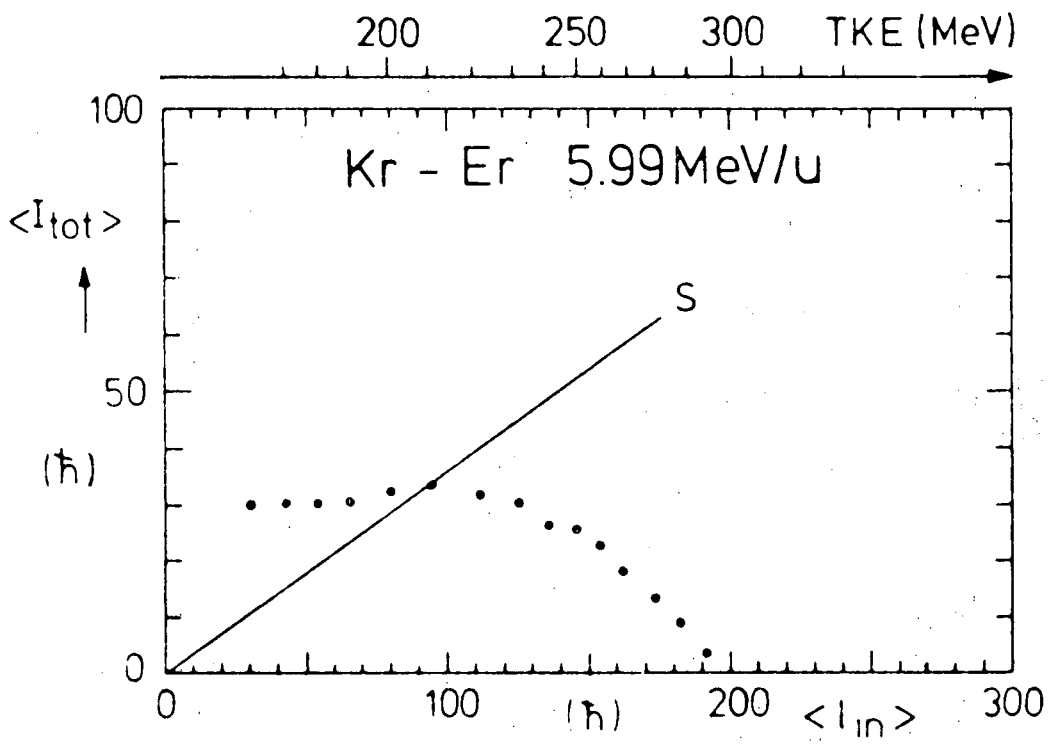

XBL 842-704

Fig. 13

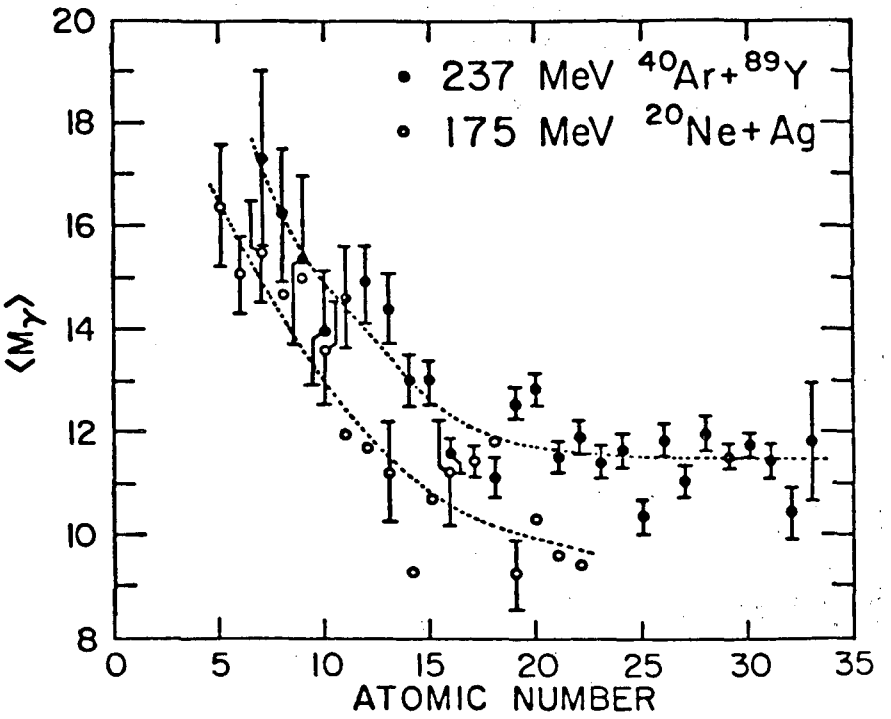

XBL 841-483

Fig. 14

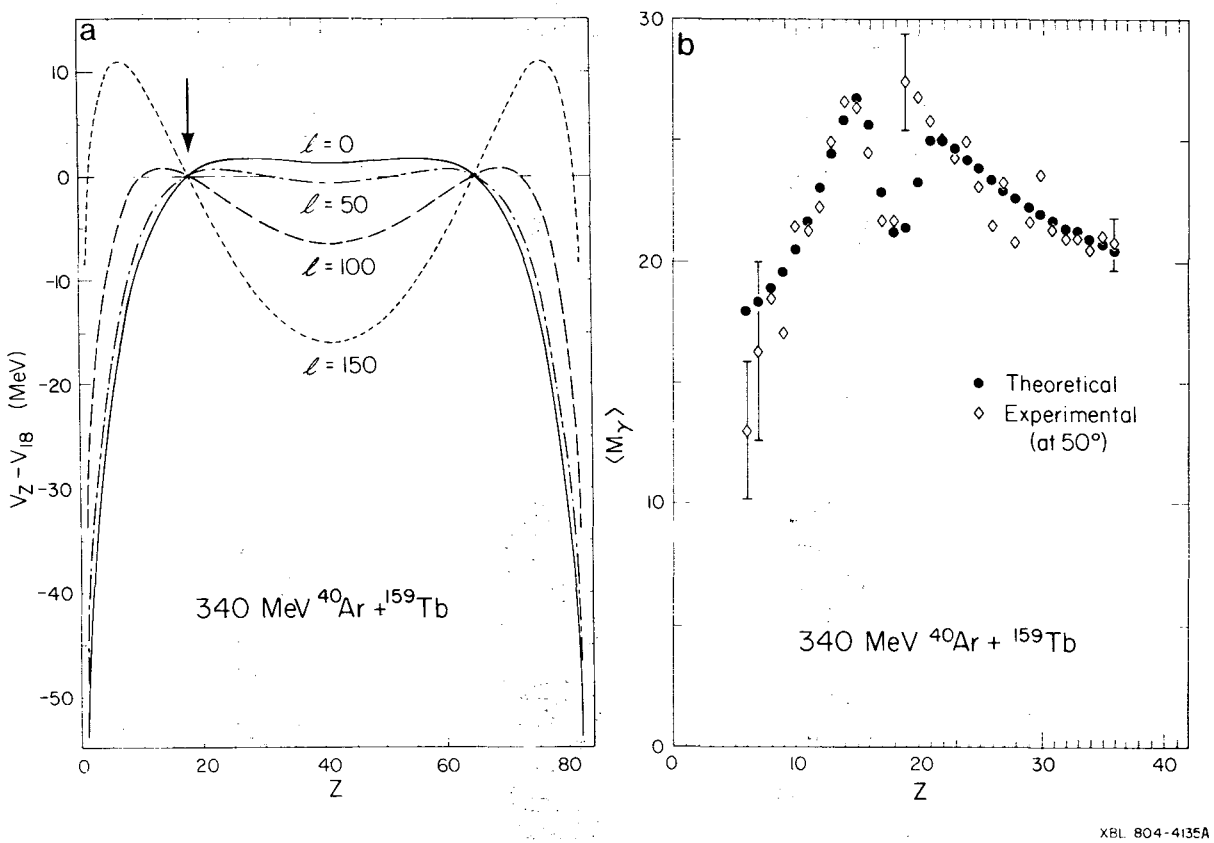
a
$V_Z - V_{18}$ (MeV)
10
0
-10
-20
-30
-40
-50
0
20
40
60
80
Z
$\ell = 0$
$\ell = 50$
$\ell = 100$
$\ell = 150$
340 MeV ^{40}Ar + ^{159}Tb
b
$\langle M_Y \rangle$
30
20
10
0
0
10
20
30
40
Z
Theoretical
Experimental (at 50°)
340 MeV ^{40}Ar + ^{159}Tb
XBL 804-4135A

Fig. 15

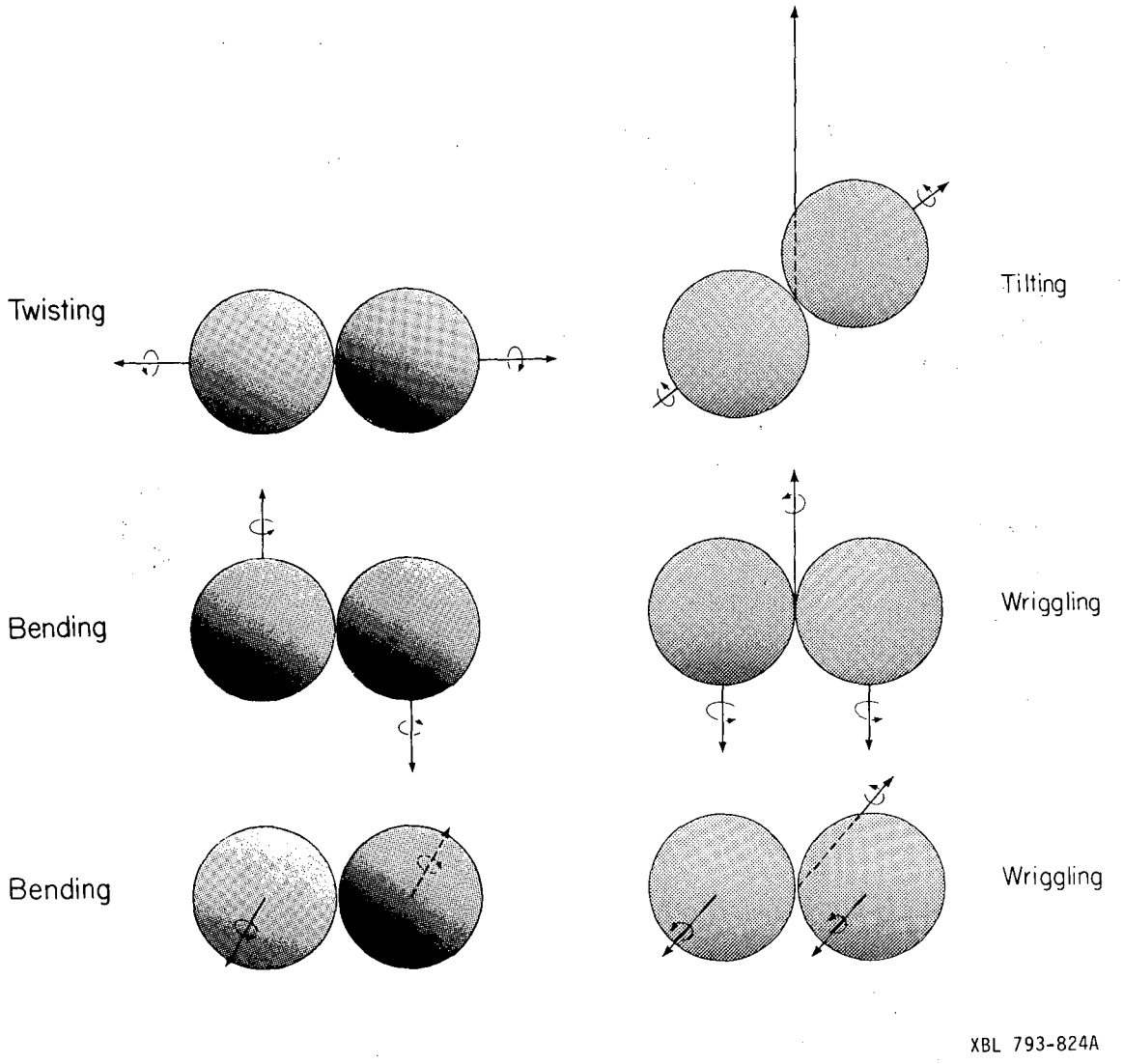
Twisting
Tilting
Bending
Wriggling
Bending
Wriggling
XBL 793-824A

Fig. 16

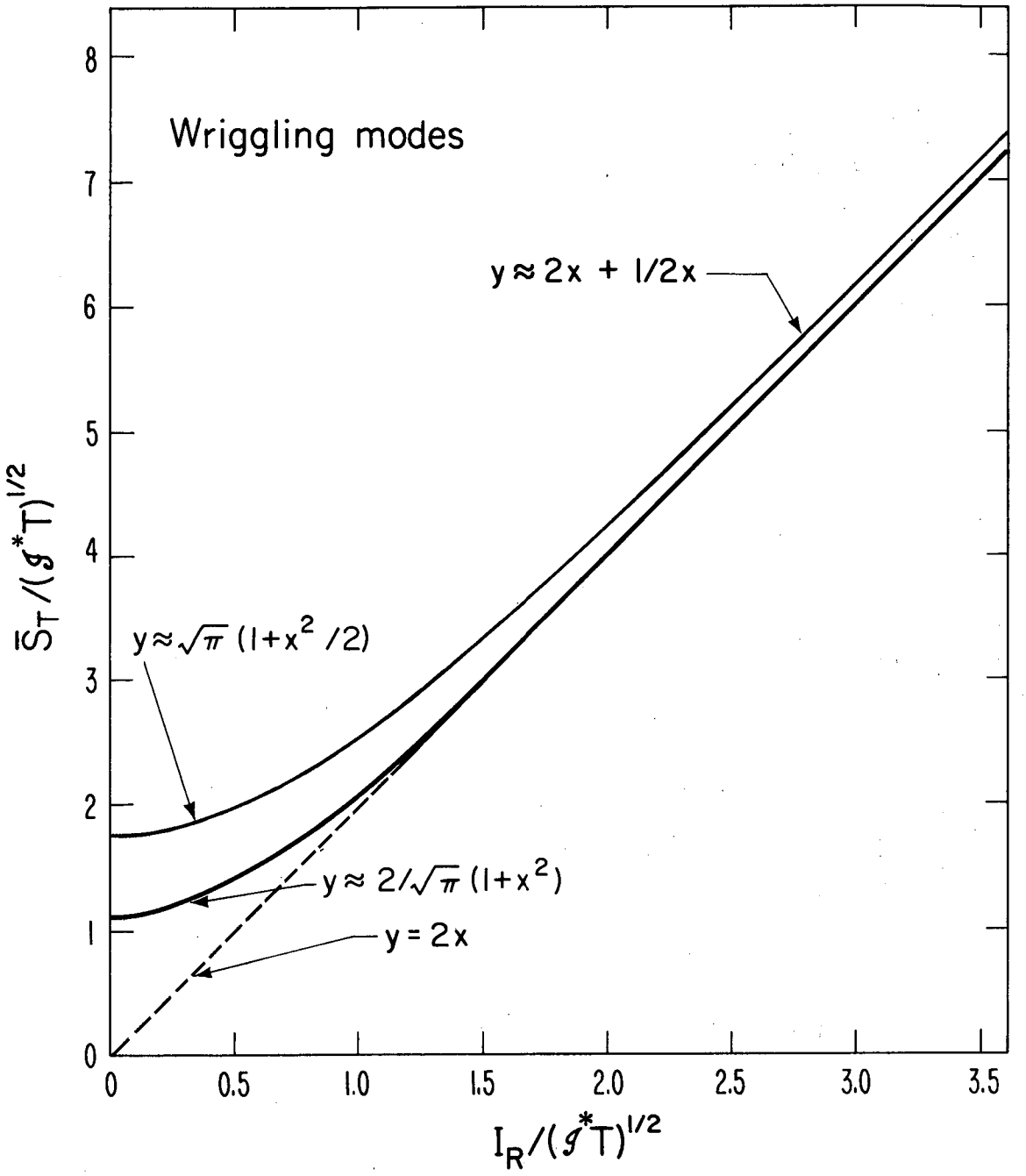

XBL 793 - 822

Fig. 17

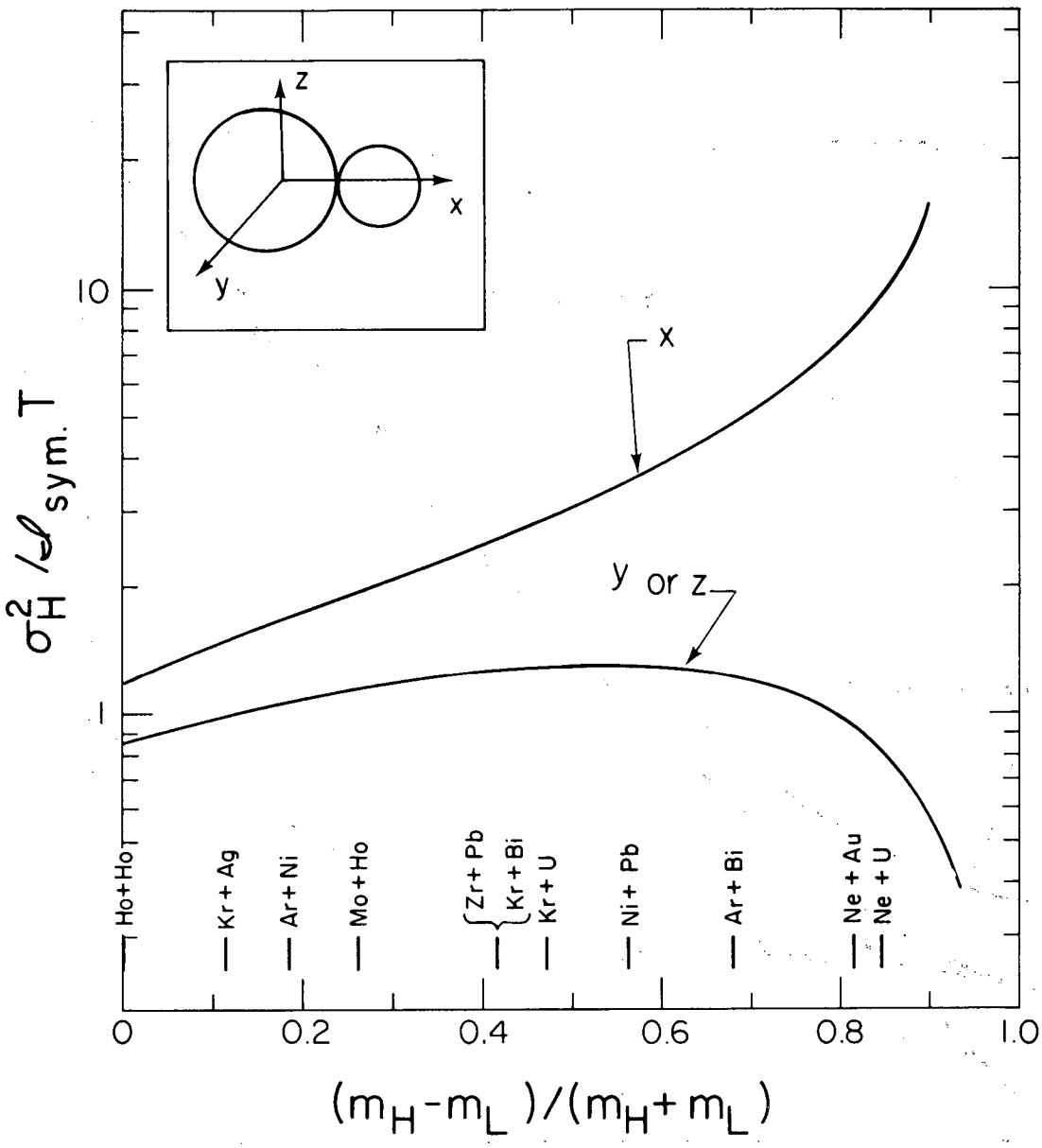

XBL 821-4405A

Fig. 18

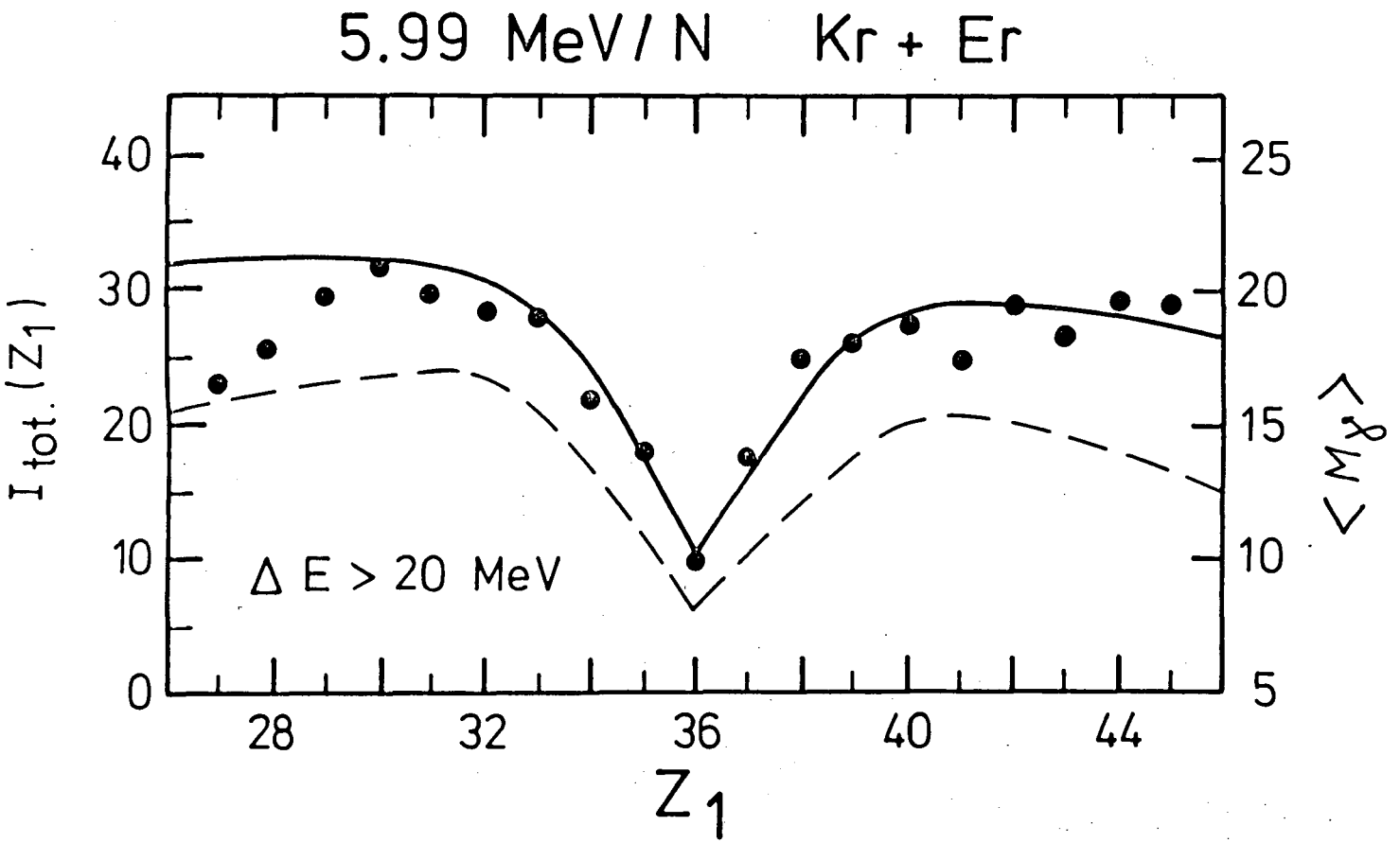

XBL 842-614

Fig. 19

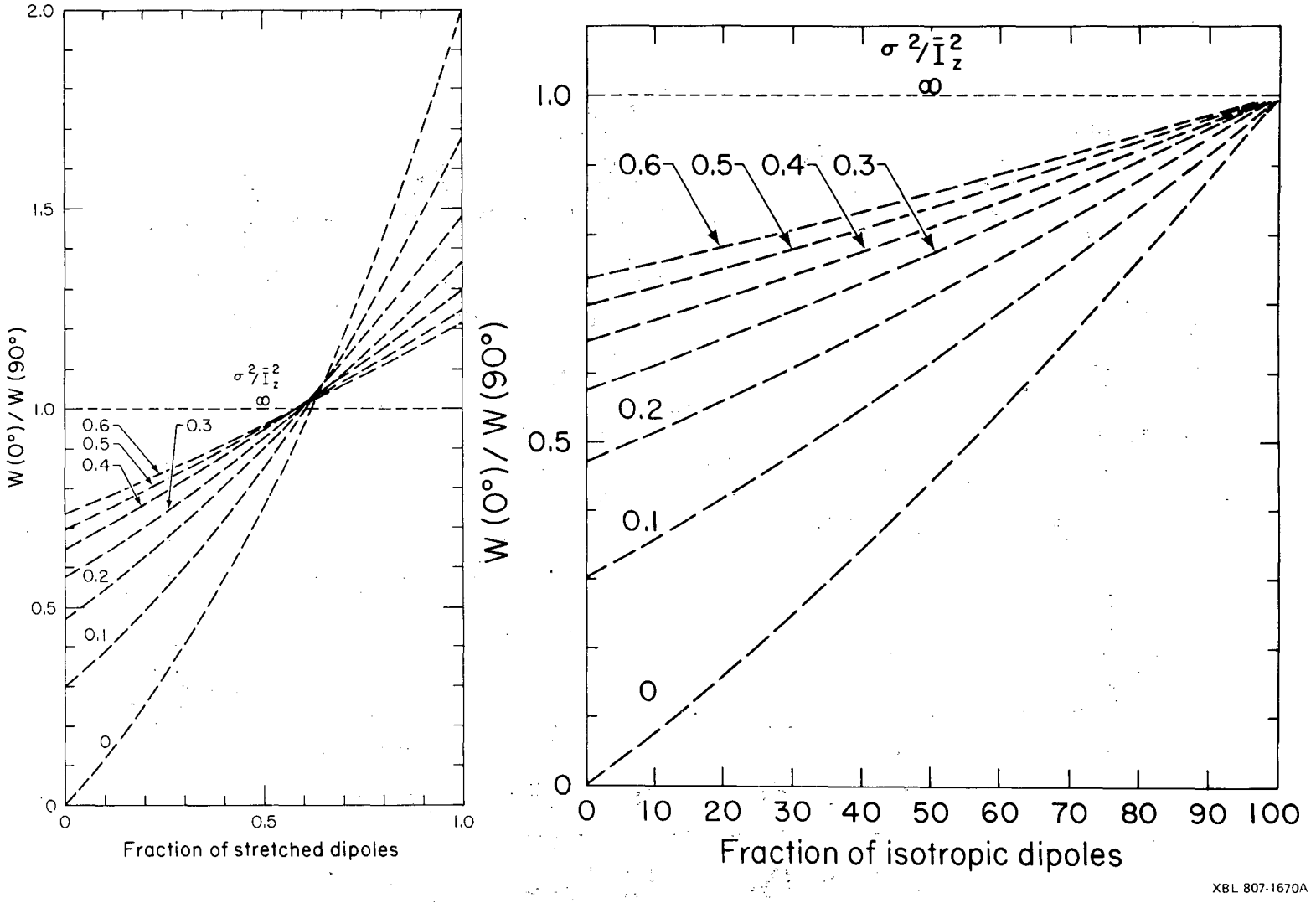
2.0
1.5
1.0
0.5
0
W (0°) / W (90°)
0
0.5
1.0
Fraction of stretched dipoles
$\sigma^2/\bar{I}_z^2$
∞
0.6
0.5
0.4
0.3
0.2
0.1
0
1.0
0.5
0
W (0°) / W (90°)
0 10 20 30 40 50 60 70 80 90 100
Fraction of isotropic dipoles
XBL 807-1670A

Fig. 20

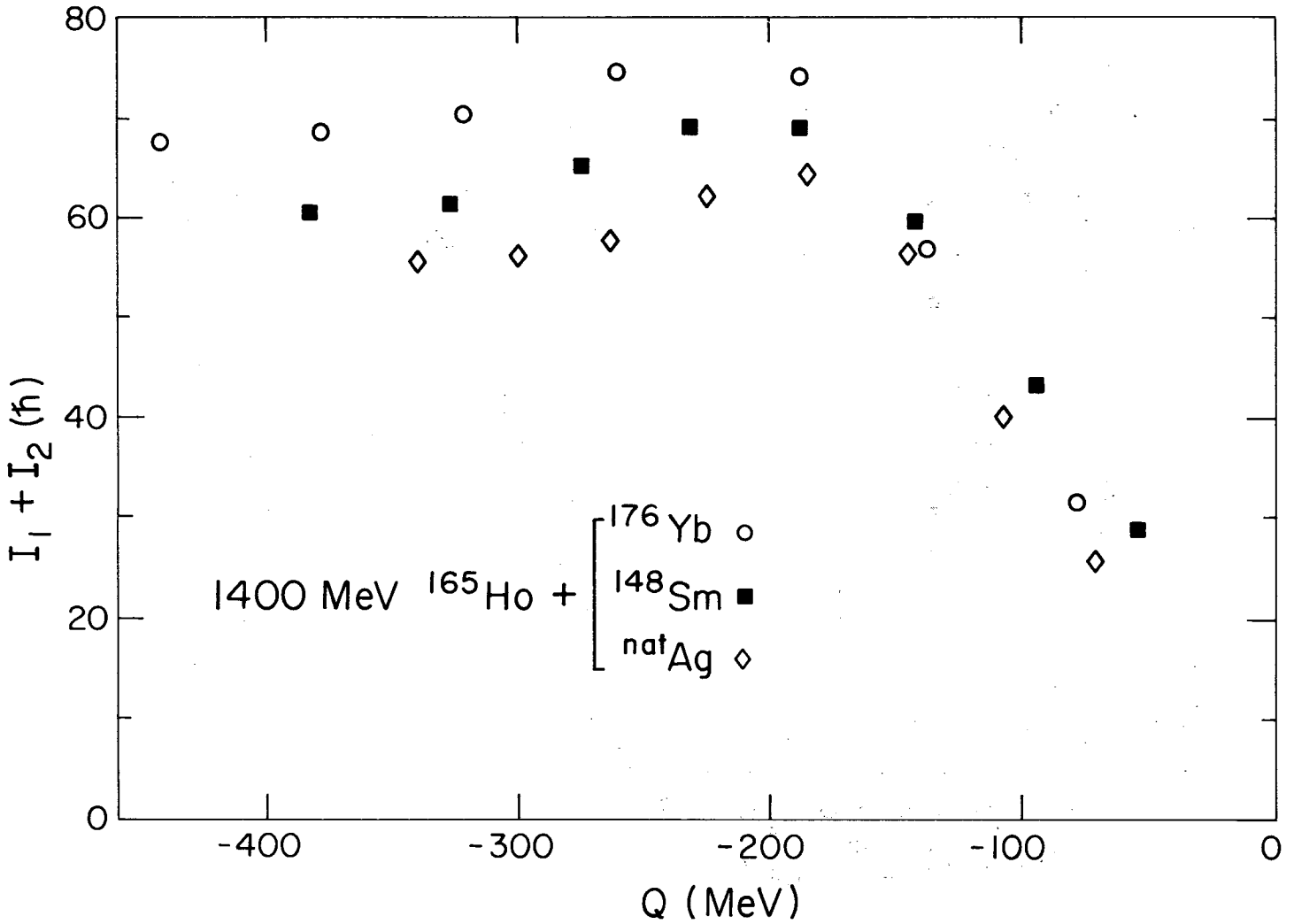

XBL 824-327

Fig. 21

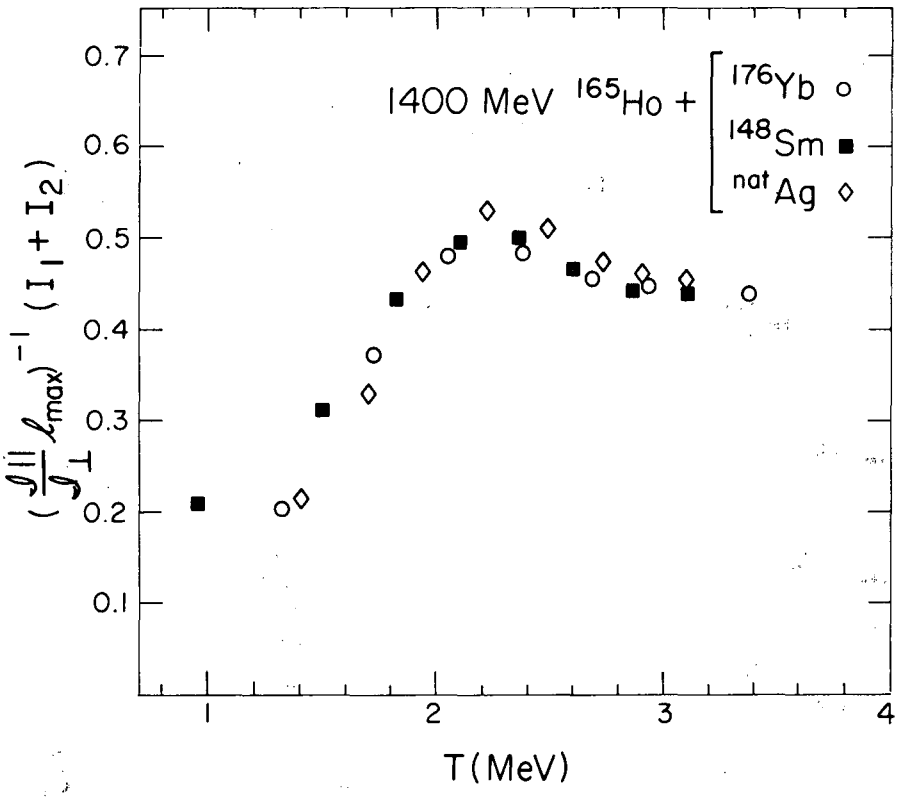

XBL 824-335A

Fig. 22

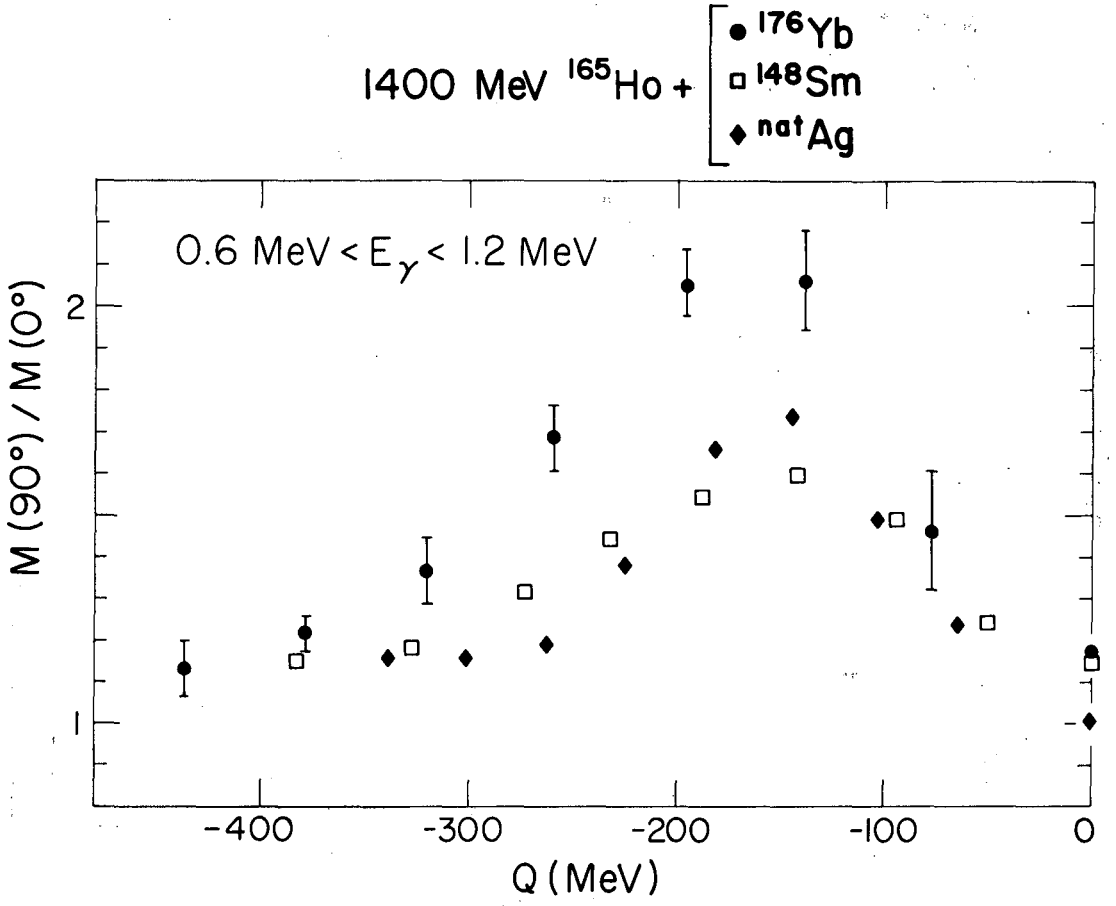

XBL 824-333A

Fig. 23

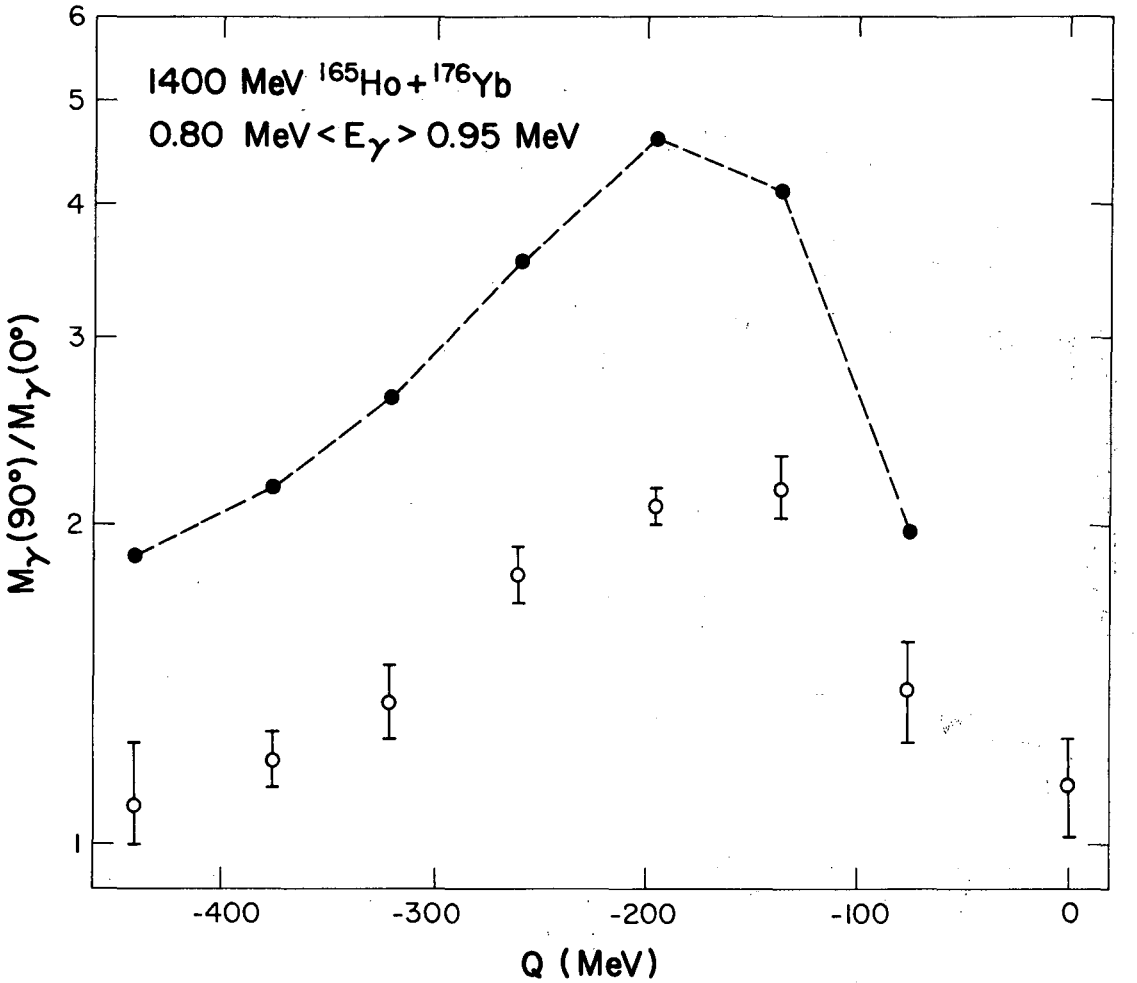

XBL 824 - 338

Fig. 24

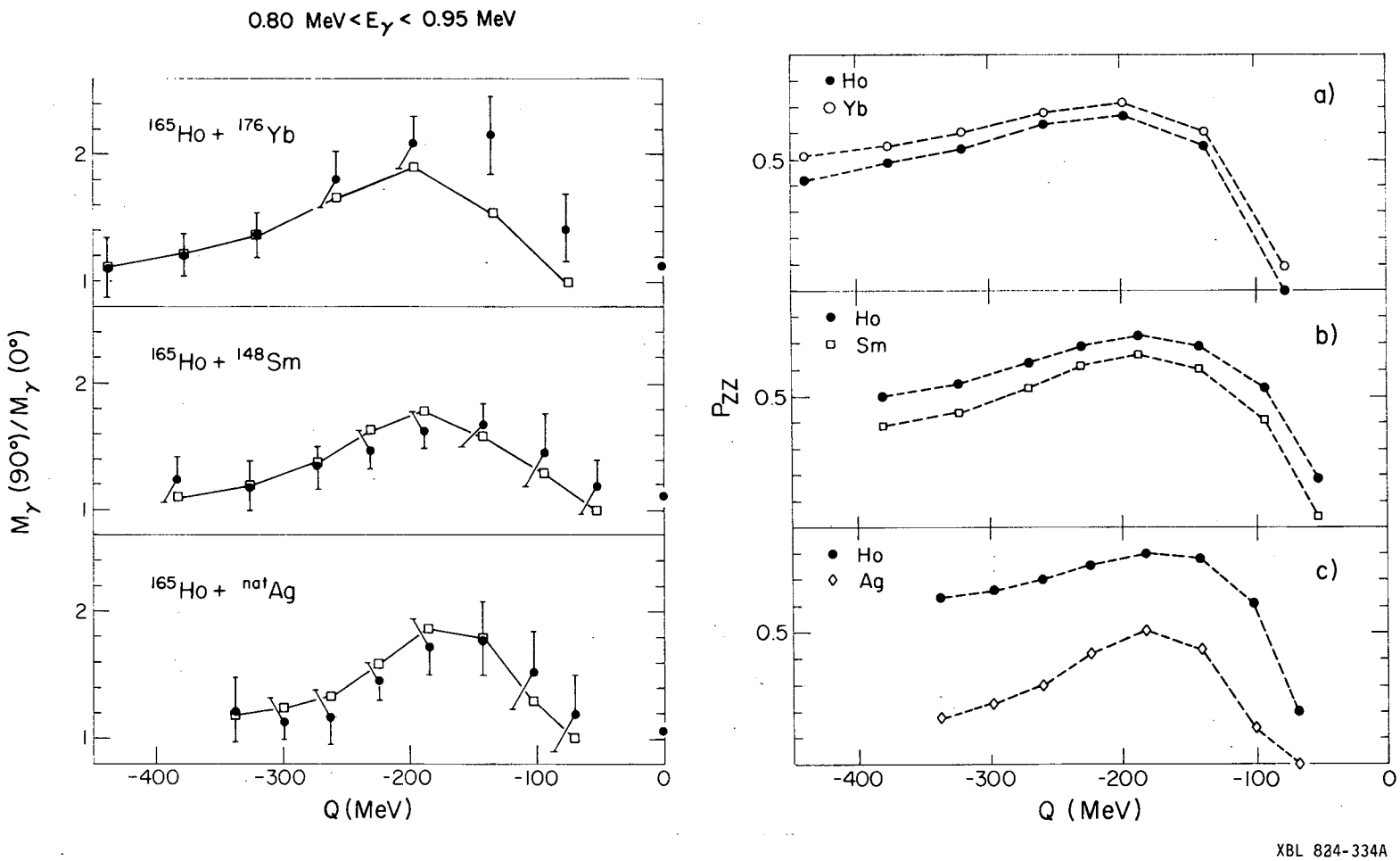
0.80 MeV < E_γ < 0.95 MeV
^{165}Ho + ^{176}Yb
^{165}Ho + ^{148}Sm
^{165}Ho + ^{nat}Ag
M_γ (90°) / M_γ (0°)
Q (MeV)
Ho
Yb
Sm
Ag
a)
b)
c)
P_{ZZ}
XBL 824-334A

Fig. 25

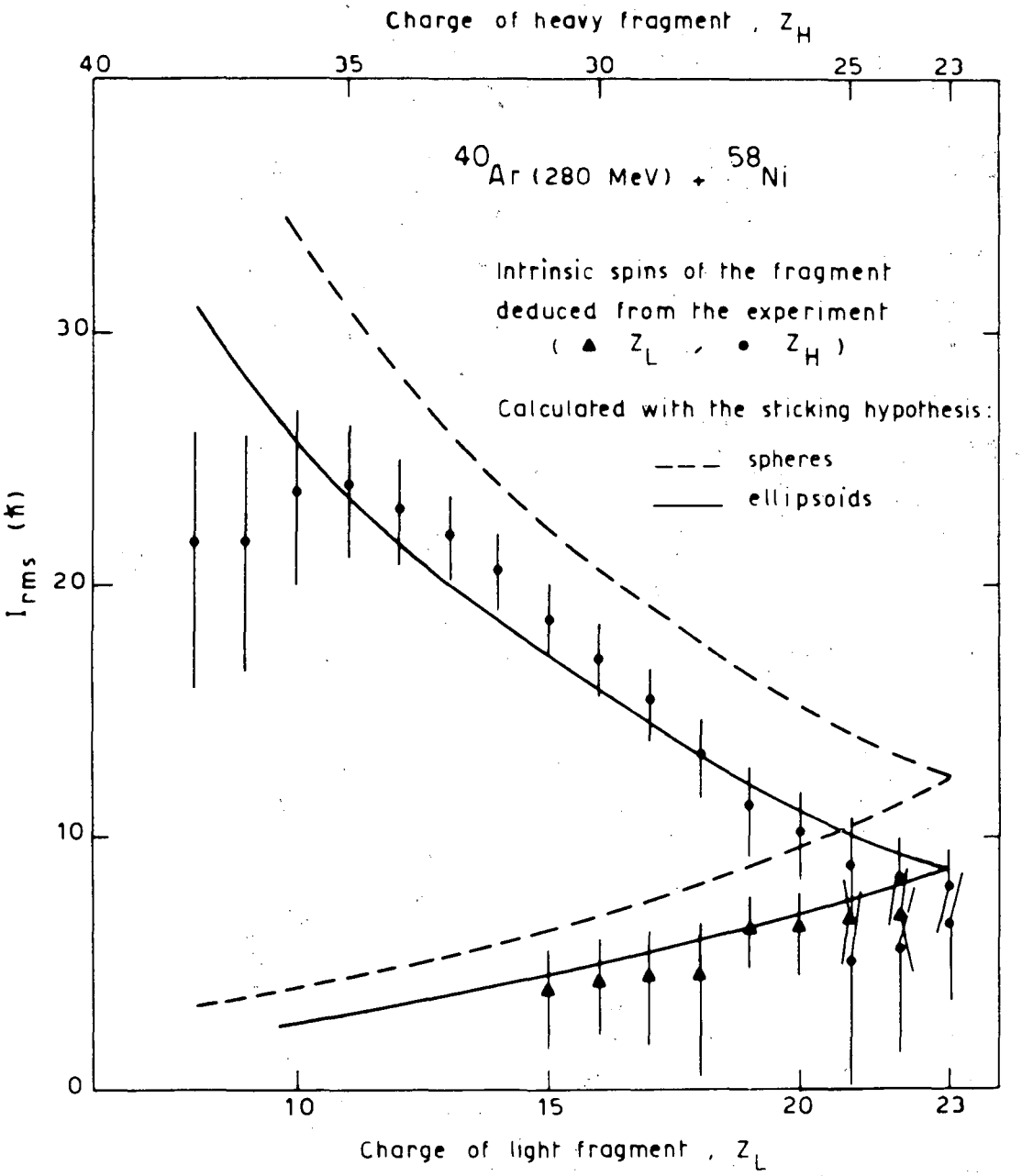

XBL 842-613

Fig. 26

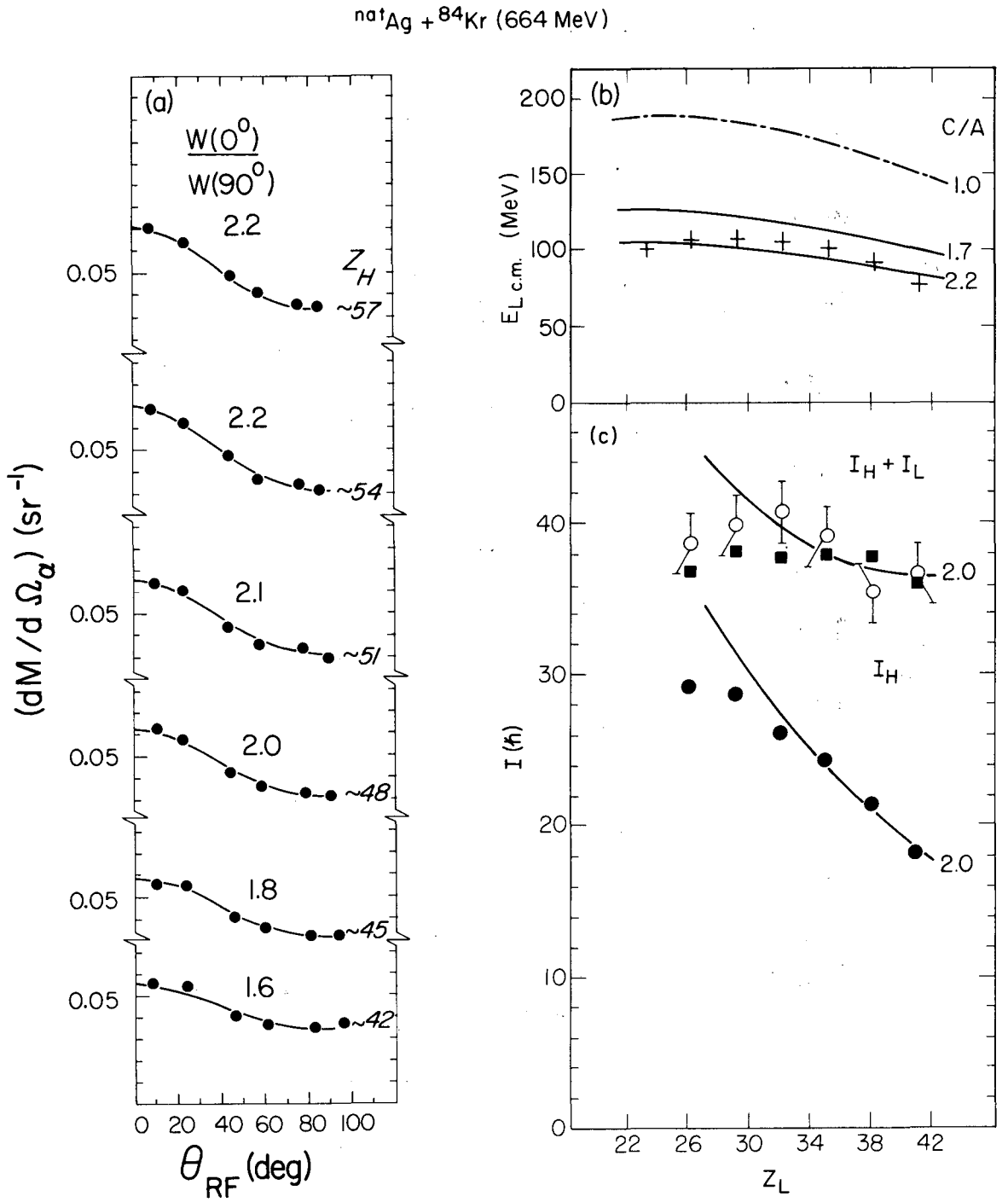

XBL 807-3458B

Fig. 27

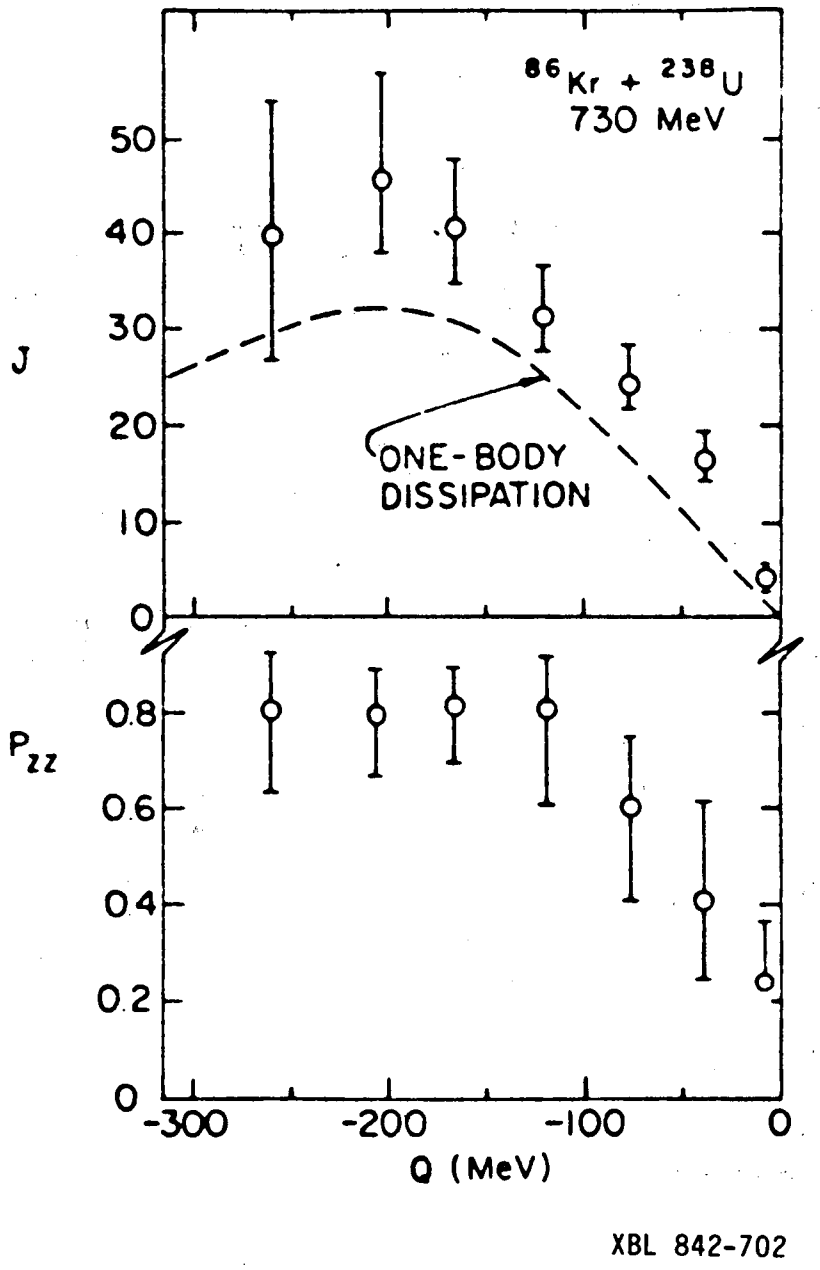

XBL 842-702

Fig. 28

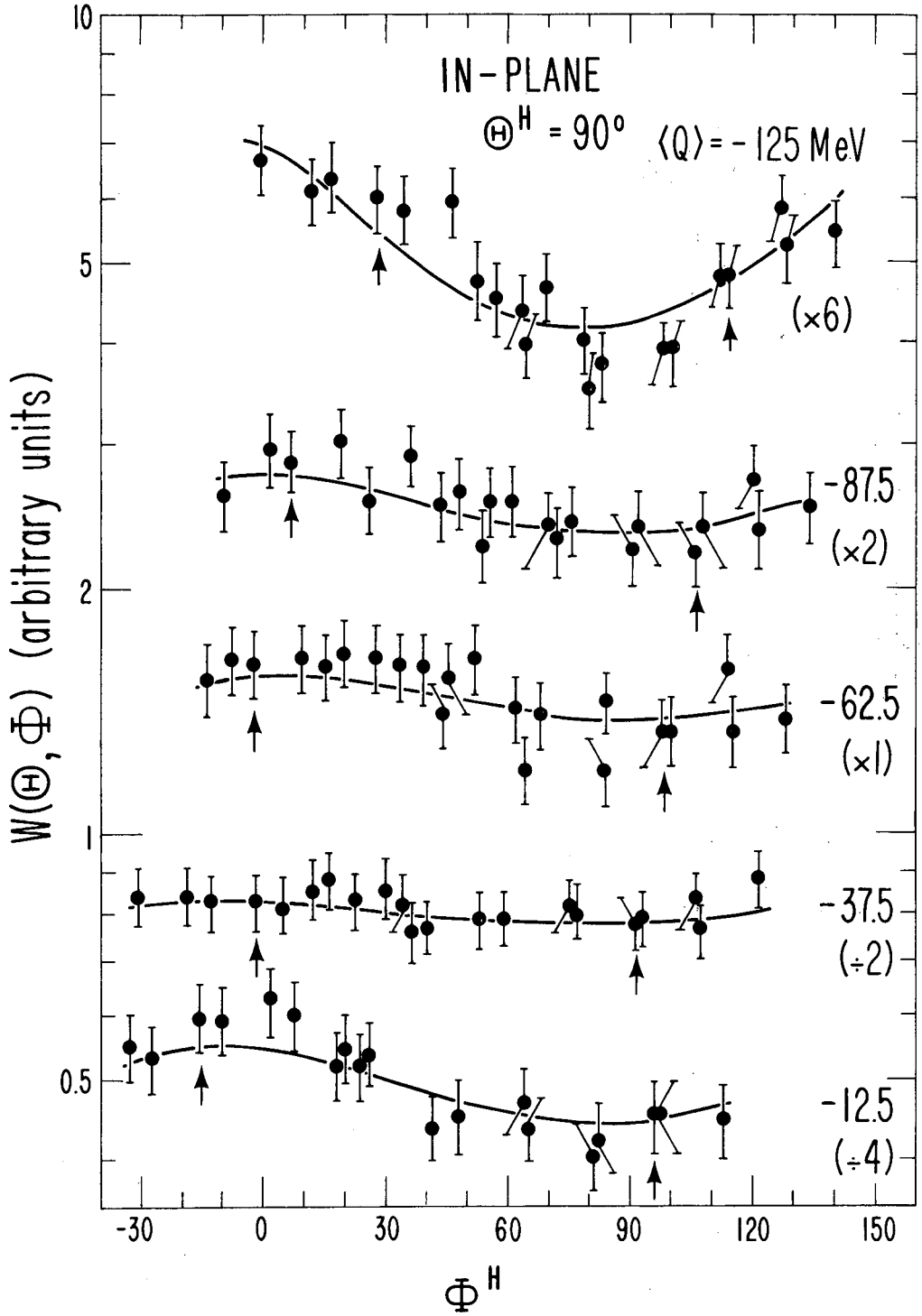

XBL813-2180

Fig. 29

283

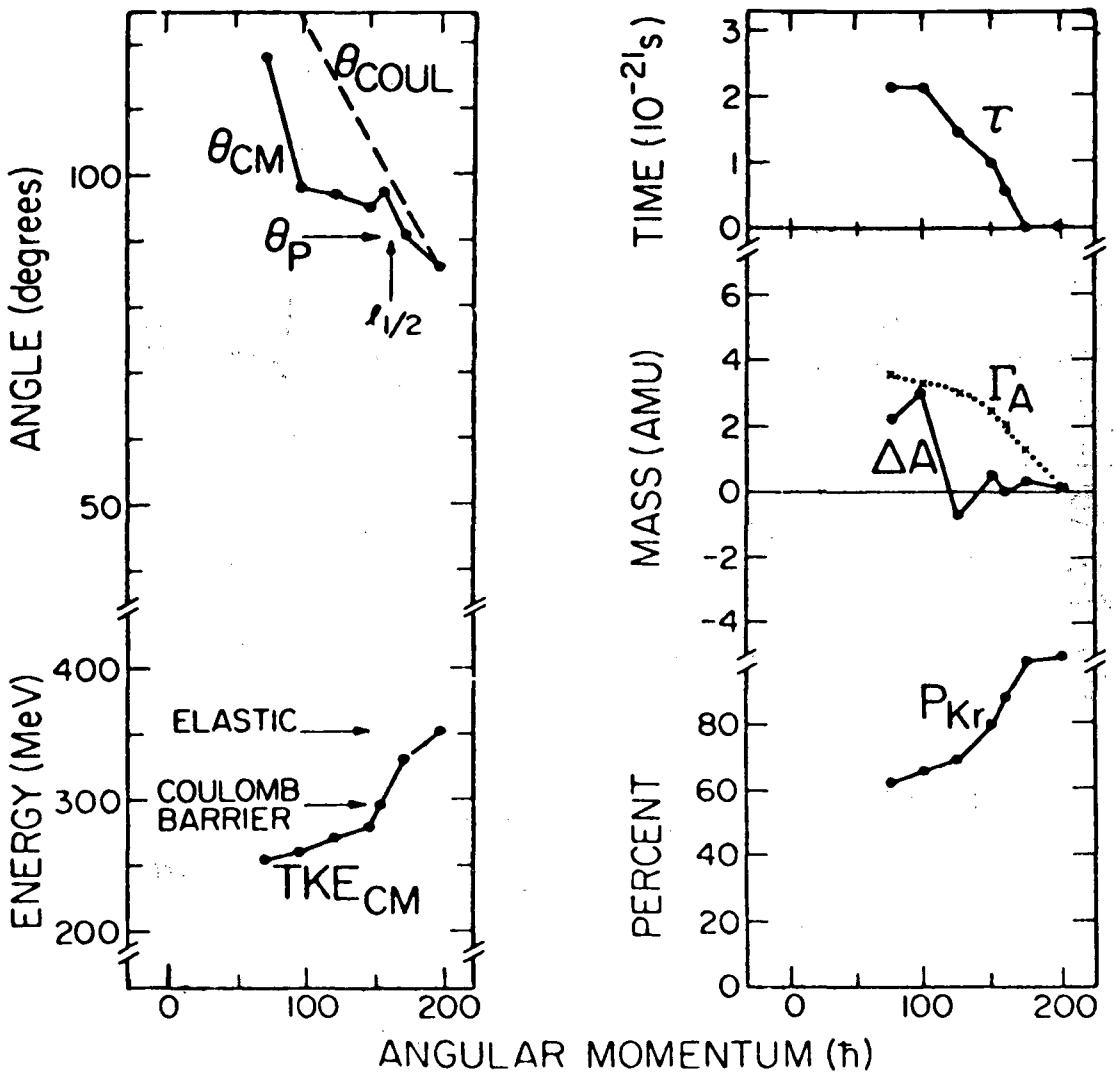

XBL 842-785

Fig. 30

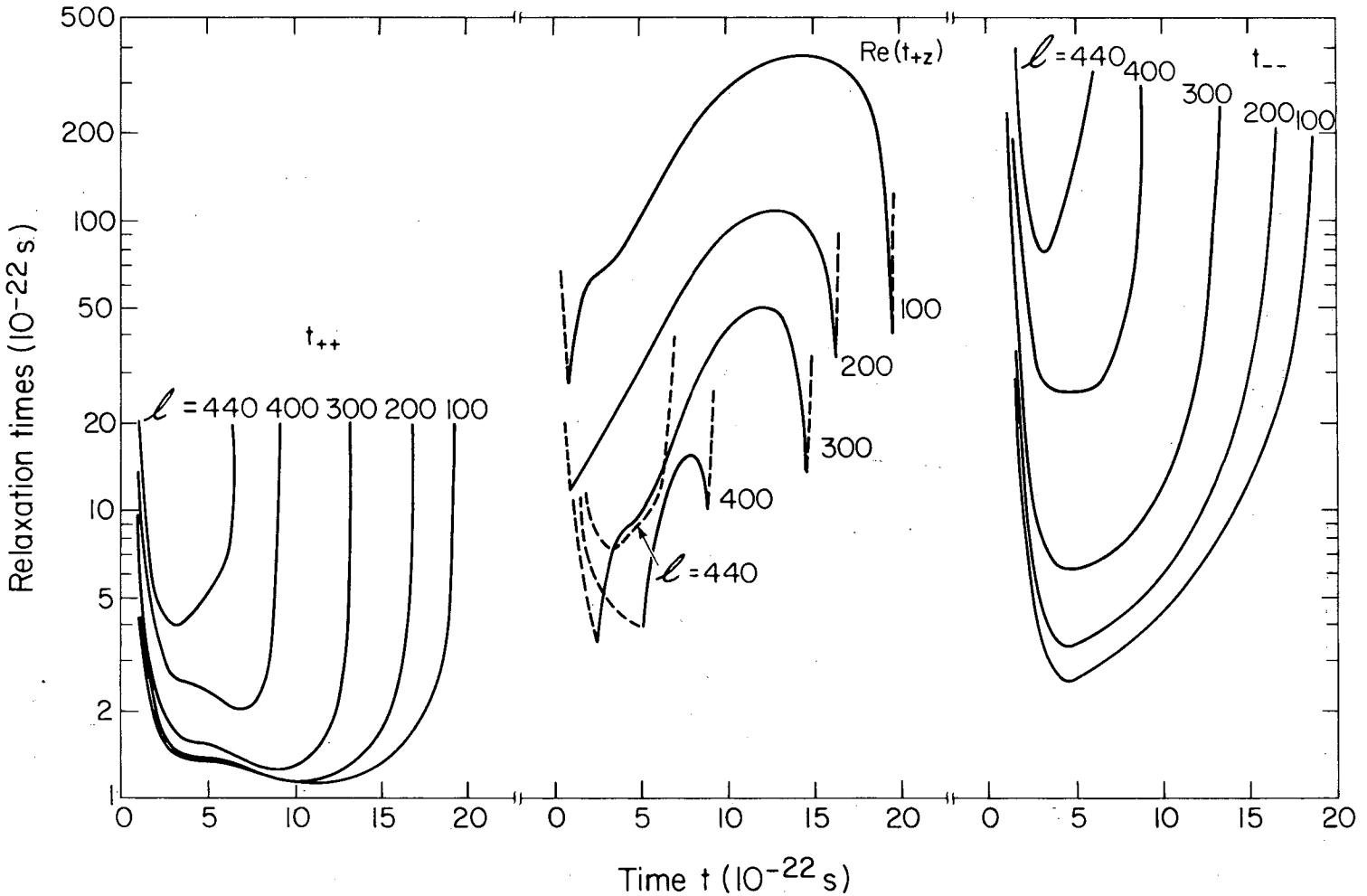

XBL 841-23

Fig. 31

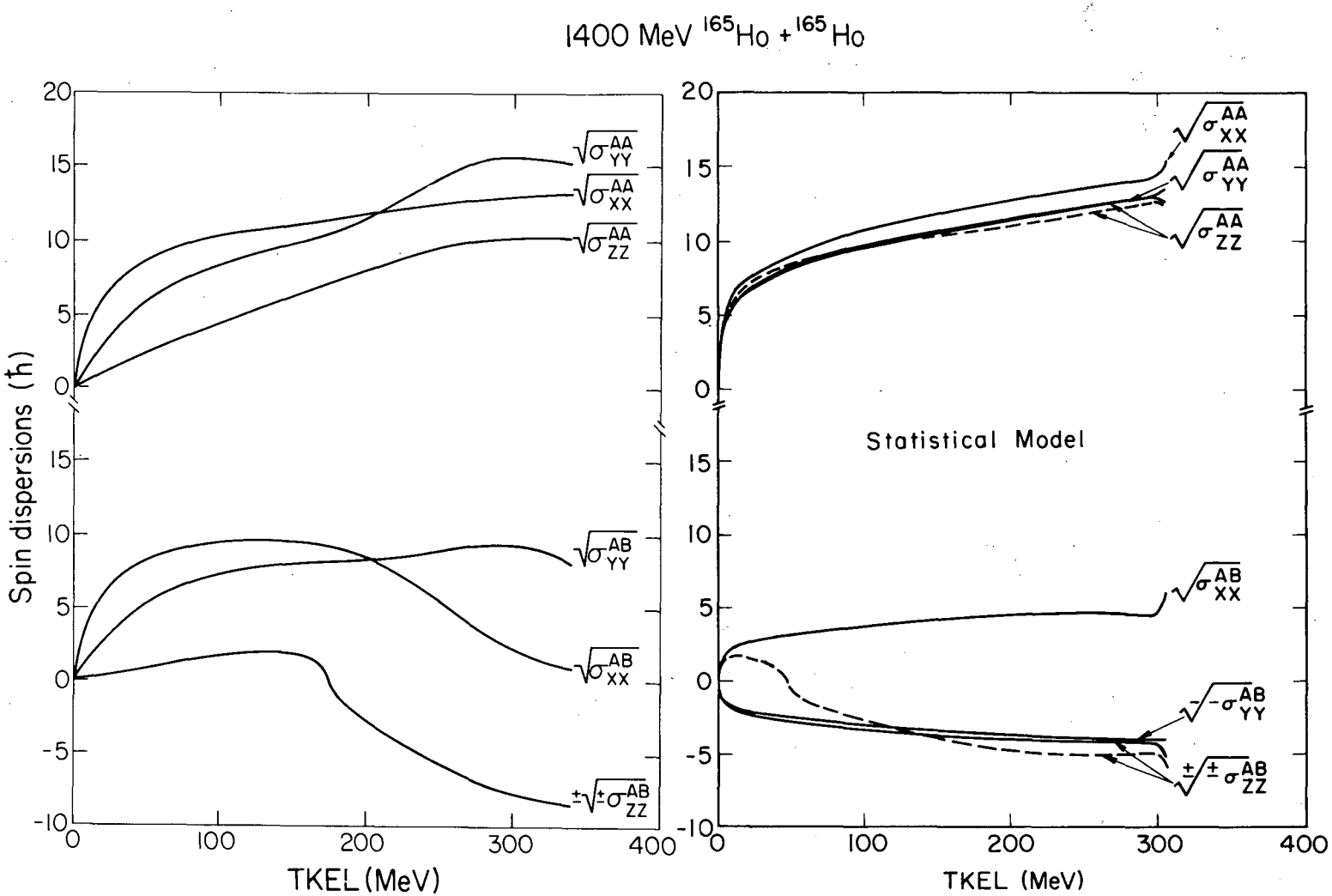

XBL 841-7504A

Fig. 32

This report was done with support from the Department of Energy. Any conclusions or opinions expressed in this report represent solely those of the author(s) and not necessarily those of The Regents of the University of California, the Lawrence Berkeley Laboratory or the Department of Energy.

Reference to a company or product name does not imply approval or recommendation of the product by the University of California or the U.S. Department of Energy to the exclusion of others that may be suitable.

TECHNICAL INFORMATION DEPARTMENT
LAWRENCE BERKELEY LABORATORY
UNIVERSITY OF CALIFORNIA
BERKELEY, CALIFORNIA 94720